Evaluation of Polymer Relaxation Dynamics

Using Laser Speckle Imaging and Dynamic Mechanical Analysis

TUDelft

A.K. Wiltink

Evaluation of Polymer Relaxation Dynamics

Using Laser Speckle Imaging and Dynamic Mechanical Analysis

by

A.K. Wiltink

to obtain the degree of Master of Science
at the Delft University of Technology,
to be defended publicly on Friday September 10, 2021 at 13:00.

Cover image, Camera, credits: Christoph Niemann [1]

An electronic version of this thesis is available at `http://repository.tudelft.nl/`.

TUDelft

Abstract

On the road towards developing truly self-healing polymer coatings, autonomous gap closure behavior is an important step. Stored entropic energy in a polymer could act as driving force for this closure. To make proper use of this concept it is important to develop characterization protocols able to relate entropy release to gap closure dynamics and ultimately to polymer architecture. Dynamic mechanical thermal analysis (DMA) and Laser Speckle Imaging (LSI) have previously been used in separate studies to quantify entropic energy change and measure local polymer dynamics, respectively.

This work aims to develop an LSI-based protocol able to relate entropic induced length changes measured in DMA to polymer relaxation dynamics. To this purpose a set of non-healing epoxies with different molecular weight between crosslinks was tested both in DMA and LSI. A recently developed analysis protocol was used to extract, from DMA data, the entropy change at the glass transition region related to displacement (i.e. shape memory effect). With the help of a micro-tensile tester and a temperature control system, LSI allowed quantifying the local dynamics of the studied polymers as function of temperature and strain. The overall relaxation dynamics in stress relaxation tests measured with LSI were then compared to the DMA results.

A relation between the strain relaxation dynamics in LSI, crosslinking density, entropy release and tan δ variation with temperature was found. This was done by comparing the frequency and intensity of local displacements measured with LSI to delta length and tan δ obtained with DMA. Furthermore, this research revealed an interesting discrepancy between local strain relaxation and stress relaxation times, as the local strain relaxation time extracted with LSI was shown to be longer than the overall stress relaxation time measured by the micro-tensile tester in the same test. The characterization and data analysis protocol explored here paves the way towards experimental methods that allow a more direct correlation between coating design parameters, such as crosslinking density and chain flexibility, and local entropy driven damage closure.

Acknowledgements

Like the picture on the cover illustrates, you sometimes have to look differently at something in order to see the possibilities. This is certainly one of the things I discovered during this research and I could not have done it on my own, so I would like to take this place to express my gratitude to many people.

First and foremost I would like to thank Santiago for his supervision during this project: without all the good feedback and brainstorm meeting I could not have changed my ideas into the result it is now. Sybrand, I would like to thank you for the sharp questions that have helped me steer this research in the right direction. Marlies, you have been invaluable for all your help in the lab and good advice to make my own decisions and work towards an end at some point. Johan and Durga, thanks for the support in the labs and for steering me in the right direction when it was needed. For this thesis we borrowed a micro tensile tester from our friends at 3ME, Kees, thank you very much. Julie Teuwen, many thanks for being part of my thesis committee.

Sèra, Mark and Caspar, thanks for all the good discussions, coffee and lunch breaks and support in the lab. All of NovAM, thanks for the good time I have had although Covid made our corridor a quiet place from time to time. I look forward to the long promised NovAM dinner to end our time together cheerful.

Many thanks to my parents for their infinite support during the eight years my student life now already lasts (and the final months the internship will add to those). Of course I would like to thank all my friends that have made my time in Delft, and my life in the future, such a wonderful time! Roos, thanks for following my tracks and help me refresh my knowledge every year and of course just for being you. Last, but certainly not least, I would like to thank Mattie for reading this document an infinite times and more.

A.K. Wiltink
Delft, September 2021

List of Figures

List of Tables

Contents

<div align="right">

1

</div>

<div align="right">

Introduction

</div>

Extending the lifetime of a product is an important motivation for material research, a longer life means more efficient use of materials and thus resources. In light of the growing population and limited sources of raw materials this need will only increase over the coming decades.

Since the lifetime of a product largely depends on its materials, researchers have developed materials that last longer. Developing self-healing materials is a route to do so, since the ability to self-repair makes for longer lasting materials. Self-healing polymeric materials can be divided into two different classes: extrinsic and intrinsic healing. Extrinsic covers all polymers that have containers with healing agent inside that will be released if a crack occurs; breaking the containers, filling the gap and reacting with its surrounding in order to heal the damage [2]. The intrinsic healing strategy is based on reversible chemistries that reconnect the polymer chains after a damage occurs [3]. The material focus of this thesis lies on the development of intrinsic self-healing polymers.

In order to make self-healing polymers, the material will need local temporal mobility to repair damages. Mobility is needed to close the damage and reconnect the reversible chemistries. Local because only a small area surrounding the damage should be involved. Temporal because after healing the mobility should be reduced again. In this thesis the steps of healing described as: surface rearrangement, surface approach, wetting, diffusion and randomization are divided into gap closure and healing [4]. This is illustrated in Figure 1.1.
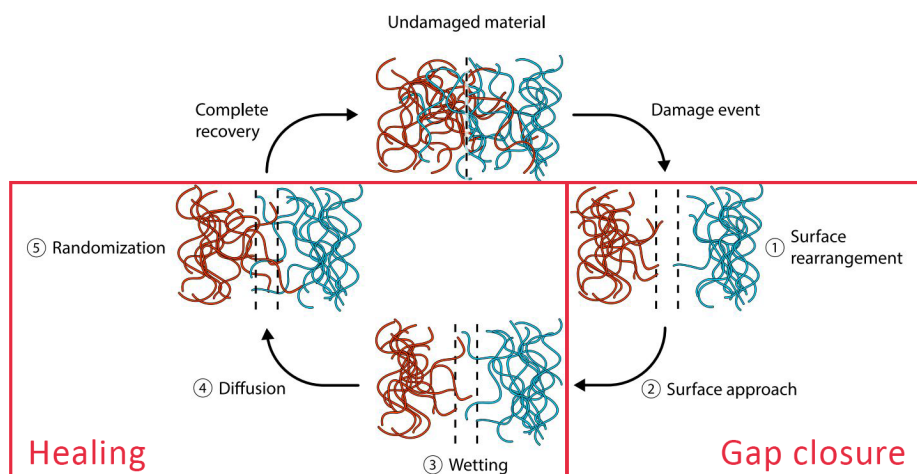
Figure 1.1: The five stages of intrinsic healing redefined for this work in the gap closure and healing stages, adapted from Susa (2019) [5].

<div align="center">

1

</div>

Most research on intrinsic self-healing polymers is focused on the healing stage and gap closure is often forced by applying pressure and/or heat. However, for truly self-healing polymers the gap closure stage should also take place autonomously. In order to develop polymers that possess good gap closure properties, this property has to be made measurable and quantifiable. This is an important step towards truly autonomous self-healing polymers. In order to understand what is happening, one route is to understand what kind of dynamics take place during the whole process depicted in Figure 1.1, and how these influence gap closure. The subject of measuring gap closure dynamics will be discussed in the next section and the emerging research gap relevant for this thesis will be concluding the chapter.

1.1. Background

Every chemical process is governed by reaction kinetics and thermodynamics, there is no difference for self-healing polymeric materials [6]. As mentioned before, the intrinsic self-healing process should proceed without any active interference from outside the system for it to be truly autonomous. In terms of self-healing dynamics this means that any energy required for polymer chains to move (i.e., gap closure) and for healing reactions should come from somewhere. During the damage-making process, energy can be stored by the material known as entropic energy storage [7]. The release of this energy can be used to close the gap. This phenomenon is best known and visible in shape memory materials and a measuring protocol has been developed to quantify entropy storage and release for these materials [8].

Using Dynamic Mechanical Analysis (DMA), a change in length can be measured and converted into entropy storage and release. This protocol and its use will be explained below. Another method to measure polymer dynamics is with Laser Speckle Imaging (LSI), where local dynamics can be traced over time in a spatial manner. Both techniques are advantageous in different ways and their use to measure and quantify self-healing polymer dynamics will be explained in the following subsections.

Before elaborating on these two protocols, another definition important for this work has to be discussed, namely bulk material and especially the difference between a coating and bulk material. Coatings are attached to a substrate and their mobility is thus limited. Thickness plays a role as well, since most coatings are applied as thin as possible in order to have the right properties while minimizing weight and material. Bulk material properties may differ from coating properties because of these circumstances. In case of gap closure properties, the amount of surrounding material could be of great influence on the behavior. Therefore, when investigating polymers these differences should be taken into account. DMA is a bulk material technique since it requires free standing films for investigation, while LSI can measure coatings as well, and thus a translation from the one technique to the other is very useful and an important contribution of this thesis.
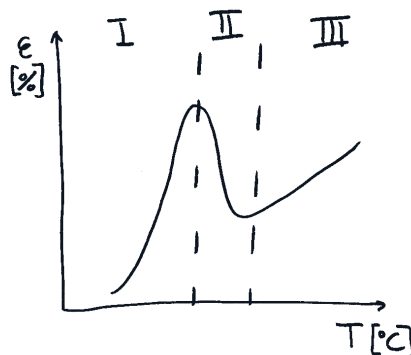
Figure 1.2: DMA result as strain vs temperature. [I] viscoelastic length extension, [II] entropy driven retraction and [III] further extension [9].

1.1.1. Dynamic Mechanical Analysis

DMA is used to measure the viscoelastic behavior of polymers by applying a strain and measuring the stress or vice versa. A protocol has been developed where dynamic and static modes are combined in a strain-controlled thermal ramp DMA experiment [8]. An oscillating force is applied on top of a static force to keep the sample in the elastic regime. The amplitude is kept constant and the overall length change is measured, as illustrated schematically in Figure 1.2.

Entropy change can be calculated with the values extracted from DMA experiments. For this, length change will be converted into entropy change. These results present a bulk material property and can be used for comparison with a coating as illustrated in Figure 1.3. Here gap closure ($\delta_{closure}$) of a coating is compared to entropy release (ΔS_R), measured as bulk property for the same polyurethane with different soft phase fractions (X_{SF}). Previous work has shown a linear relation between the two properties for the same polymer applied as free standing film (ΔS_R on the x-axis) and coating on steel ($\delta_{closure}$ on the y-axis) as depicted in Figure 1.3d [9].
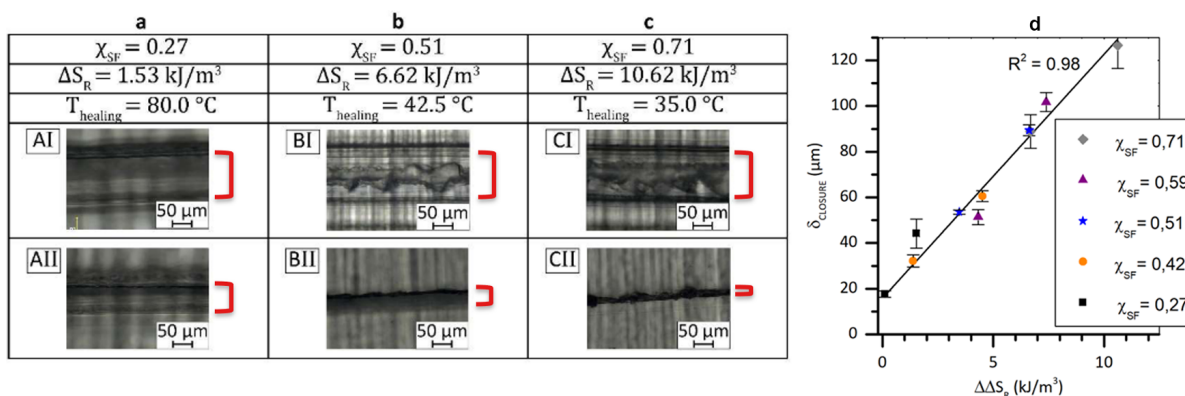
Figure 1.3: a,b,c) Comparison of three polyurethanes with different soft phase fraction (X_{SF}) where entropy release (ΔS_R) and scratch width after healing are compared. d) plot of the linear relationship obtained between gap closure and entropy release [9].

More entropic energy release shows more gap closure, which is an interesting property for self-healing coatings as discussed before. In order to understand the underlying principles it is necessary to investigate what happens during that gap closure phase. So an in-situ spatial and temporal technique is necessary to follow the process while it is happening. LSI could be such a technique, its relevance and working principle will be explained in the next section.

1.1.2. Laser Speckle Imaging

LSI is a measurement technique comparable to other optical techniques, like for example Digital Image Correlation (DIC) [10]. Here, a speckle pattern is painted on the surface of the area of interest, this pattern is recorded during the experiment, and by following the speckles the motion can be tracked very carefully.

With LSI the pattern is not physically presented on the to-be-investigated object but it is the effect of laser light that is reflected by a turbid material. Since laser light is monochromatic, has a coherent light beam and a single wavelength, the wavelets will be in phase when they enter the (turbid) material. These in-phase wavelets are illustrated in Figure 1.4 by comparing laser to LED and natural (sun) light. After these coherent wavelets have entered the material they will encounter scattering centers and proceed on a 'random walk' until they leave the material [11]. Because of the 'random walk' that is different for every single wavelet the returning wavelets will no longer be in phase. These phase differences result in local maxima and minima observable as a speckle pattern. When scattering centers will move (due to polymer dynamics for example) the resulting pattern will displace as well, following the motion of the material.

By taking many pictures of this changing pattern and comparing them with each other, you obtain the method that is called LSI. As shown in previous research a lot is possible with LSI, like following phase transitions in drying of paint [13], morphing of liquid crystals [14] or self-healing dynamics [15]. This
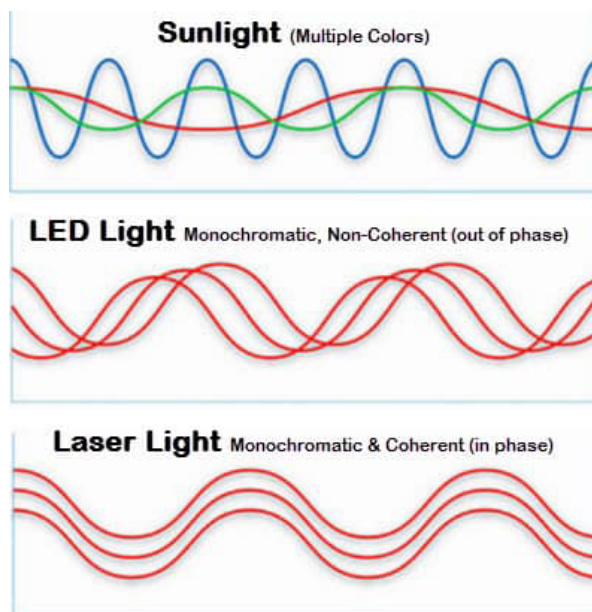
Figure 1.4: Schematic representation of laser waves in comparison to natural white light (sunlight) and led light [12].

looks promising for the development of a testing method to measure entropy storage and understand better what is happening during relaxation of materials by probing polymer dynamics.

1.2. Research Objectives and Thesis Layout
The research gap emerging from literature can be defined as the lack of a method that can be used to quantify entropy storage and release during damage making and subsequently gap closure of polymer coatings. LSI has been proven suitable to probe polymer dynamics during different processes, and thus is the main subject for this work. The aim of this work will be to establish a link between temperature-dependent material behavior measured with DMA and relaxation dynamics measured with LSI. The establishment of such link will aid as a step towards the ultimate aim of being able to fully quantify gap closure behavior of polymer coatings.

The research question has been formulated as follows: *How can temperature-dependent material behavior measured by DMA be linked to polymer dynamics measured with LSI?* In order to answer this question multiple research objectives will be addressed:

- Assess whether it is possible to measure polymer dynamics with LSI during a thermal ramp and relate them to material properties obtained with DMA.

- Assess the possibilities regarding measuring polymer dynamics with LSI that are relatable to length change, used for entropy calculations, measured with DMA.

- Assess the relation between stress relaxation and local strain relaxation by comparing LSI and micro tensile tester results.

- Review the obtained results by comparing LSI and DMA results.

This thesis is written in order to provide the reader with a clear and structured overview. First the material choice is substantiated and the synthesis procedures are described in Chapter 2. In Chapter 3, methods used for this thesis are examined and explained. The test results obtained are presented in Chapter 4, and the interpretation of those results is discussed in Chapter 5. Finally, this work is concluded in Chapter 6.

2

Materials

In this chapter the choice of material will be substantiated in Section 2.1. The chemicals used and synthesize method are described in Section 2.2.

2.1. Polymer Choice and Structure

The techniques investigated in this study dictate certain requirements for the materials to use. For the LSI study it is important that the material is turbid such that the laser light will be reflected and a speckle pattern is created. In order to investigate entropy storage and release, DMA experiments are necessary and therefore the samples should be of a certain stiffness. If the sample becomes too soft it will collapse under its own weight. Since polymer dynamics around the *glass transition temperature* (T_g) are the subject of interest, the material should have the T_g range in the measurable range. This range lies above room temperature, and due to LSI set-up limitations below 120°C. Lastly it is important that the thermal stability of the material is good (not more than 1wt% weight loss) in the temperature range of interest. Finally, it is important to synthesize the samples in order to have control over the components and if deemed necessary make subtle changes for result comparison.

The polymers selected for this research were expected to be suitable for DMA and LSI tests in the facilities used, both are epoxy networks that are synthesized by reacting a resin and a hardener. For this research stage it is not necessary to work with the self-healing ability of the polymer, since storage and release of conformational entropic energy within viscoelastic polymers is the subject of interest. This, in other research defined as shape memory behavior, is a feature many polymers possess, not reserved to self-healing polymers [16]. By removing the self-healing component it is easier to look at gap closure dynamics separated from other processes. Therefore it has been decided to work with epoxy networks only consisting of two components that react together. Junction points in the epoxies provide rigidity resulting in conformational entropy changes during displacements of the samples.

One epoxy is based on an epoxy network thoroughly investigated previously by the NovAM research group and a common base composition for aircraft coatings, chosen because of the available knowledge on the synthesis procedure and its characteristics. For this study a non self-healing variant is used based on previous work [17]. The other epoxy network is based on an epoxy that has shown good entropy storage and release behavior in previous research [18].

The use of two chemistries whose composition can be controlled up to a certain degree provides the possibility to create two polymers with different junction density and T_g. This is useful to compare and interpret DMA and LSI data and validate the testing protocol here introduced.

2.2. Polymer Synthesis

The amine group of the hardener will react with the epoxy group of the resin in multiple additions to form the polymer network, resulting in a thermosetting polymer. This process is illustrated and explained in Figure 2.1.

Reaction (A):

Reaction (B):

Reaction (C):

Figure 2.1: Reactions of the resin and hardener. Reaction A shows the first reaction between amine (blue) and epoxide (yellow), ideally Reaction B occurs next, forming the epoxy junction point (green). The hydroxyl group (pink) formed could also react with the epoxide forming an unwanted addition product, depicted in Reaction C. [19].

The resin used for both epoxies is Epikote828 and was provided by AkzoNobel. The hardeners used are Ancamine2500, provided by AkzoNobel, and JeffamineD-230, purchased from Sigma-Aldrich (Poly(propylene glycol) bis(2-aminopropyl ether)). Since Epikote828 and Ancamine2500 are commercial products not all components are known, but the known parts are depicted in Figure 2.2 and their reactive groups are indicated in blue for the amines and yellow for the epoxides, similar as in Figure 2.1. The knowledge of these products is originated from the work of M. Abdolahzadeh [17]. All the reagents were used as received without further purification.

Figure 2.2: The three known monomers used for synthesis with their reactive groups indicated in blue (amine) and yellow (epoxide). Since Epikote828 and Ancamine2500 are commercial products not all components are known, but the known parts are depicted in this figure.

Titaniumdioxide (TiO_2) nanoparticles of 21nm particle size, purchased from Sigma-Aldrich, were used to make the samples suitable for LSI analysis (turbid instead of transparent), by adding only 0.5wt% of the total weight of the other components. Epoxy networks were synthesized by reacting Epikote828 and Ancamine2500 or JeffamineD-230, the gram equivalent and corresponding weight ratios are depicted in Table 2.1.

The synthesis procedure followed is based on previous work carried out at the NovAM group with similar epoxies [17][20] and information obtained from the work of M. Urban [21]. For the remainder of this report the samples prepared will be named based on the hardener that is used, sometimes in combination with their batch number. For the two variations two batches are produced so they are

Table 2.1: Components used for epoxy network synthesis.

Component	Reactive groups [g/eq]	Weight ratio
Epikote 828	188	1
Ancamine 2500	135	0,72
Jeffamine D-230	124	0,66
TiO2 nanoparticles	-	0,005 (of total weight)

named: Anc_B1, Anc_B2, Jeff_B1 and Jeff_B2. If a number of the same tests is executed using the same batch a test number is added to indicate which sample is used and which test number it is, e.g. Anc_B1-1.

Synthesis Procedure EpiAnc Samples
First, in order to decrease viscosity, approximately the right amount of resin (Epikote) is put in the oven at 80°C for 15 minutes. The resin is added to the weighted TiO_2 nanoparticles in a jar suitable for a speedmixer and mixed for 30 seconds at 800rpm. Subsequently this mixture is put back in the oven (80°C) for 5 minutes and the hardener(Ancamine) is added for the last 2 minutes in a separate cup, to drop viscosity. After this, the jars are degassed for 5 minutes in the oven, reducing air bubbles. Thereafter, the right amount of hardener is added to the resin nanoparticle mixture and everything is put in the speedmixer to mix under vacuum for 3 minutes. The mixture is poured on a Teflon mould. The mould exists of a Teflon plate with five separate moulds as illustrated in Figure 2.3. After pouring, the mixture is spread out by hand carefully in order to fill the five moulds entirely. The samples are left to cure at room temperature for 24 hours, after which the samples are cut out in the desired sample geometries as illustrated in Figure 2.3 and put in the oven at 100°C for a 24 hour second step thermal cure. After the room temperature cure not all crosslinks are made and the samples are easier to cut than after the second step thermal cure, moreover the induced stresses from cutting will be removed during the second step thermal cure as a form of heat treatment because the samples are heated above their T_g. The latter also ensures the alignment of samples in the moulds with respect to each other does not matter any more, the material characteristics are isotropic since stresses from processing and cutting are removed.
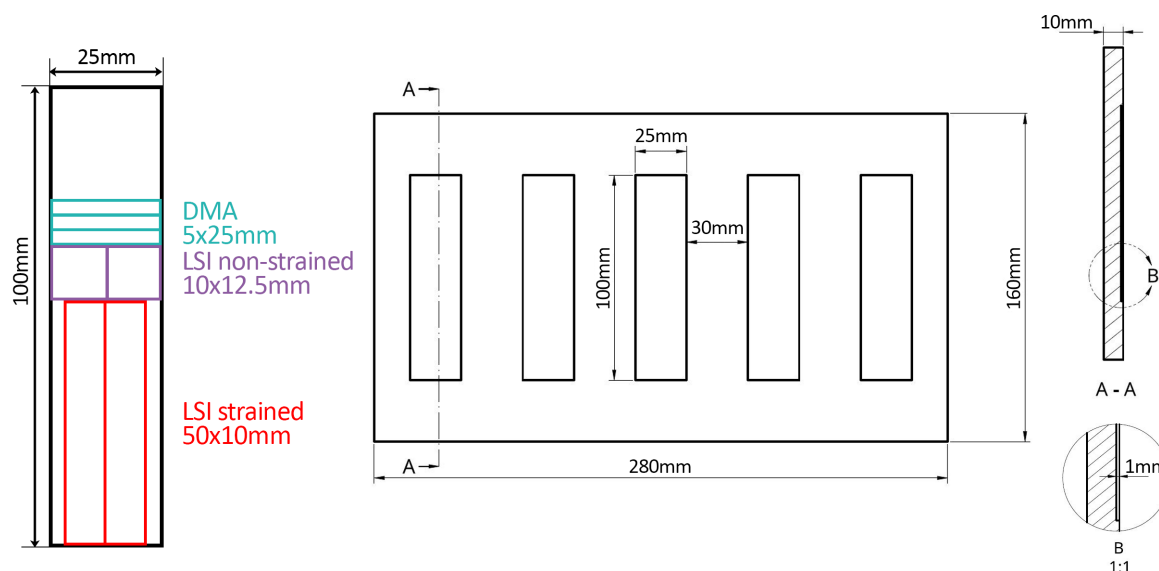

Figure 2.3: Geometry of the mould used for sample preparation, and the dimensions of the samples after cutting.

Synthesis Procedure EpiJeff Samples
The procedure is comparable to the above mentioned method where Ancamine is used instead of Jeffamine, but there are two important differences. The first is that Jeffamine is less viscous, so no

preheat is needed before adding it to the Epikote nanoparticle mixture. The other one is that the times and temperatures after the mixture is poured into the Teflon mould are different. The samples are left to cure at room temperature for 10 minutes, after which the mould is put in the oven at 80°C overnight. Next the desired sample geometries are cut out and put in the oven at 180°C for a 2 hour second step thermal cure.

Expected Material Characteristics

After synthesis networks are formed resulting in stiff and turbid samples. Taking into account the polymer structure certain material characteristics are expected. Epoxies belong to the group of thermosetting polymers that cannot melt, but have a T_g range. Thermosets are amorphous solids and therefore isotropic, the disorder of chain configuration ensures material characteristics to be the same in all directions. Their flexibility is dependent, among other things, on the crosslinking density; more junction points results in a stiffer less deformable material [22].

As illustrated in Figure 2.2 an important difference between the amines used is their length. For Ancamine 2500 only the known monomer is depicted, but more non disclosed monomers are present in the mixture. This monomer is shorter than the Jeffamine D-230, which has a repetitive unit leading to a longer chain. Longer chains result in more flexibility and thus a lower T_g range. Since the Ancamine 2500 mixture consists of several monomers it is expected that a more heterogeneous network will be formed, because it exists of more components. Heterogeneity will lead to a network with locally different T_gs that broaden the overall T_g range measured. The well defined Jeffamine D-230 epoxy is expected to show a narrower T_g range, because of a more homogeneous network.

Intermolecular interactions influence T_g range temperatures for both epoxies, stronger bonds between chains increase the energy needed for displacement and thus a higher T_g range is expected [22]. Van der Waals interactions and hydrogen bonds between chains in the cured epoxy network could increase the T_g range. The presence of OH-groups could result in hydrogen bonds between chains, but this effect is expected to be similar for both epoxy variations since stoichiometric mixed epoxies result in the same number of OH-groups present.

<div align="right">

3

</div>

Methods

In this chapter a closer look will be taken at the methods used. In Section 3.1 two thermal characterization methods are described that aid in the characterization of the thermal behavior of the polymers produced. Next, in Section 3.2, the DMA procedure to measure entropic energy is explained. Lastly, in Section 3.3, the LSI set-up, working principle, data analysis and used set-ups for this thesis work are presented.

3.1. Thermal Characterization

Since the focus of this research lies on temperature dependent material behavior, it is important to know the thermal characteristics of the samples made. Polymers could go through all kinds of thermal transitions and epoxies may face a post-curing phase if heated to certain temperatures for a considerable amount of time. This behavior is important to test and will aid in better understanding the dynamic behavior of the synthesized epoxies. The two methods used are described here.

3.1.1. Thermal Gravimetric Analysis

By measuring the weight during heating the thermal stability of a material is measured. Test results could give unreliable data if the material degrades in the temperature range of interest (dictated by the DMA and LSI tests). With Thermal Gravimetric Analysis (TGA) this stability can be measured.

A PerkinElmer TGA 4000 was used for the analysis. Under nitrogen a 10°C/min heating rate is used until 500°C is reached, in order to fully degrade the material. The weight of the sample, approximately $1mg$ for all samples, is measured at the beginning of the heating ramp and taken as 100wt%. Data extracted from this experiment could look like the graph in Figure 3.1.
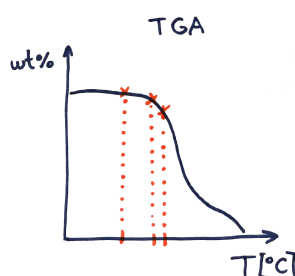
Figure 3.1: Schematic representation of a TGA measurement, with the weight percentage on the y-axis and the temperature on the x-axis. The 1wt%, 5wt% and 10wt% points are indicated in orange.

The 1wt%, 5wt% and 10wt% weight loss temperatures are important data points to extract from this experiment. They can be used for comparison between sample batches and to set the maximum test

temperature. The temperature during a test should stay below the 1wt% weight loss temperature in order to have reliable results, otherwise the material starts to degrade which influences the results.

3.1.2. Differential Scanning Calorimetry

With the Differential Scanning Calorimetry (DSC) technique thermal transitions can be measured, such as the glass transition temperature (T_g) or the melt temperature (T_m). A TA Instruments DSC250 differential scanning calorimeter was employed to study T_g, which will be used as characterization method and to compare different samples and batches. Samples of approximately $5 mg$ were used. The method consists of two heating ramps under nitrogen. The first ramp is used to erase the thermal history, by heating the samples above their T_g, and the second to measure the T_g range. The heating rate is 5°C/min from -30°C until 170°C. The result is a graph of heat flow (Q) versus temperature (T) and is illustrated in Figure 3.2, where the heat capacity of the material changes, visible as a step indicating the T_g range.

Figure 3.2: Schematic representation of a DSC measurement in the 'exo up' mode to get positive heat flow rates for exothermic processes. Here only part of the second second heating ramp is shown that contains the step with onset and endset points, which mark the T_g range, indicated in orange

The T_g range is defined as the range from onset until endset point, T_g for this work is defined as midpoint between onset and endset points. During this transition the dynamic behavior of the polymer changes and influences the measurements. Besides showing this influence, DSC is also used to compare the T_g range before and after LSI experiments in order to conclude if the T_g range has shifted. If the epoxy has cured further during the test (and therefore dissipating energy) than the T_g range would be expected to shift towards higher temperatures. A denser crosslinked epoxy needs more energy to be able to move (i.e., soften), and thus higher temperatures, before it goes through T_g.

3.2. Characterize Entropy Storage and Release with DMA

It is possible to measure entropy storage and release with DMA as mentioned in Section 1.1. The procedure developed measures the material response to temperature and a static and dynamic force by means of a length change. Polymers exhibit viscoelastic length transitions (VLTs) in the T_g range which are manifested by a length extension and retraction measurable with DMA [8][18][23][24][25].

3.2.1. Protocol Explained

The protocol developed imposes a strain, because of the temperature increase the polymer chains become more mobile and the materials softens so the dynamic force (maintaining 0,1% strain) will drop. The static force is linked to this dynamic force so it will drop as well. The static force, indicated in Figure 3.3A in blue, ensures the dynamics force (F_d in red) is maintained in the material's tensile region.

The induced strain at lower temperatures stores energy during elongation by decreasing the conformational entropy of the network. During elongation the polymer chains are being ordered (stretched) because the viscous network component enables some flexibility, this is only possible until a certain degree of displacement due to crosslinks as illustrated in Figure 3.3B. This elongation is possible because upon entering the T_g range, stiffness decreases as kinetic energy and free volume increase so

the polymer exhibits more viscous character [8].

At some point during the temperature increase, elongation transforms into retraction because sufficient energy is available to the chains in order to increase the entropy of the system again. This increase of entropy is the energetic more favorable state of the polymer network. After the retraction phase elongation continues, which is attributed to rearrangements of the network under the constant applied static force. The whole process is depicted in Figure 3.3C. The point of maximum elongation is located before the maximum value of $\tan(\delta)$ but within the T_g range.
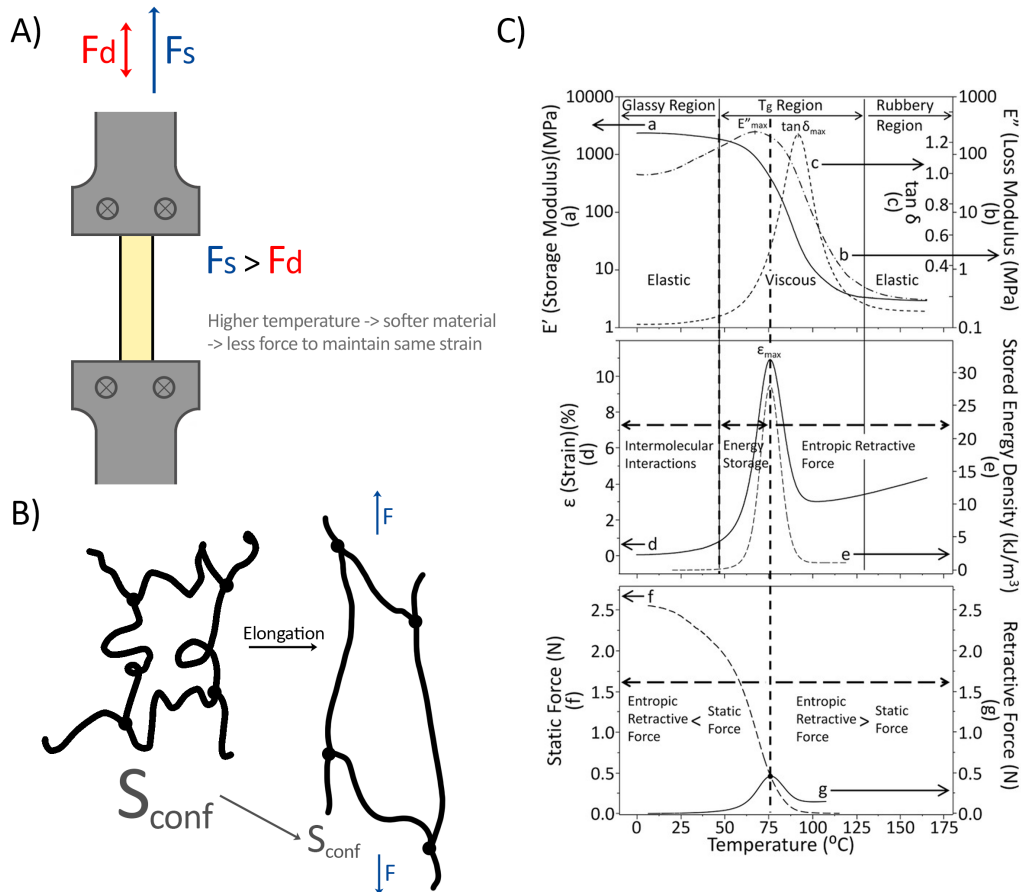

Figure 3.3: **A)** Illustration of a clamped sample (yellow) in the DMA tension geometry set-up (grey), dynamic force (F_d) and static force (F_s) are indicated in respectively red and blue. **B)** Schematic representation of crosslinked polymer chains before (left) and after (right) elongation that results in a decrease in conformational entropy, storing energy. **C)** DMA result divided over three graphs, a-c show the material characteristics obtained during a DMA strain-controlled temperature ramp, d and e depict the strain and obtained stored energy density in the second one and in the third graph, f and g, the applied static force (F_S) and generated retractive force are depicted. The three temperature dependant material ranges are indicated: glassy, T_g and rubbery region. Figure C) is obtained from Hornat(2017) [8].

These length changes can be quantified in terms of entropy storage and release following thermodynamics of molecular network and rubber elasticity theory [22][26][27]. These values have previously been related to VLTs induced shape memory behavior and gap closure [28][18].

3.2.2. Implementation at NovAM

For this study a strain controlled DMA of TA Instruments is used, the *G2-RSA Solids Analyzer*. Samples with dimensions between 4-6mm wide, 0,7-1,1mm thick and a length of approximately 20-25mm were clamped in a tension geometry set-up with a 10 mm loading gap, as depicted in Figure 3.3A. The experiment is executed in a forced convection oven under nitrogen to perform the heating ramp. The test procedure is set following 4 steps in the TRIOS software:

1. *End Of Test Conditions*: A temperature of 20°C is set.

2. *Conditioning Options*: Axial force adjustment is set and active mode is selected in tension. The force tracking mode is selected with a 125% Axial force > Dynamic force setting. Important is that in the advanced section priority is given to data sampling over force control.

3. *Conditioning Transducer*: The spring mode is selected as well as the override configuration. Before every test a transducer zeroing will take place selecting the low range, which makes sure the settings are suitable for the stiffness of the sample used.

4. *Oscillation Temperature Ramp*: A ramp rate of 2°C/min from room temperature (20°C) until 130°C is set. The test parameters are set to an amplitude of 0,1% strain ($10\mu m$) and a frequency of 10 Hz.

In the work of C. Hornat, effects of different settings on the results are evaluated [29], for this work the settings are adapted from previous research [8][9]. After the settings are selected, the exact sample geometry should be measured and the sample is clamped, results are obtained via the TRIOS software.

3.2.3. Data Analysis

The experimental data will provide for the necessary information to calculate entropy changes (ΔS). As derived in previous research from thermodynamics and rubber elasticity theory [30][31], decrease in entropy can be estimated as depicted in Equation 3.1 [9]. The protocol developed by the research group of M. Urban is based on coupling Equation 3.1 with Equation 3.2 as derived from classical thermodynamics, which results in Equation 3.3 [8][24]. In Equation 3.3 the maximum entropy storage is calculated by taking the values at maximum elongation (ϵ_{max}) and comparing them to the values obtained in the glassy regime (i, initial) of the polymer.

$$\Delta S = -\frac{\nu_j R}{2}[\alpha^2 + \frac{2}{\alpha} - 3] \qquad \text{,with } \nu_j = \frac{\rho}{M_j} \tag{3.1}$$

$$\Delta S_S = -T_{\epsilon I} S_{\epsilon I} + T_i S_i \tag{3.2}$$

$$\Delta S_S^{max} = \frac{R\nu_j T_{\epsilon_{max}}}{2}(\alpha_{max}^2 + \frac{2}{\alpha_{max}} - 3) - \frac{R\nu_j T_i}{2}(\alpha_i^2 + \frac{2}{\alpha_i} - 3) \tag{3.3}$$

Where α is the extension ratio L/L_0, α_{max} is L_{max}/L_{glass}, α_i is $L_{glass}/L_{glass} = 1$, M_j is the molecular weight between crosslinks or entanglements, R is the gas constant and ρ is density. When calculating entropy release (ΔS_R), Equation 3.2 is used, where ϵI is ϵ_{min} and i is ϵ_{max}, to rewrite Equation 3.3. The result of this modification is depicted in Equation 3.4.

$$\Delta S_R^{max} = \frac{R\nu_j T_{\epsilon_{min}}}{2}(\alpha_{min}^2 + \frac{2}{\alpha_{min}} - 3) - \frac{R\nu_j T_{\epsilon_{max}}}{2}(\alpha_{\epsilon_{max}}^2 + \frac{2}{\alpha_{\epsilon_{max}}} - 3) \tag{3.4}$$

As can be seen in Equation 3.1 some crosslinks or entanglements (junction points) are necessary in order to store entropic energy. If there are no entanglements or crosslinks the molecular weight between entanglements can assumed to be: infinity $M_j \to \infty$ resulting in a ΔS of zero or $M_j = 0$ resulting in a non valid fracture.

Estimation Procedure ν_j and M_j

In order to use Equations 3.3 and 3.4, a value for ν_j is necessary, and the resulting M_j value is useful to compare the epoxies made. The value for M_j can be calculated in different ways, one is based on estimating values for ρ and ν_j ($M_j = \rho/\nu_j$). The density is obtained by measuring several sample geometries and their weight, all resulting in approximately $1.1 g/cm^3$. In order to estimate ν_j the value for stress at maximum elongation ($\sigma_{SF.at.\epsilon_{max}}$) is assumed to be equal to the resulting retractive stress (σ_R) [9]. Here $\sigma_{SF.at.\epsilon_{max}}$ is the stress measured at maximum elongation, σ_R is calculated following Equation 3.5 where ν_j is varied until Equation 3.6 holds.

$$\sigma_R = \nu_j R T_{max} \frac{\alpha_{max} - 1}{\alpha_{max}^2} \tag{3.5}$$

$$\sigma_R = \frac{F_R}{A} = \sigma_{SF.at.\epsilon_{max}} \tag{3.6}$$

The junction density and molecular weight between crosslinks obtained following this procedure will be called $M_jest.$ and $\nu_jest.$ for the remainder of this report. In Chapter 4, a comparison will be made with other methods to obtain these values and explanation will be given regarding the obtained results. It is expected that the Jeff chemistry is the network with a lower crosslinking density and thus more flexibility, because of the longer amine chains, leading to better entropic energy storage and release.

3.3. Laser Speckle Imaging

LSI is a non-invasive optical measurement technique to probe (near) surface dynamics in the mm range. Its working principle, set-up at NovAM, data analysis possibilities and proposed protocols will be discussed in this section.

3.3.1. Working Principle

As discussed in Section 1.1 the interference pattern of reflected laser light is used to probe dynamics taking place in the sample. During the measurement frames are shot of the changing speckle pattern. The principle is shown graphically in Figure 3.4 for probing the dynamics of a self-healing coating [15]. A sample is prepared and placed under a laser beam in step one, two and three. Step four shows the frame collection over a period of time. These frames depict the speckle pattern. The fifth step is the LSI analysis to extract how much those speckles have moved. By comparing the raw speckle pattern frames taken over time (t) for a certain frequency (τ), a micromechanical map can be created that shows the amount of displacement depicted as the d_2-number.
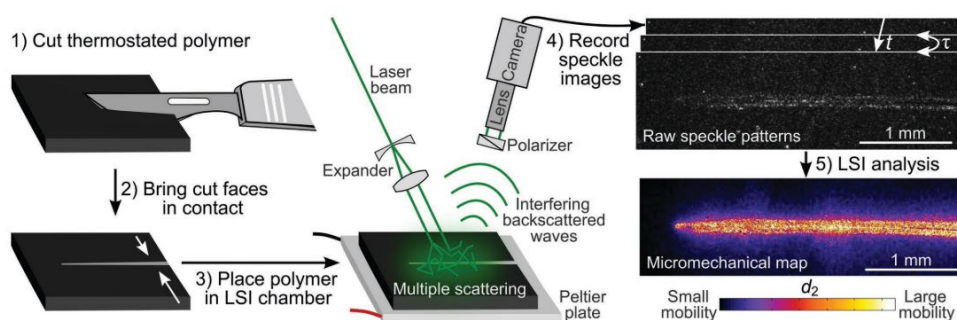

Figure 3.4: Illustration of the LSI working principle as depicted by van der Kooij et al. [15].

3.3.2. Set-up at NovAM

The LSI set-up is shown in Figure 3.5, the laser path and main components are highlighted:

- A: Camera

- B: Objective

- C: Polarizer

- D: Beam expander

- E: Laser light source

The camera has a Charge-Coupled Device (CCD) of 8 bits, which is 480x680 pixels with a physical pixel size of 9,9μm. The camera has a frame rate of 60fps and is connected to the objective. This objective is used to first focus the sample at a certain size regulated by the zoom, after which the diaphragm is used to control the speckle size. Before the light enters the objective a polarizer reduces the specularly reflected light component. The beam expander regulates the spot size of light that illuminates the sample. The laser light source produces a blue laser beam with a wavelength of 473nm.
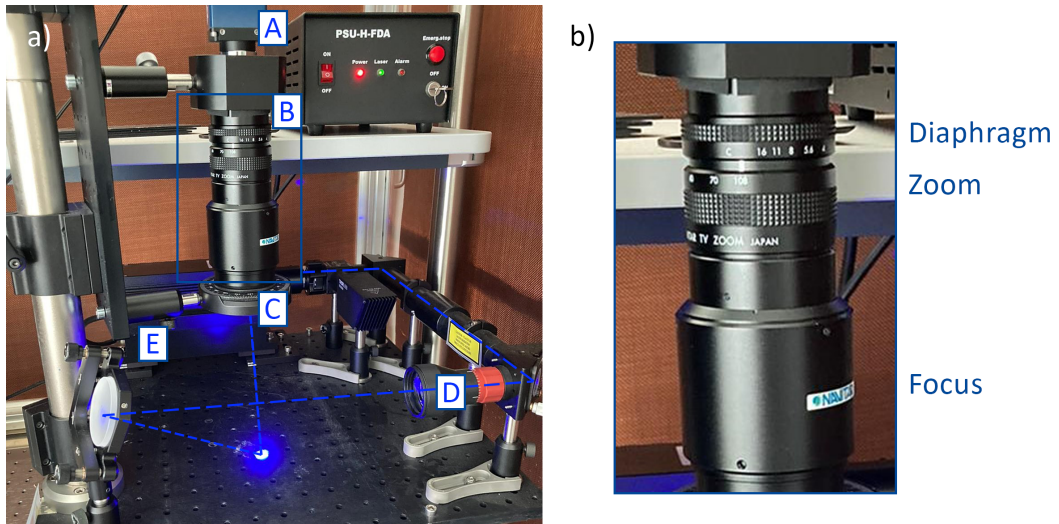
Figure 3.5: NovAM LSI set-up where a) shows an overview and the dotted line illustrates the laser path and b) shows the components of the objective.

3.3.3. Data Analysis

Three software packages developed in Wageningen were used to extract information from the LSI measurements [32]. *LSI_Speckle_Size_Analysis* defines the speckle size of speckles in a certain frame, *LSI_2D_d2* is used to extract coloured spatial maps for a certain τ and thus check the spatial homogeneity, *LSI_g2_d2* is used to calculate the averaged g_2 and d_2 (Equation 3.7) values for a defined frequency range and thus provide insight in the development of dynamics over time.

Each series of measurements results in many frames that individually do not show anything, as can be seen in Figure 3.6, where a single LSI frame is shown. Grey and white speckles are visible, but the relation to the other frames is needed in order to produce useful results. First the speckle size has to be checked, because the size of each speckle is of influence on the result. If a speckle is smaller than a pixel, then the pixel will show an averaged value of the speckles it covers. On the other hand, if every speckle consists of many pixels less information can be extracted from the frames. A speckle size of 2-3 pixels has been established as desirable [33] [34] [35].
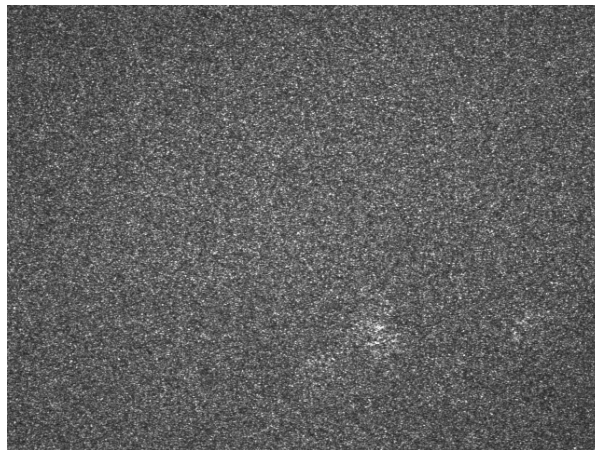

Figure 3.6: Frame taken in a LSI experiment, shown is the speckle pattern as recorded.

The second step is to check if the displacements occur homogeneously over the whole area measured. This is done by calculating the Intensity Structure Function d_2 represented in Equation 3.7 [36].

$$d_2 = \frac{\langle (I(t) - I(t+\tau))^2 \rangle >}{\langle < I(t) \rangle \cdot \langle I(t+\tau) \rangle}$$

(3.7)

The grey value or intensity of a pixel at a certain time $I(t)$ is compared to the intensity of the same pixel some time later $I(t + \tau)$. If the intensity has changed noticeably the d_2 value will be high and if not it will have a lower d_2 value. Plotting these values on their place in the picture (x, y) yields a coloured picture as illustrated by Figure 3.7. The autocorrelation functions $g_2(t, \tau)$ and $d_2(t, \tau)$ can be calculated by taking the averaged intensity fluctuations over a whole indicated Region Of Interest (ROI). If the data is not homogeneous in that area, for example in Figure 3.4 where a cut is made and dynamics are different according to their position, close or further away from the cut. If that is the case the result will average all the displacements occurring and the resulting averaged d_2 values are not reliable. First the homogeneity of a ROI should be checked, if necessary the ROI should be adjusted, before extracting the averaged d_2 values.
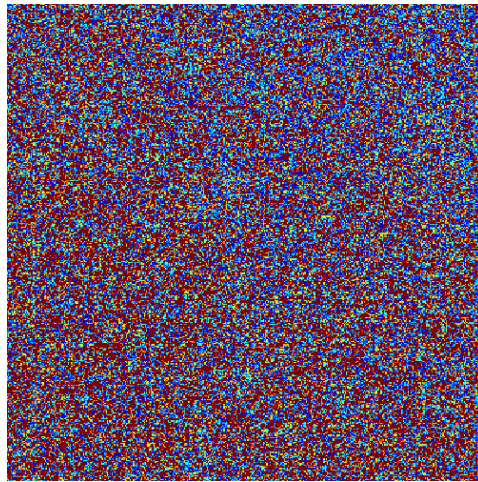
Figure 3.7: Frame taken in a LSI experiment and analysed using the *LSI_2D_d2* software. Red pixels represent more displacement than the blue ones. This picture shows data homogeneous over the whole area.

The Intensity Autocorrelation Functions $g_2(t, \tau)$ and Intensity Structure Function $d_2(t, \tau)$ are used to extract d_2 values over a time and frequency range, resulting in 3D plots where d_2 values are shown versus (t) and (τ).
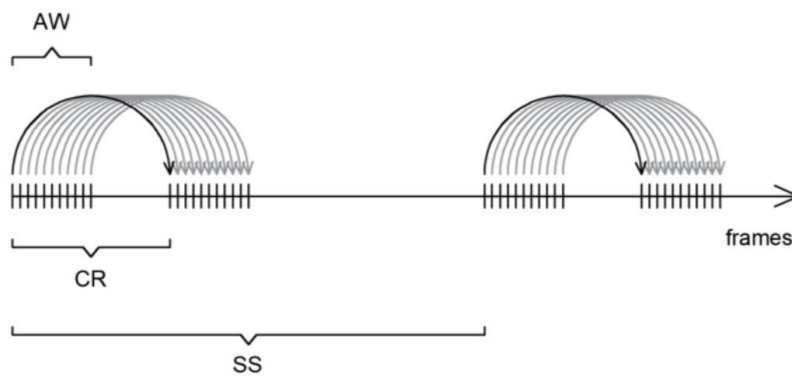

Figure 3.8: Graphic representation of data analysis of LSI frames, where AW is the averaging window, CR the correlation range and SS the step size [37].

The method to extract these data is illustrated schematically in Figure 3.8. An average is taken over a group of frames in order to filter out single frame artifacts. Each frame of the group will be correlated with a frame a certain number of frames further in time, defined by the correlation range (CR), which can be related to the frequency as $\tau = CR/framerate$. A small CR will show high frequency dynamics while a large CR depicts slower dynamics. Since the change between frames is measured as an intensity number, more change will result in a higher intensity number (higher d_2 value). This process is repeated to obtain the development of the dynamics over time by looking at frames every number

of frames, the step size (SS). A smaller step size will give you more data points but may enlarge the computing time.

By comparing the same dataset over a range of τ's, a frequency sweep is conducted. By comparing the speckle displacement for different frequencies the presence of both fast and slow dynamics can be investigated. Which can produce interesting information about the type of dynamics occurring, while the d_2 value provides information about the amount of displacement.

To illustrate this a colour map (Figure 3.9) and 3D plot (Figure 3.10) of the same dataset is created. The dataset is produced from a tensile test in LSI; after 120 seconds an epoxy sample was stretched for 30 seconds after which the elongation was kept constant so the sample relaxation was measured. The polymer dynamics measured during this test are shown in terms of type (τ), and amount of displacement (d_2).
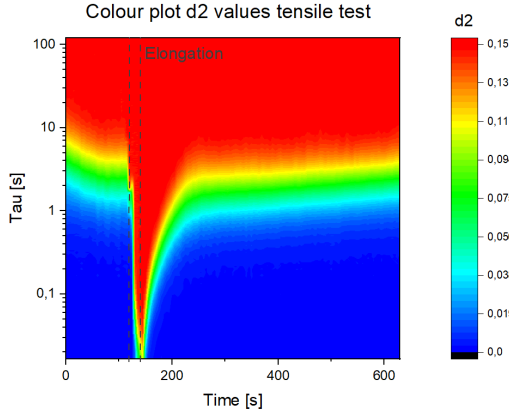
Figure 3.9: Colour plot of the d_2 values obtained from a tensile test on an epoxy sample.
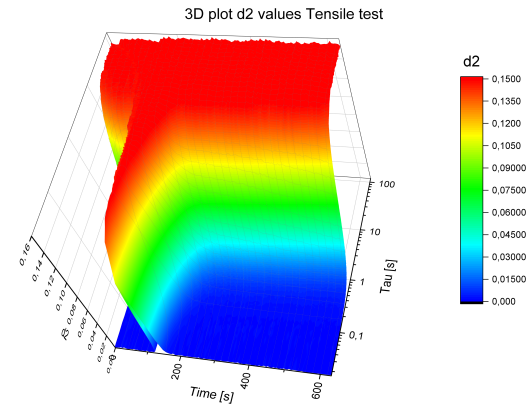
Figure 3.10: 3D plot of the same test as in Figure 3.9.

As can be seen, by the presence of the red colour (higher d_2 values) for higher τ's (from 10s upwards), there are some baseline dynamics occurring always, for a higher tau. Once the elongation starts, at 120 seconds, the d_2 value increases over the whole range of τ. At 150 seconds when the elongation stops but the distance is kept constant the d_2 values for the lowest τ's drop quickly, but the higher the τ the slower, in time, this drop occurs. Resulting in both fast and slow relaxation shown in these pictures.

3.3.4. Computation of the Local Relaxation Time

Furthermore, the autocorrelation function (g_2) can be fitted to extract the local relaxation time, τ_0, that belongs to certain moments in time. This fitting is based on the Siegert relation to calculate the normalized field autocorrelation function $g_1(t, \tau)$, depicted as Equation 3.8 [13]. Fitting those g_1 curves with Equation 3.9 provides the time evolution of the characteristic relaxation time τ_0 (stretching exponent α is not used in this research).

$$g_1(t, \tau) = \frac{1}{\sqrt{\beta}}\sqrt{g_2(t, \tau) - 1} \tag{3.8}$$

$$g_{1\text{-fit}}(t, \tau) = \exp[-\gamma[\tau/\tau_0(t)]^{\alpha(t)}] \tag{3.9}$$

Where β and γ are numerical constants that have been established in previous research [13][37] and are dependent on material properties and set-up configurations. The characteristic relaxation time depicted by $\tau_0(t)$, and $\alpha(t)$ is the stretching exponent. The characteristic relaxation time will be used to extract information on the material behavior and compare between different tests.

3.3.5. Non-strained and Strained Temperature Ramp Tests

The feasibility of the LSI protocol to measure local entropic induced displacements has to be investigated as stated in the research objectives in Section 1.2. Since the proven DMA method is based both

on a temperature ramp and dynamic material behavior, the tests for this research are based on these two aspects as well. First a temperature ramp similar to the ramp during the DMA test will be conducted on non-strained samples, and the material response in terms of dynamics measured by LSI will be analyzed. Secondly, a temperature ramp will be conducted on strained samples. A micro-tensile tester will elongate the samples, to an extent similar to the length change measured in DMA, after which the relaxation dynamics are measured for different temperatures.

Temperature Ramp with a Non-strained Sample

The set-up used for the non-strained temperature ramp is illustrated in Figure 3.11A, all the components are shown except the computer that collects the frames shot by the LSI camera. A hot stage is placed under the camera and used to heat the sample. A thermometer to measure the sample temperature at the begin and end of each test is shown. The measured values and fitted lines can be found in Appendix E. In Figure 3.11B the set-up is shown with the laser turned on and a box that covers the hot stage to reduce air flow.

The test procedure is schematically illustrated in Figure 3.11C. The heating rate set on the hot stage is one degree per minute faster in order to mimic the DMA heating ramp on the sample surface, some heat is lost because the heating does not take place in an oven. The test is executed twice for every batch of material made.
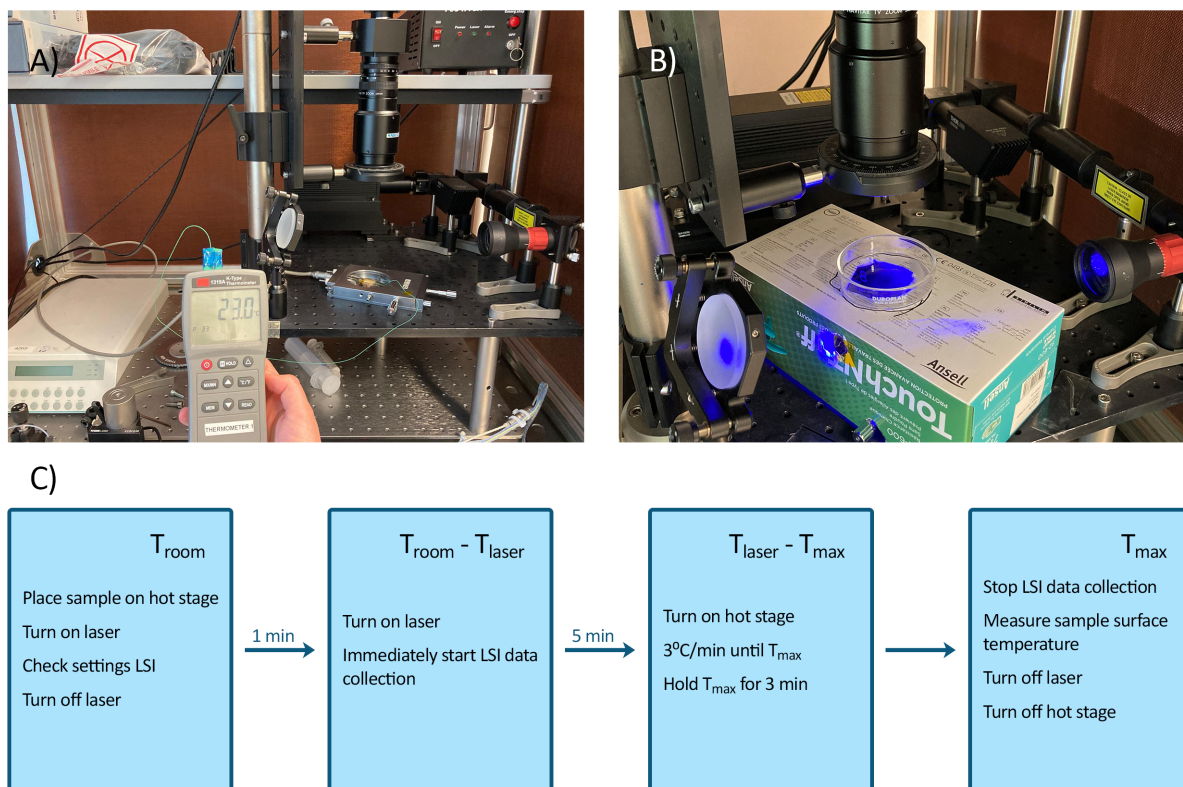
Figure 3.11: **A)** Test set-up for non-strained samples, the hot stage with sample is located under the camera, the thermometer is connected to the sample and indicates 23°C. **B)** The same set-up in a cardboard chamber to reduce airflow and hold the heat. Holes are present to not interrupt the laser-path and influence the signal. **C)** Schematic representation of the test procedure.

Temperature Ramp with a Strained Sample

The set-up used for strained sample temperature ramps is illustrated in Figure 3.12A and 3.12B. All components are shown except the computers connected to the LSI and to the micro-tensile tester.

The test procedure is depicted schematically in Figure 3.12C. The test is repeated for different temperatures in the DMA temperature range of the two epoxies of interest as illustrated in Figure 3.12D by the coloured crosses and circles.
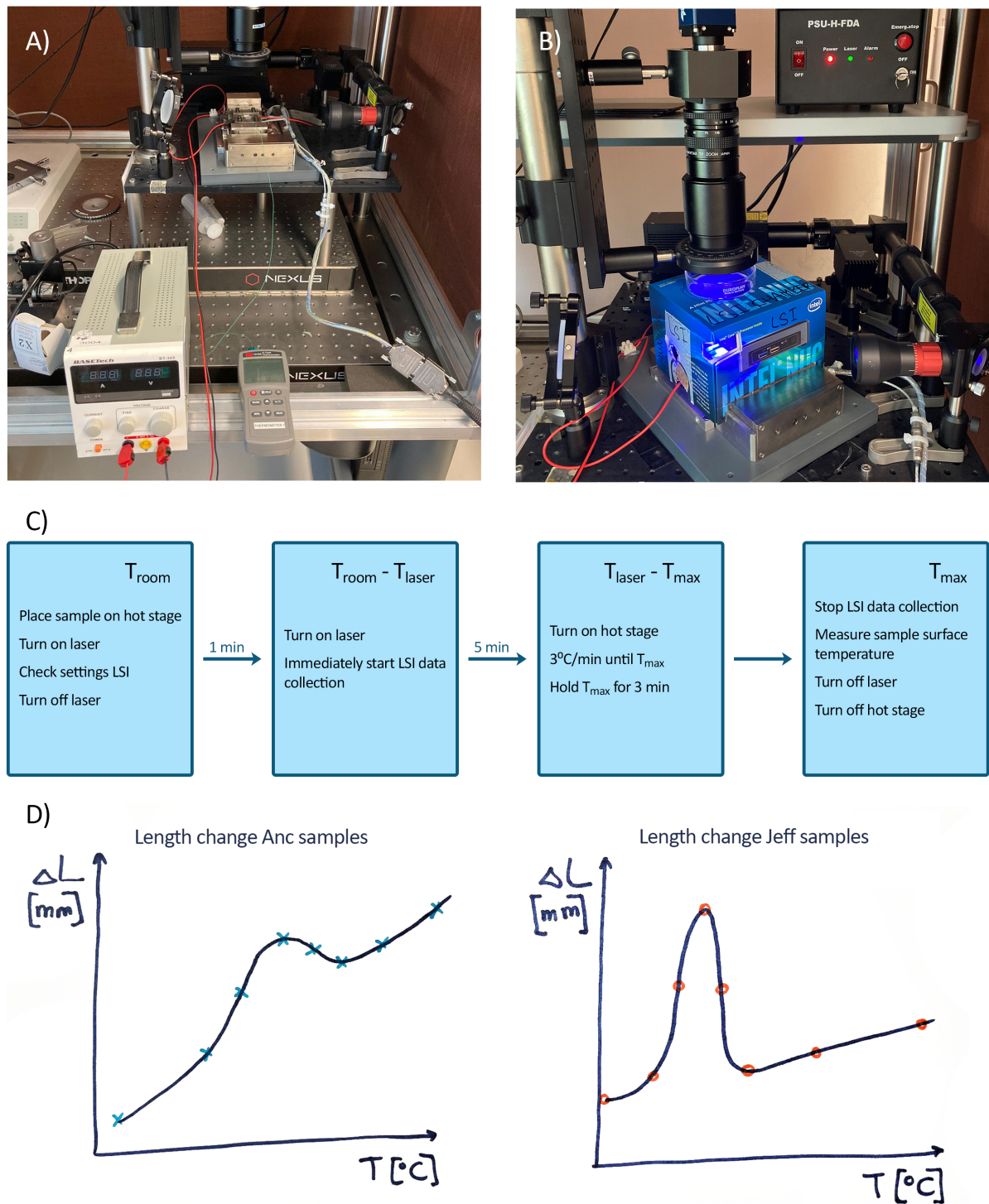
Figure 3.12: **A)** Test set-up for strained samples, micro-tensile tester, resistor heating device mounted on it, voltage control box and thermometer are depicted. **B)** The same set-up in a cardboard chamber to reduce airflow and hold the heat. Holes are present to not interrupt the laser-path and influence the signal. **C)** Schematic representation of the test procedure **D)** Indication of the LSI test temperature selection based on DMA results. Blue crosses indicate the temperatures for the Anc test and orange circles for the Jeff sample tests.

Micro-tensile Tester
The micro-tensile tester has two clamps connected to a screw thread so it can displace over one axis, elongating the clamped sample. The tensile tester can apply a maximum load of $5kN$ and a maximum displacement of $10mm$. The displacement speed has a range of $0.005 - 1.5mm/min$ with a speed control accuracy of better than 1%.

The software that comes with the device, *Microtest*, allows you to control the micro-tensile tester. Extension and force results are shown during testing. Before starting a test, sample details and elongation speed are set after which the force is set to approximately $0N$. The motor can be stopped and started again while data collection of the resulting force continues.

The micro-tensile tester used for this thesis is depicted in Figure 3.13A. The heat required for temperature ramp tests is generated with two resistors that are mounted between the clamps and just below the sample, as depicted in Figure 3.13B.
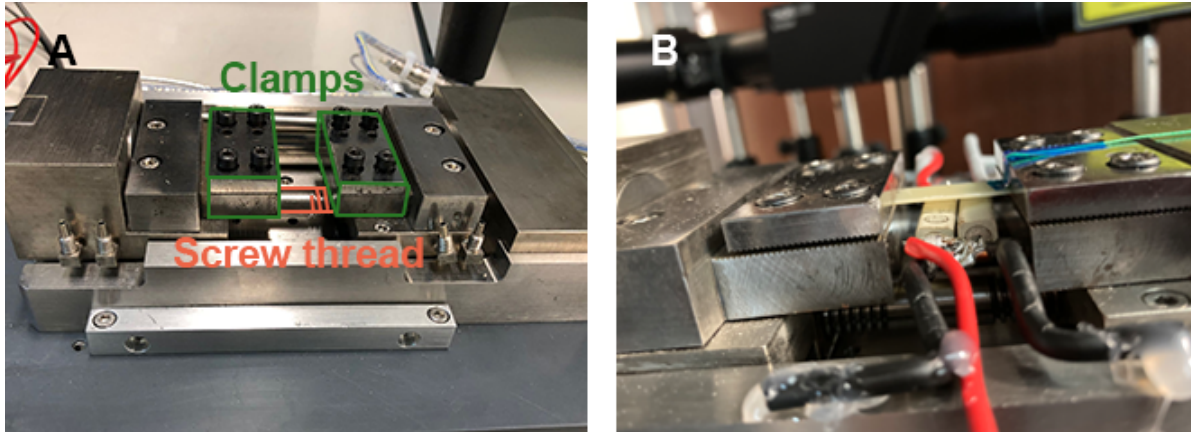
Figure 3.13: **A)** The micro-tensile tester used for this thesis. **B)** Clamped sample and mounted resistors for heating.

4

Results

In this chapter the results obtained during TGA, DSC, DMA, LSI and micro-tensile tests are provided in their respective sections.

4.1. Thermal Characterization Results

The graphs of all separate TGA and DSC measurements can be found in Appendix D.

TGA results are used to check if the maximum DMA and LSI test temperature of 120°C does not exceed the 1wt% weight loss temperature. In Figure 4.1 the averaged temperatures of 1wt%, 5wt% and 10wt% weight loss are depicted. The values are averaged over four measurements per material, two batches and two tests each. The error bars indicate the scatter between batches and tests.
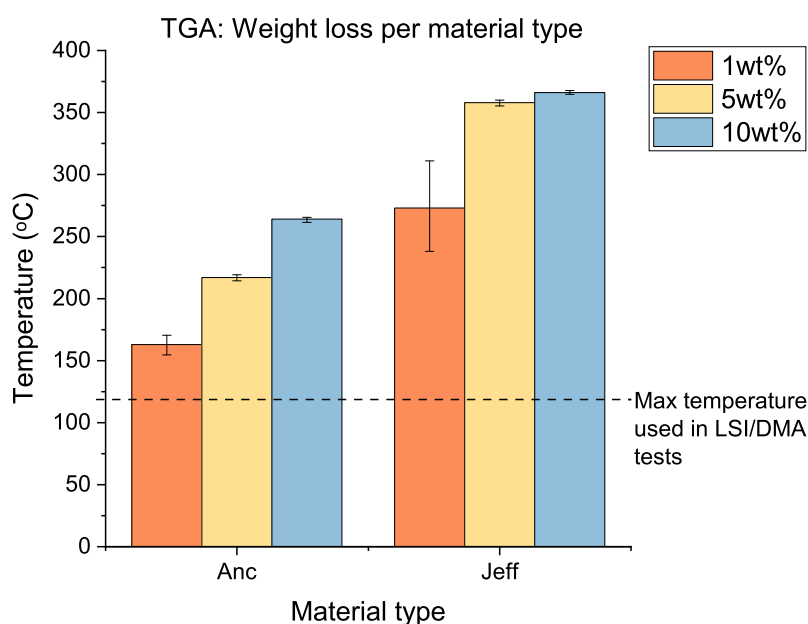
Figure 4.1: TGA results indicating the one, five and ten percent weight loss. The dotted line indicates the maximum test temperature, the 1% weight loss temperature should not come below this line.

The temperatures at which polymers start to lose weight can be linked to chemical reactions occurring at elevated temperatures. Polymer chains consisting of bonds that can resist these reactions until higher temperatures are considered to be temperature stable polymers. The Anc samples show degradation at temperatures approximately 100°C lower than the Jeff samples. This difference can be explained by the difference in crosslinking density, a lower crosslinking density gives the polymer

chains more freedom to move upon heating and create more free volume within the network. By expanding, energy can be dissipated, while denser crosslinked networks will show quicker chain scission at lower temperatures [38]. This results indicates that the Jeff network has a lower crosslinking density than the Anc network. The high temperatures at which 1wt% weight loss occurs also suggest that no byproducts like water are present in the polymer, since evaporation would result in weight loss as well.

Next, the results from DSC measurements are shown in Figure 4.2. The T_g range is defined by onset and endset points, determined by the *Onset Point* and *Endset Point* analysis executed by the *TA Instruments TRIOS Software*. Apart from a T_g range, T_g has also been defined as point with the *Half Height Midpoint Type* analysis. It can be seen that Anc has a broader T_g range, around 70°C, than Jeff, where the T_g range lies between 30°C and 40°C. The broader T_g range for Anc shows the influence of amine used on the dynamic behavior of the material. The error bars are the result of averaging the values over four tests per batch.
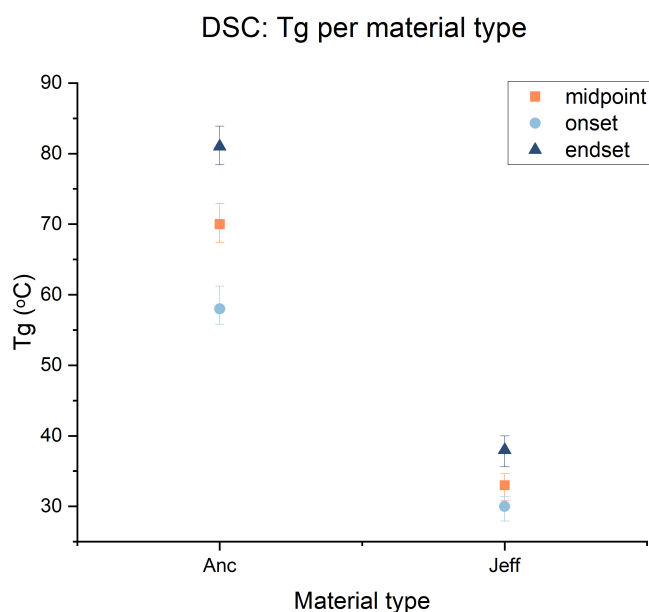
Figure 4.2: DSC results indicating T_g midpoint, onset and endset points.

T_g is influenced by thermal history, polymer chemistry and intramolecular interactions. The lower T_g range of Jeff samples suggests more chain flexibility and free volume resulting in less energy needed (lower temperatures) before the polymer softens. This gives another indication that Jeff samples are less crosslinked compared to the Anc samples. The broader T_g range of the Anc samples (30°C) can be attributed to the mixture of amines that is used to form the network, leading to more network heterogeneity and local variation in crosslinking density. Different parts in a heterogeneous network have their own temperature at which they become flexible resulting in a broader range of temperatures for which the overall polymer network softens. The amine used to form the Jeff network only consists of one type of monomer reducing the T_g range to a temperature span of only 10°C.

4.2. DMA Results

DMA experiments are used to calculate the ability of each material to store and release entropic energy, which is based on the length change measured under both static and dynamic loads. One example of the measured length change for each epoxy type is depicted in Figure 4.3. The ratio between the initial, maximum and minimum length change is used. The dotted red lines indicate the local maximum and minimum of the delta length curve. Each material type has been tested six times, three runs have been executed per material batch (12 tests total). A complete list of all DMA graphs produced can be found in Appendix B, all tests show similar results and therefore reproducibility.
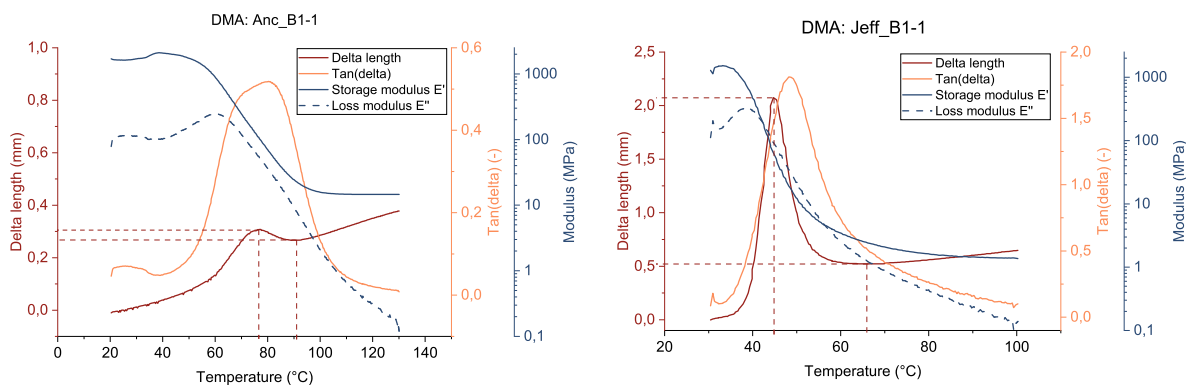
Figure 4.3: DMA temperature ramp data of the Anc_B1 (left) and Jeff_B1-1 (right) samples, where the blue lines depict the modulus data, orange line $\tan(\delta)$ and red the length change. The dotted red lines indicate the local maximum and minimum of the length change used for entropy calculations.

The DMA graphs show a few interesting material properties for both materials. Anc seems to have a double $\tan(\delta)$ peak but the absolute value is clearly lower than that of the Jeff sample (note the difference in axis range). The relation between $\tan(\delta)$ and the moduli is defined as $\tan(\delta) = E''/E'$, so when $\tan(\delta)$ is 1 the loss and storage modulus are equal to each other. When E'' exceeds E', the material is more viscous and $\tan(\delta)$ has a value greater than 1. The implication of this relation for the tested samples is visible in Figure 4.3, Jeff has a $\tan(\delta)$ exceeding 1 and shows more elongation as compared to Anc where $\tan(\delta)$ stays well below 1. Crosslinking density influences mobility of a material, which is reflected by the $\tan(\delta)$ and delta length curves. A $\tan(\delta)$ of lower than 1 is expected for polymers with a high crosslinking density, like the Anc samples.

When the temperature ranges of $\tan(\delta)$ peaks are compared to the obtained T_g ranges with DSC, both the second Anc and the single Jeff peak lay at temperatures slightly higher. Both $\tan(\delta)$ peaks of Anc are suggested to be the result of the various components present in *Ancamine D-230* broadening the T_g range. The maximum length extensions lay at a temperature before the $\tan(\delta)$ peak (the second peak in the case of the Anc sample), and slightly after the T_g range as measured by DSC, for both materials.

Entropy storage and release has been calculated, as explained in Section 3.2, the results are depicted in Figure 4.4. In orange entropy storage (ΔS_S) is shown and in blue entropy release (ΔS_R). In order to calculate ΔS_S the length increase from initial length until local maximum is used. For ΔS_R the decrease from local maximum until minimum is used. Both local maximum and minimum are highlighted in Figure 4.3 by red dotted lines. The error bars show variations between the different measurements per material type.
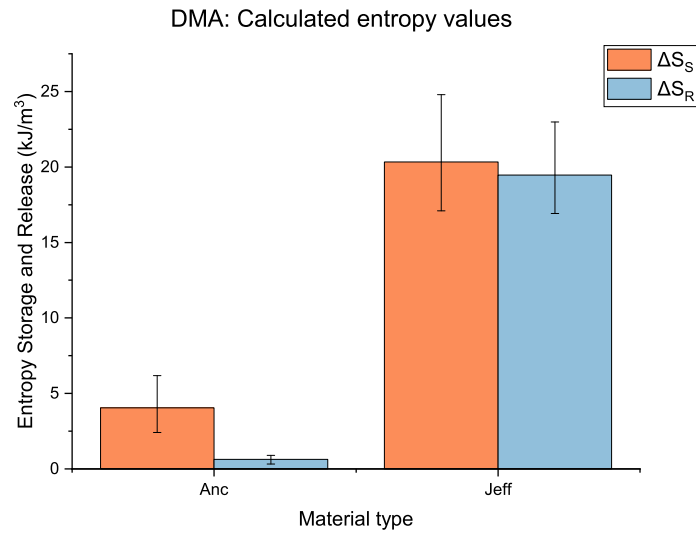
Figure 4.4: Calculated entropy values from DMA results. ΔS_S indicates entropy storage and ΔS_R indicates entropy release.

For the calculations an Excel spreadsheet is used that was developed in previous research [25]. A screenshot of this sheet containing all the calculated values for ΔS_S and ΔS_R can be found in Appendix A.

A comparison has been made for Anc and Jeff based on the ΔS_R values obtained in previous studies, depicted in Figure 4.5. The values in blue are results from other studies. The first four (E-1.05 - E-EDR) are obtained from a study done by C. Hornat (2020) that are synthesized with Jeffamine D-230, the same as used for this study [18]. The polyurethane samples depicted next (TS PUR and TP PUR), are polyurethanes that are mentioned in the article of C. Hornat (2017) where the DMA protocol to quantify entropy is explained. Lastly, the Montano samples have been used in a study where gap closure behavior has been related to entropy release [25], the adjacent number denotes the soft phase fraction in the polyurethane used. The line of $tan(\delta) = 0$ is highlighted by a dashed line.
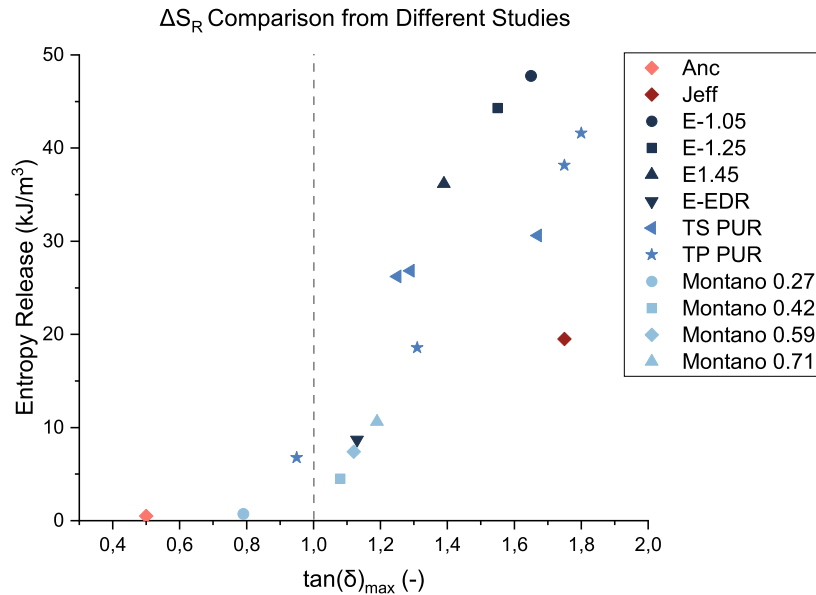
Figure 4.5: Entropy release values obtained from different studies for comparison. E-1.05, E-1.25, E-1.45 and E-EDR are comparable epoxies to Jeff [18], from [8] TS PUR (thermosetting polyurethane) and TP PUR (thermoplast) are obtained, the last four are TP PUR as well with varying soft phase fraction denoted by the adjacent number [25].

ΔS_R has been chosen for comparison since the amount of entropy release is the important parameter for gap closure. Storage is expected to take place during damage-making, displacing material around the gap, subsequently entropy release is responsible for gap closure [7]. A clear trend is visible where more entropy release can be coupled to higher $tan(\delta)_{max}$ values. Almost all polymers used for previous research have a $tan(\delta)_{max}$ higher than 1. The *Montano Polyurethanes* with a lower $tan(\delta)_{max}$ value have shown insufficient gap closure in previous research [9], suggesting lower ΔS_R and $tan(\delta)_{max}$ are an indication of little displacement and relaxation dynamics at T_g, influencing damage closure. The comparison, between the different studies mentioned here, suggest a correlation between $tan(\delta)_{max}$ values of a polymer, the measured entropy release and damage closure behavior.

The epoxies for this study are based on the same epoxy, only the amine is different. Considering the epoxy is the same, the results indicate a large influence of amine selected on entropy release obtained.

DMA measurements can also be used to determine the crosslinking density (ν_j). This can be done by calculating the average molecular weight between crosslinks ($\overline{M}_j$) and taking the density (ρ) divided by it ($\nu_j = \frac{\rho}{M_j}$) [28]. $\overline{M}_j$ is calculated with Equation 4.1 derived from rubber elasticity theory [39] [40].

$$\overline{M}_j = \frac{3\nu\rho RT}{E'} \tag{4.1}$$

In Equation 4.1 the rubber modulus of the material is used (E' at T_g + 50°C), ν is the front factor (a value of 1 is assumed [39]), ρ the density ($1.1 g/cm^3$ experimentally obtained), R the gas constant ($8.31 J/(Kmol)$) and T the temperature in Kelvin at T_g + 50K. The values obtained following this method are named $M_j msrd.$ and $\nu_j msrd.$ for the remainder of this report.

Results from DSC and DMA measurements are summarized in Table 4.1. Here $T_g midpoint$ results from DSC measurements, ΔS from DMA, the ν_j and M_j values are calculated using Equation 4.1 and estimated with the aforementioned method explained in Section 3.2.3. The Anc samples have a higher T_g and show smaller entropy storage and release. The Jeff samples on the other hand show a lower T_g, but a higher change in entropic values.

Table 4.1: Material characteristics obtained from DSC and DMA tests. Annotation *msrd.* refers to measured (defined in Equation 4.1) and annotation *est.* refers to estimated (defined in Section 3.2.3).

Material	$T_g midpoint$ [°C]	ΔS_S [kJ/m^3]	ΔS_R [kJ/m^3]	$\nu_j msrd.$ [mol/m^3]	$M_j msrd.$ [g/mol]	$\nu_j est.$ [mol/m^3]	$M_j est.$ [g/mol]
Anc	70	4.0	0.5	1104	996	467	2717
Jeff	35	20.0	19.5	145	7564	163	7048

There is good agreement between the measured and estimated values for M_j and ν_j of the Jeff samples, but little for the Anc samples. A difference greater than 50% for Anc samples, as opposed to the 10% difference for Jeff samples. Since the estimation method is based on the rubber elasticity theory, it could be that applying this to a crosslinked network causes the discrepancy. Another explanation for the discrepancy is the assumption that the retractive stress is equal to the stress measured at maximum elongation, it may be that this assumption thus does not hold for polymers with a lower viscous component ($tan(\delta)_{max}$ < 1). Other parameters that influence ν_j calculations might be neglected is this approach as well, for example dangling chains, intramolecular chain interactions, etc [41] [42]. The difference is noted, but is considered beyond the scope of this research.

A higher crosslinking density (ν_j) is expected for the epoxy synthesized with an amine consisting of short monomers. This is visible when comparing Anc (short amine chains) and Jeff (longer amine chains), since Anc has a higher crosslinking density. A lower T_g is also expected for a smaller crosslinking density [43], because the network is less rigid so less energy is needed for the chains to move. A network were the viscous component is dominant during the VLTs induced elongation is expected to show a high maximum strain and thus entropy storage (ΔS_S). Crosslinks (or junction points) are necessary in order to retrieve this energy, otherwise the viscous displacement will result in a permanent shape change instead of energy storage in the form of conformational entropy change. Crosslinks pre-

vent permanent shape changes and thus the chain elongation results in energy storage retrieved upon heating further, appearing as sample retraction.

It can be concluded that to ensure high entropy release, resulting in more displacement for gap closure, sufficient crosslinks or junction points are needed to store entropic energy, but also high flexibility of the chains between crosslinks is needed ($(tan(\delta)_{max}$ > 1) in order to change the entropy of the system.

4.3. Tensile Test Results

The micro-tensile tester used to obtain LSI temperature ramps for strained samples imposes a displacement and measures the resulting force, which can be converted into stress ($\sigma = F/A$). Tensile tests have been executed at different temperatures controlled by a resistor heating device (as depicted in Figure 3.13). An example result is given in Figure 4.6, during all the LSI temperature ramp tests for strained samples such results have been obtained.

The course of all tests follows a similar pattern, a local minimum in stress is present when the resistor heating device is turned on. The local minimum could be attributed to the sudden increase in temperature causing a temporary relaxation where the polymer rearranges itself after which a new equilibrium is reached. After ten minutes, when the prescribed strain is reached the stress relaxation is measured. Stress relaxation can be denoted by the change in stress or the time it takes to reach an equilibrium. The first is measured by taking the difference in stress ($\Delta\sigma$) between right after elongation and where the curve flattens. The time it takes before stress does not change anymore (the stress curve is flattened) is denoted by t_σ, both parameters are illustrated in Figure 4.6.
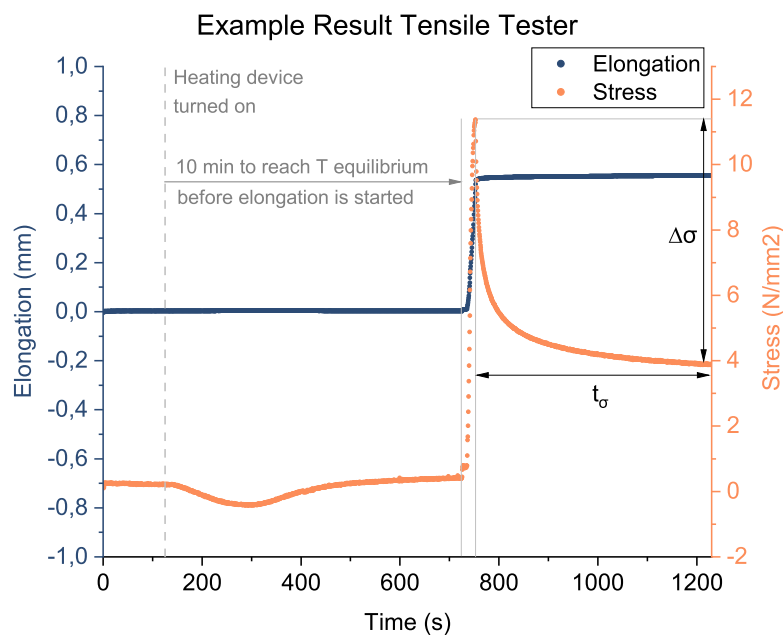
Figure 4.6: Example of a result obtained with the tensile tester during a test of the LSI temperature ramp for strained samples. The decay in stress is depicted as $\Delta\sigma$ and the stress relaxation time as t_σ.

After two minutes the resistor heating device is turned on, a momentarily decay in stress is measured after which a new equilibrium is reached. Once an isothermal temperature is reached, after 10 minutes, the sample is strained to a predefined length. Stress increases during this straining event after which stress relaxation is measured. The stress relaxation for this work has been defined by the decay in stress ($\Delta\sigma$) and the time to reach a plateau value (t_σ).

In Figure 4.7 stress relaxation is depicted versus temperature at which the strained LSI test has taken place, as measured by the micro-tensile tester. T_g ranges measured with DSC are highlighted. If relaxation had not reached a plateau value before the end of test a time of $600s$ is noted, this is highlighted by the dashed line.
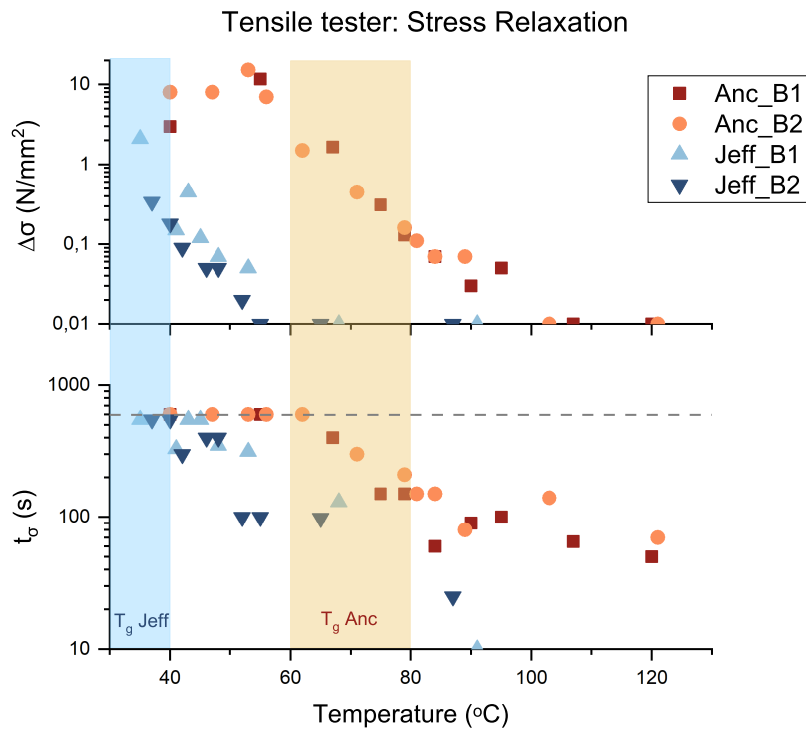
Figure 4.7: Stress relaxation obtained during LSI temperature ramp tests with strained samples, measured by the micro-tensile tester. Top, decay in stress during relaxation. Bottom, relaxation times obtained from the same tests. T_g measured with DSC is marked by a coloured bar per sample composition. If relaxation had not reached a plateau value before the end of test a time of $600s$ is noted, this is highlighted by the dashed line.

A constant decay in $\Delta\sigma$ throughout the T_g range is shown for both samples in the top graph. An increase in $\Delta\sigma$ is visible before T_g for the Anc samples.

The bottom graph in Figure 4.7 shows a decay in stress relaxation times throughout the T_g range as well. Both graphs clearly show temperature dependency of stress relaxation behavior.

4.4. LSI Results

LSI measures local displacement over a frequency range by comparing frames with an increasing time interval $(\tau(s))$. The amount of displacement measured is captured by the autocorrelation function (d_2), where a high value depicts more displacement (i.e. higher dynamics) than a lower value. Combining these gives you a color plot as explained in Section 3.3. The x-axis denotes time or temperature (for a constant temperature increase over time).

4.4.1. Experimental Considerations

Because of the nature of the test set-up it is challenging to control all test conditions that influence the results, most noticeably temperature and airflow.

The true test temperatures have been established in several ways. Due to the nature of the LSI set-up, it was not possible to measure the temperature during each test. The laser signal should not be disturbed and thus placing a thermocouple on the spot of measurement was not possible. Furthermore, for the LSI tests on strained samples, in order to not disturb relaxation dynamics, the resistors heating the sample could not touch it. The distance to the sample caused a temperature gradient over the sample, but the laser spot on the sample is small enough to assume a constant temperature over the region of interest.

The measured temperatures before and after tests and the gradients measured are depicted in Appendix E.

For the non-strained sample temperature ramp, start and final temperatures were measured and a linear line was fitted through those points to establish the true temperature ramp. Rate of heating was tuned in a manner so the surface temperature increased with approximately 2°C/min, comparable to DMA heating rate.
The test temperature of the tests on strained samples has been measured directly after every test. All obtained results were used to predict the voltage to use for the next test.

In color plots from LSI measurements the signal seems to fluctuate at higher temperatures. A hypothesis was formed that the signal is influenced by airflow due to the increased heat of the resistors and the sample since there is no closed oven around it. Because the laser light is reflected by tiny scatterers (the TiO_2 nanoparticles), it is plausible that moving air also influences the signal because it contains small (dust) particles as well. To test this hypothesis four trials were executed with an airblower and a cardboard box. The results of these trials are depicted in Figure E.15 in Appendix E.
From all tests executed to determine test temperatures and the influence of airflow it has been concluded to use the temperatures as measured directly after every test and to perform the tests in a cardboard chamber to reduce airflow.

4.4.2. LSI Temperature Ramp Results
In this Section, results of the LSI temperature ramp tests with non-strained and strained samples are presented respectively.

Non-strained Sample Temperature Ramp
Results from the temperature ramp for non-strained samples are depicted in Figure 4.8. $\tau(s)$ is represented on the y-axes, where a small number denotes fast dynamics. d_2 denotes displacement, a high number represents more displacement than a lower number. For Anc, two distinct temperature ranges of increased frequencies at which high displacements occur (e.g. faster dynamics) around 60°C and 85°C. For the Jeff samples one such an area can be distinguished right at the beginning of measurement, around 50°C.
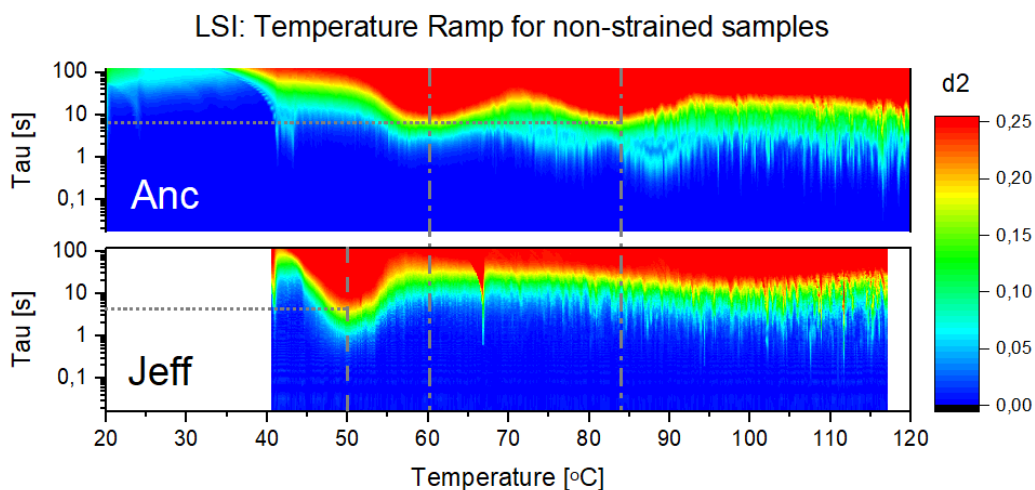
Figure 4.8: LSI temperature ramp for non-strained samples. In the upper plot the Anc result is shown and in the lower one the Jeff result, temperatures where fastest dynamics occur are highlighted with dotted lines.

A decrease of the faster dynamics at elevated temperatures is notable, a decrease suggests that although more energy is available (higher temperatures), this energy is not used for ever faster displacements (of the polymer chains for example). An explanation for this phenomenon could be that the local minimum are related to thermal transitions in the material associated with dynamics, like T_g or

conformational entropy changes. Color plots obtained from measurements of different batches showed good reproducibility between and amongst batches, all LSI plots obtained can be found in Appendix C.

A remark should be made regarding the first 20°C of the Jeff measurement, since turning on the laser increases temperature already the starting temperature lies at 40°C. For the Anc samples a correction was made by including temperature increase solely from the laser until 40°C, at this point the hot stage was turned on and further increased the sample temperature. This could not be incorporated in the Jeff measurement.

From LSI results the local strain relaxation time ($\tau_0(s)$) can be extracted by a fitting procedure, clarified in Section 3.3.4. As shown in literature this can be used to investigate the viscosity of a material [13]. A viscous material has shorter relaxation times and when it becomes more elastic relaxation times increase. It is expected that τ_0 will decrease when heating the epoxies, since the material becomes more viscous when going through T_g. From the temperature ramps and tau plots as seen in Figure 4.8 τ_0 can be obtained as function of temperature. A plot as depicted in Figure 4.9 is constructed to compare both polymers.
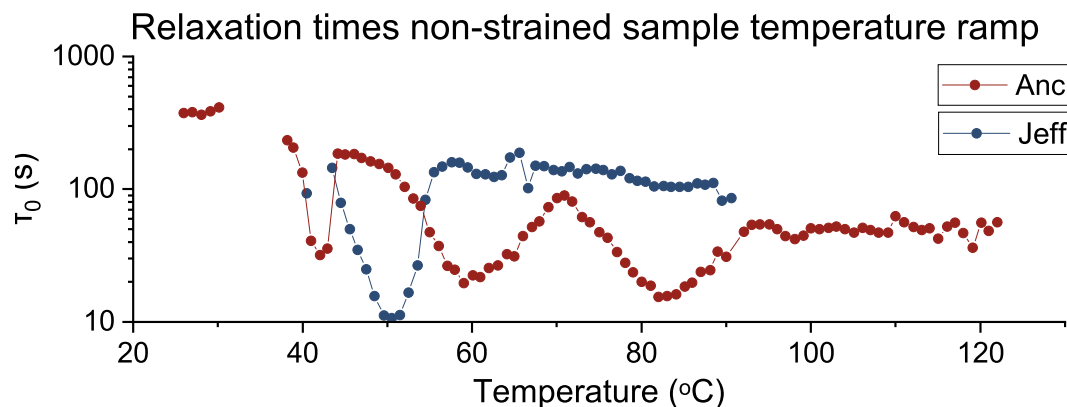
Figure 4.9: τ_0 for both samples, obtained from the non-strained sample temperature ramp LSI measurements. Viscous behavior is shown by shorter relaxation times while elastic behavior results in longer times.

Anc results for temperatures between 32°c and 38°C where unfit for the fitting procedure, so the invalid values are left out, but an overall trend of higher relaxation times can be observed for the pre-T_g temperature range. Only one local minimum at 40°C is standing out, which can be attributed to the moment where the hot stage was turned on.

Two local minimum in the Anc curve during the T_g range can be observed, and one local minimum in the Jeff curve. After T_g, relaxation times remain more or less constant for both materials. Although a bit longer times are observed for the Jeff samples.

Strained Sample Temperature Ramp

Color plots obtained from LSI tests with strained samples are displayed over a timescale instead of temperature, since every separate test is executed at a certain temperature. In Figure 4.10 a color plot of such a test is shown. Color plots obtained from measurements of different batches showed good reproducibility between and amongst batches, all LSI plots obtained can be found in Appendix C.
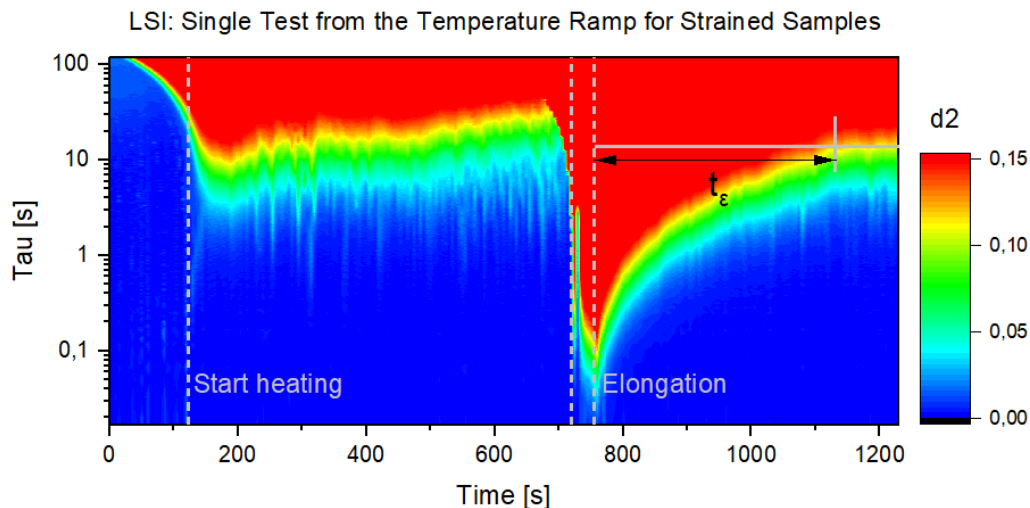
Figure 4.10: Color Plot from a single test of the temperature ramp for strained samples. The moments in time where heating starts and elongation takes place are indicated by dashed lines. The strain relaxation time is extracted from LSI color plots as illustrated here by t_ϵ

At 0s the resistor heating device is off and the sample is non-strained. After two minutes the heating device is turned on and will heat the sample to a given temperature, this event increases the dynamics measured immediately. Ten minutes later, at isothermal conditions, the sample is strained to a predetermined level while the polymer strain dynamics are measured by LSI. once the strain level is reached the micro-tensile tester stops and measures stress relaxation while LSI measures local strain relaxation. During elongation d_2 clearly increases over a wide frequency range (tau), when straining stops the number of frequencies over which displacements take place drops. Relaxation time can thus be measured with LSI by defining it as the red area (and how quickly it reduces).

That an area of increased dynamics is visible before the heating device is turned on, is the result of the computing method used to create the d_2 numbers. As explained in Section 3.3.3 frames are compared to a set of frames a certain moment in time further away (the correlation range). In this way, for longer correlation ranges (high numbers of tau), a high d_2 value is generated if displacement has occurred in the future and it seems as. This issue will be discussed in Section 5.2.1.

Post-curing during the tests has been investigated by testing all used samples after their LSI test with DSC. A change in T_g indicates a change in polymer architecture, this could influence the dynamics measured in LSI. No change in T_g was found, all DSC results can be seen in the last section of Appendix D.

In Figures 4.11 and 4.12 elongation is shown for two samples of the same material at different temperatures. A dotted line at $tau = 50s$ is added in both graphs as a baseline to show the overall increase in frequency for higher temperatures (i.e. the standard dynamics appear to be faster at elevated temperatures). If the relaxation dynamics are compared between the two tested temperatures a clear difference is visible. Both samples are elongated over the same distance, but their response is very different. At 40°C, well below T_g, a gradual decay in dynamics is visible over time. At 120°C only the elongation itself stands out, the expected subsequent relaxation is very fast and hardly distinguishable from this plot.
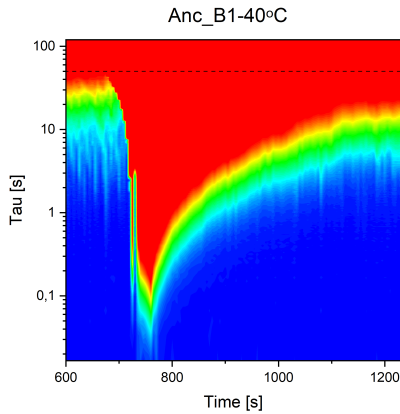
Figure 4.11: Tensile Test Result Anc-40°C   Figure 4.12: Tensile Test Result Anc-120°C
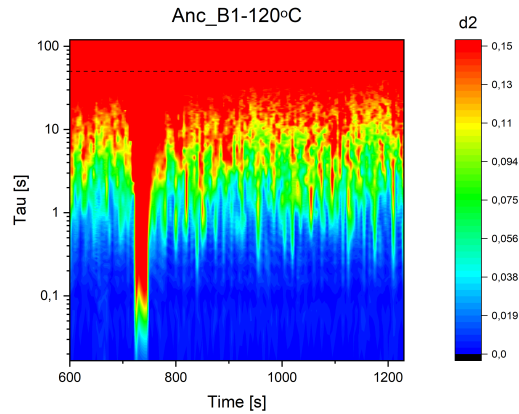
The area of relaxation can be analysed for all separate LSI tests by converting Figure 4.11 into Figure 4.13, and doing so for all tests at different temperatures. This is done by counting the number of frequencies during elongation and relaxation that have a d_2 number above a certain threshold value: N_{tau}. The threshold value is the calculated average d_2 number, which is different per measurement because of uncontrollable environmental conditions, but will always be the tipping point between high and low d_2 numbers. The displayed d_2 numbers per moment in time are cumulative, which means that if a displacement has occurred on a short timescale it always also has occurred for longer timescales. The implication of this is that a high N_{tau} number is related to fast dynamics; a lot of frequencies have a high d_2 number. Obtained results for all strained sample temperature ramps executed are depicted in Figure 4.14.
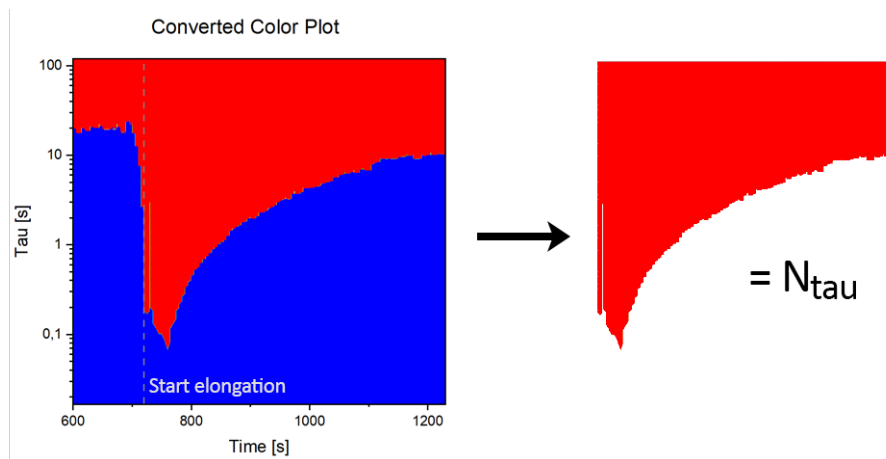
Figure 4.13: Graphic representation of the method used to convert the color plots into measured relaxation.

From Figure 4.14 two things can be noted. The difference between Jeff and Anc is clearly visible in the N_{tau} value obtained. A higher N_{tau} number is related to faster dynamics, so Jeff samples show faster dynamics during relaxation than Anc samples.
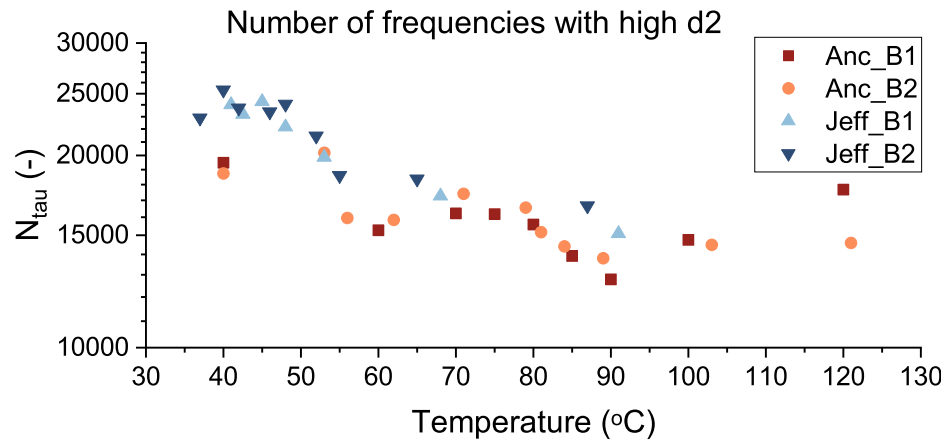
Figure 4.14: Strained sample temperature ramp with relaxation depicted as N_{tau}.

5

Discussion

In this chapter a comparison is made between DMA, LSI and Tensile test results. First, the interpretation of obtained results is done in Section 5.1. Some final remarks on the methods used are given in Section 5.2

5.1. Interpretation LSI Results

The goal of this research was to link LSI measurements to the DMA-protocol developed for entropy quantification. The hypothesis is that length changes measured in DMA are distinguishable with LSI by means of changing dynamics. In this section a comparison will be made between DMA and LSI to validate this hypothesis.

5.1.1. Non-strained Sample Temperature Ramp

A comparison between DMA results and the LSI color plots is depicted in Figures 5.1 and 5.2. In both figures first DMA results, as discussed previously in Section 4.2, are shown. The LSI result is captured in color plots that are presented on the same temperature axis as the DMA plots. The dashed grey lines indicate local maximum, minimum and inflection points of the $tan(\delta)$ curve. Using these lines a qualitative comparison can be made between DMA and LSI measurements.
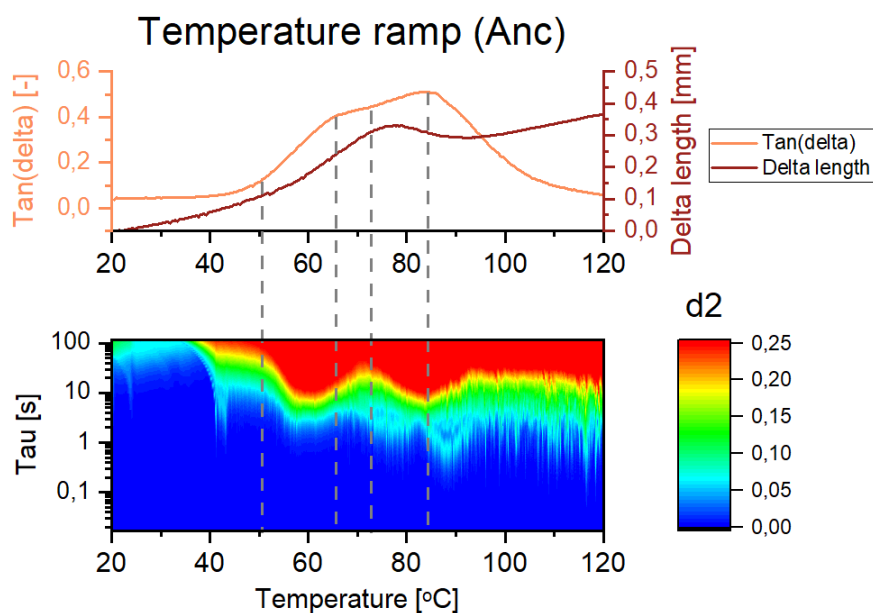
Figure 5.1: DMA and LSI comparison non-strained Anc sample LSI temperature ramp
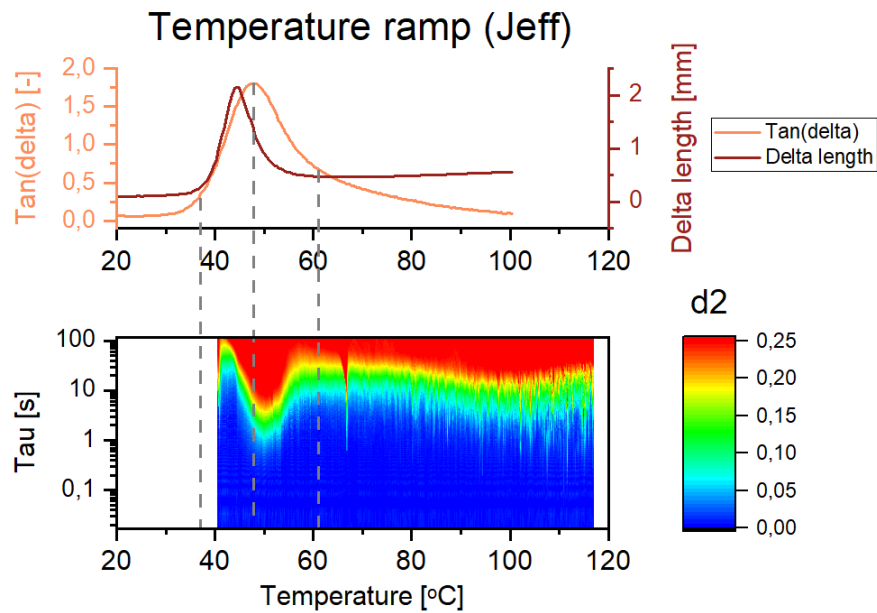
Figure 5.2: DMA and LSI comparison non-strained Jeff sample LSI temperature ramp

It can be seen that the temperature range is suitable for the Anc samples but a lower starting temperature would have been preferred when testing the Jeff samples. It appears that some dynamics are already occurring before the start of measurement. This is endorsed by comparison with DMA showing the onset of $tan(\delta)$ occurring before the start of LSI measurement, after this onset point faster dynamics are expected [24].

Both graphs show temperature ranges of faster dynamics that correspond to the DMA results. In Figure 5.1 a first increase in dynamics corresponds to the onset point of the delta length curve (i.e., the elongation phase of the sample when the energy is stored [8]). The second range of faster dynamics coincides with the second transition measured as local maximum of $tan(\delta)$.

In Figure 5.2 it is shown that both methods have captured one peak. Between 40°C-50°C the $tan(\delta)$ curve increases and the speed of dynamics increases as well, where $tan(\delta)$ is decreasing the dynamics become slower.

The observed DMA length change can be explained as first elongation governed by motion possible since the material enters the T_g range, followed by retraction due to the release of stored conformational entropy, which is released because of the increased temperature. After these two phases the extension continues because the temperatures rise above T_g and there is enough energy available for the polymer chains to move as much as possible, being restrained only by the crosslinks (e.g. the rubbery plateau).

The length change of Jeff samples clearly follows this pattern, while the Anc samples have two transitions visible in the $tan(\delta)$ curve. The color plots seem to show the thermal transitions also captured by the $tan(\delta)$ curve in DMA and not so much the length changes used to quantify entropy.

Relaxation times (τ_0) obtained from the LSI color plots for both samples are compared to DMA results, as depicted in Figure 5.3. DMA results for both materials are depicted in the top graph and τ_0 in the bottom one. The local maximum in $tan(\delta)$ are highlighted by blue and red dashed lines for Jeff and Anc respectively.
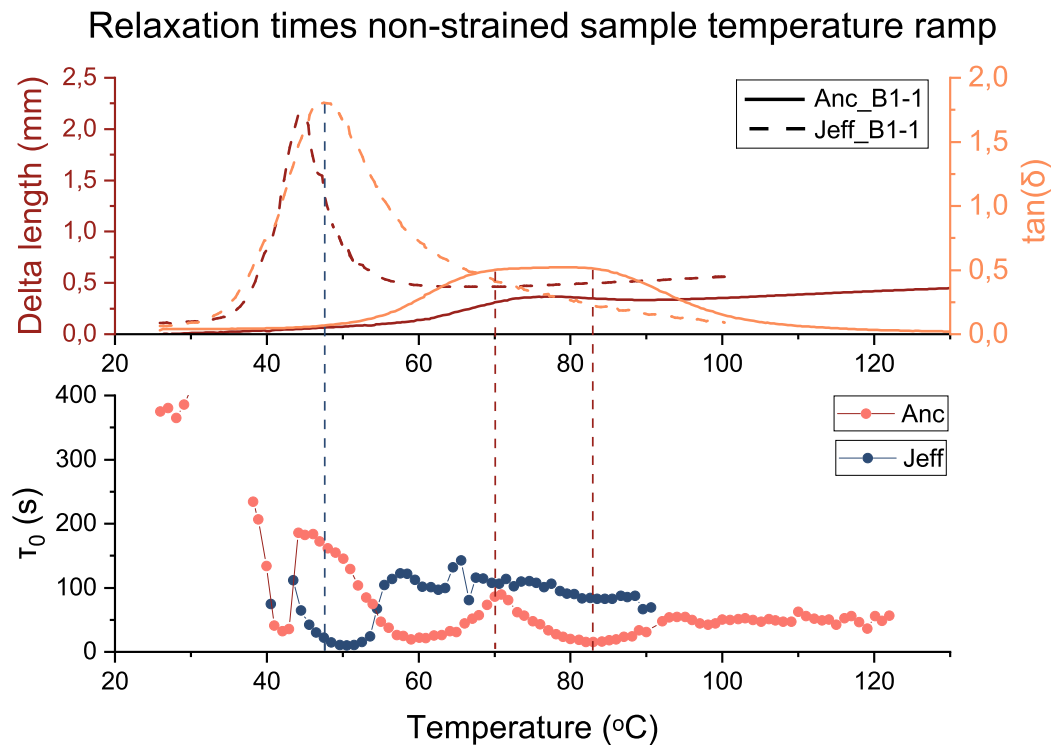
Figure 5.3: DMA and relaxation time (τ_0) comparison for the non-strained sample temperature ramp in LSI.

For the Jeff sample one local minimum can be observed that can be related to the peak in $tan(\delta)$. The τ_0 curve for Anc samples has a local maximum at 70°C and a minimum at 85°C, that both can be related to the two $tan(\delta)$ peaks observed in the upper graph. The other local minimum at 60°C seems to coincide with the temperature at which $tan(\delta)$ has an inflection point and starts to increase.

Maximum length change measured by DMA occurs right before a peak in $tan(\delta)$ (the second one for Anc), for both samples this $tan(\delta)$ peak coincides with a local minimum in τ_0. The local maximum of τ_0 that coincides with the first $tan(\delta)$ peak of the Anc sample suggests longer relaxation times and thus elastic behavior related to that transition, but further research would be needed to draw any conclusions.

It would be interesting to test a material with a single $tan(\delta)$ peak over a temperature range totally covered by LSI to see the relation between $tan(\delta)$, delta length and τ_0 more clearly. For now it can be concluded that a relation is suggested, since the dynamics measured by LSI follow the $tan(\delta)$ curve rather well, but the nature of this relation should be investigated further in order to quantify this behavior for a broader range of materials.

5.1.2. Strained Sample Temperature Ramp

The N_{tau} number is a counted number of frequencies with a high d_2 number for the entire time-span after straining (i.e., a high N_{tau} means fast displacements). It shows some similarities to DMA results as depicted in Figure 5.4. Both DMA and N_{tau} graphs are shown over the same temperature range and the maximum in $tan(\delta)$ are highlighted with dashed lines, blue for Jeff and red for Anc.
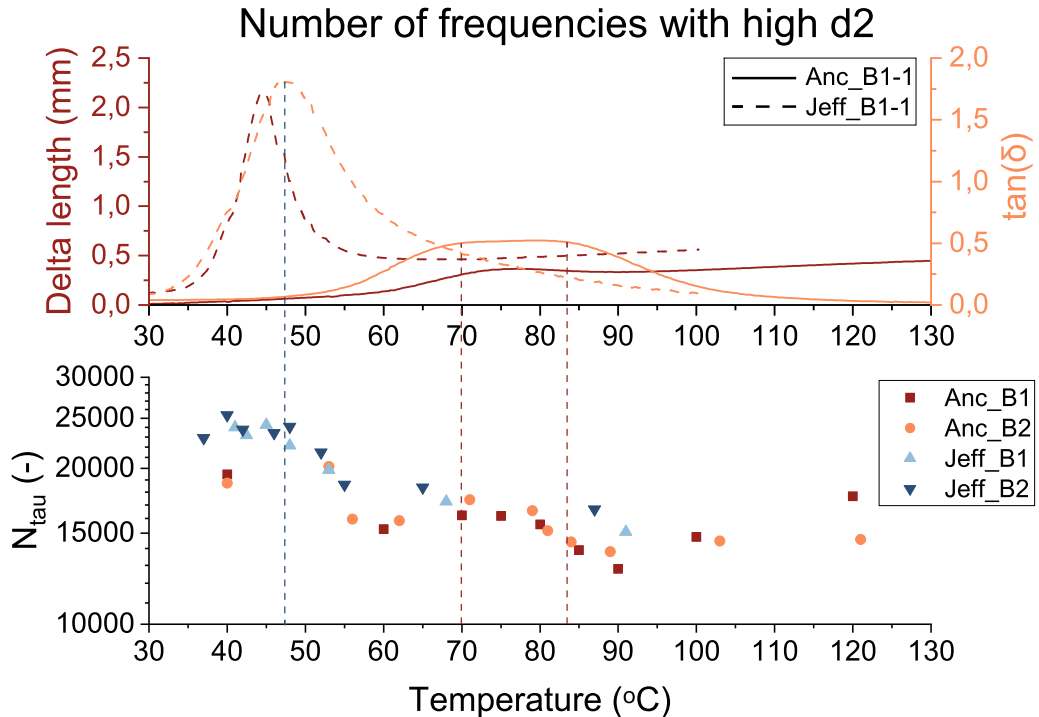
Figure 5.4: Comparison DMA and N_{tau} obtained from strained sample temperature ramp tests with LSI.

Similarities between the two graphs in Figure 5.4 are present. The $tan(\delta)$ peak of Jeff is visible in the lower graph at the same temperature range depicting high N_{tau} numbers. For the Anc sample, results in both graphs are less evident, which is also a similarity. Since delta length and $tan(\delta)$ show dependence on each other it is difficult to distinguish if the N_{tau} numbers are relatable to one of the two or both.

Noticeably is the link between a high $tan(\delta)_{max}$ value and a higher N_{tau} number. A remark should be made regarding the high N_{tau} numbers for Anc at both ends, since they show higher numbers than at the temperature range coinciding with $tan(\delta)_{max}$. These numbers don't follow the same trend as the DMA graph and more datapoints should be taken in those temperature regions in order to investigate why this happens, further research is deemed necessary.

5.1.3. Stress Relaxation versus Local Strain Relaxation

With LSI, local displacements are measured while the tensile tester measures the overall response of samples in terms of stress. By combining these results a comparison can be made between stress relaxation, as measured by the tensile tester, and local strain relaxation, as measured by LSI. In Figure 5.5 results from LSI (top graph) and the tensile tester (bottom graph) are depicted. The temperature on the x-axis reflects the temperature at which the LSI test on a strained sample is conducted. On the y-axis the relaxation times are depicted, the maximum test times are highlighted by a dashed line (due to the analysis method used for LSI results a shorter test time has been achieved there than for the tensile tester.
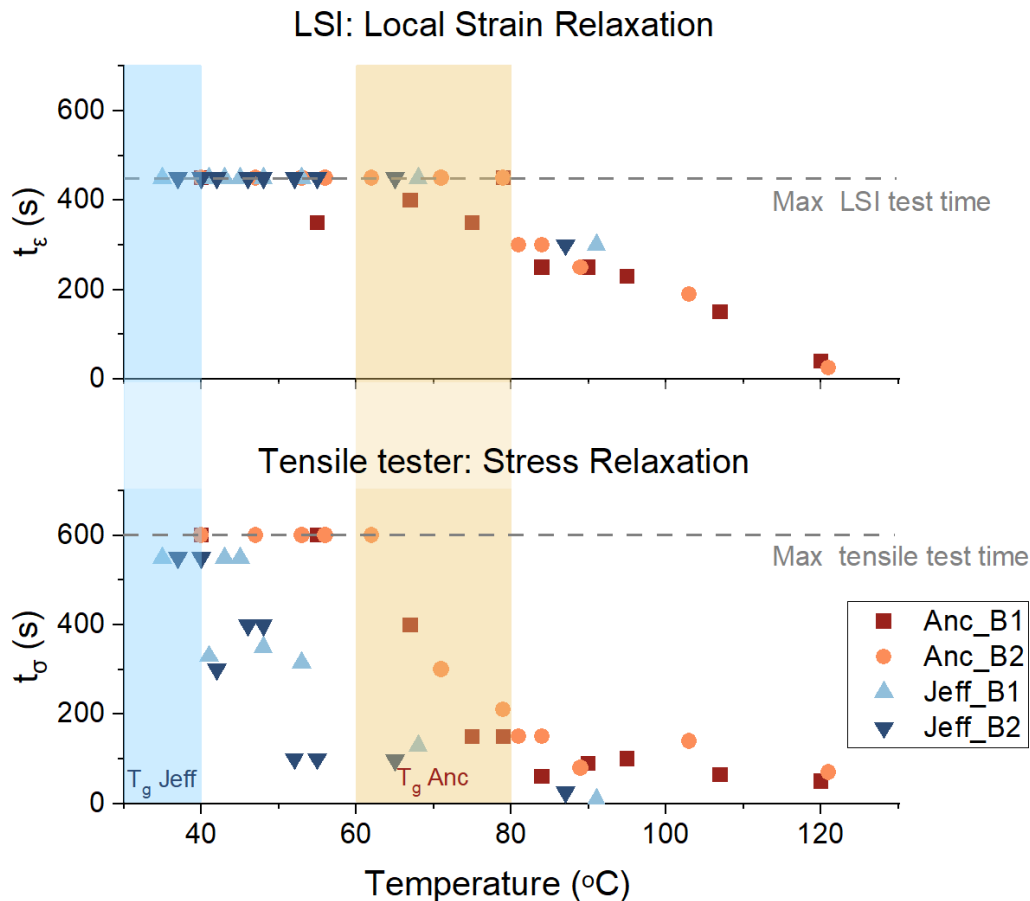
Figure 5.5: Local strain relaxation (t_ϵ) obtained from the color plots of strained samples versus stress relaxation (t_σ) obtained from the micro tensile test results.

It is immediately clear that in order to obtain the local strain relaxation times the samples should have been tested for a longer time. Nevertheless, this comparison shows that both samples exhibit longer local strain relaxation times than the overall stress relaxation time. Furthermore, a hypothesis can be formed regarding the internal energy state of the samples. After straining the sample, and thus uncoiling polymer chains, it could be that not all chains move back into their preferred state. This will change the conformational state of the sample, which induces mobility of the polymer and could result in longer local strain relaxation times measured. Further research should be conducted, over longer time frames, to see if the measured dynamics in LSI could reveal a difference in dynamics before and after relaxation that is relatable to entropy change.

5.2. Final Remarks

Some final remarks should be made regarding the methods used for the tests in this research.

5.2.1. LSI Data Analysis Software

In order to make the color plots, a matrix with d_2 values is created using the *LSI_g2_d2* software. This software compares frames with each other as discussed in Section 3.3.3. The first frame is compared with frames in the future and so the value of d_2 for that moment in time is defined. For the higher values of τ this creates a problem, because the depicted value can be viewed as a look into the future. If a frame has changed 100 seconds later the d_2 value at zero seconds for $\tau = 100s$ depicts a high value. This gives a distorted picture for slower frequency dynamics as can be seen in Figure 5.6A. Increased d_2 numbers, for higher τ, are visible before elongation starts, highlighted by the circle. Another consequence is that while doing a measurement, the maximum correlation range should already be taken into account. The software can only generate d_2 values for times up to the last measured frame minus the highest correlation range of interest, so a constant final period of the test is necessary for creating complete results.
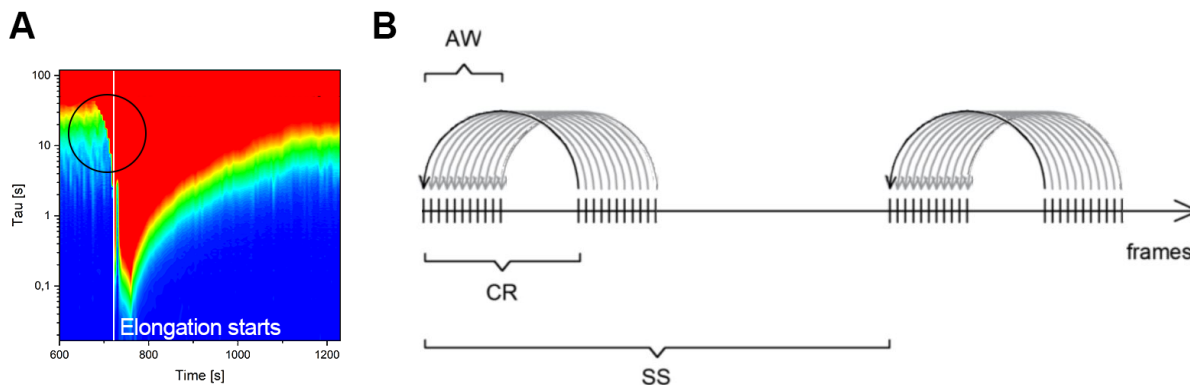
Figure 5.6: A) Example of increased dynamics before straining has started. B) Graphic representation of the proposed data analysis scheme, where AW is the averaging window, CR the correlation range and SS the step size, adapted from [37].

A solution for this problem could be to compare the frames the other way around, as depicted in Figure 5.6B. A frame at 10 seconds would then be compared to the one at zero seconds. In this manner the g_2 and d_2 values at a certain time depict the change occurred in comparison to the past and not the future. Nevertheless, it should be noted that for longer correlation ranges the values would still be distorted, because over a longer period of time the likeliness of dynamics occurring always increases. Therefore, the time range depicting high d_2 values will broaden. In order to analyze tests in the above mentioned manner, a zero measurement over a period, equal to the highest CR, is necessary before the actual test is started. This base measurement contains the frames for comparison to start with.

5.2.2. DMA Results

The protocol used to measure to entropy changes has one important limitation: the samples are tested in tension mode, but under very low stresses. If they go through their T_g range and soften there is a risk that the samples buckle under their own weight and distort the measurement. On the other hand, if a material is chosen that is very stiff for temperatures under T_g, the imposed 0.1% strain is impossible to achieve for the DMA and the test will stop automatically. The test protocol here used can thus not be used for too soft or too rigid polymers.

The method to estimate M_j and ν_j shows a discrepancy compared to the calculated values for the Anc samples, visible in Table 4.1. The method to estimate the values is based on the measured static force at maximum length change to calculate the stress, whereas the calculated method uses E'. If the material behavior is taken into account, the calculated values seem more accurate, a higher junction density leads to higher T_g. Ancamine 2500 is also expected to have shorter chains between junction points than the Jeffamine D-230, as illustrated in Figure 2.2, so a low M_j for the Anc samples makes sense too. The discrepancy cannot be explained with the information available, since the method seems accurate for the Jeff samples. Maybe the force measured by this type of DMA is different to that on the DMA by which the method is developed, so the estimation method is not universally applicable.

6

Conclusions and Recommendations

The main conclusions and resulting recommendations are addressed in this chapter. First, the research question and objectives as presented in Chapter 1 will be repeated here. Conclusions drawn are presented next. The resulting recommendations regarding future research conclude this chapter.

The research question has been formulated as follows: *How can temperature dependent material behavior measured by DMA be linked to polymer dynamics measured with LSI?* In order to answer this question multiple research objectives will be addressed:

- Assess whether it is possible to measure polymer dynamics with LSI during a temperature ramp and relate them to material properties obtained with DMA.

- Assess the possibilities regarding measuring polymer dynamics with LSI that are relatable to length change, used for entropy calculations, measured with DMA.

- Assess the relation between stress relaxation and local strain relaxation by comparing LSI and micro tensile tester results.

- Review the obtained results by comparing LSI and DMA results.

Comparing LSI and DMA

On the relation between obtained results with LSI and DMA several conclusions can be drawn:

- A difference between the two materials tested is distinguishable with LSI.

- Temperature ranges of faster dynamics measured on a non-strained sample during a temperature ramp in LSI coincide with the $tan(\delta)$ peak obtained with DMA.

- Relaxation times obtained from fitted curves of a non-strained sample temperature ramp in LSI are relatable to a peak in $tan(\delta)$, which suggests a relation between $\tau_0(s)$ and $tan(\delta)$.

- Evaluation of the number of frequencies where dynamics are occurring (N_{tau}) of strained sample temperature ramps suggest a relation to $tan(\delta)$. The Jeff chemistry, which has a higher $tan(\delta)_{max}$ number, shows higher N_{tau} numbers. This means faster dynamics are occurring during relaxation in Jeff samples as opposed to the Anc ones.

So, overall it can be concluded that thermal material properties like $tan(\delta)$ can be probed by LSI in terms of polymer dynamics. But in order to develop a technique where gap closure behavior can be quantified, much remains to be investigated.

Comparing Relaxation Times
The stress relaxation times obtained with the micro-tensile tester have been related to the local strain relaxation times in LSI. Several conclusions can be drawn:

- When the heating device is turned on during a LSI measurement, a temporary decay in stress and faster dynamics are measured for the strained sample set-up. A local minimum in τ_0 and faster dynamics are measured for the non-strained sample set-up.

- The Jeff chemistry, that showed good entropy release properties, has longer stress and strain relaxation times above the glass transition temperature range than the Anc chemistry.

- Local strain relaxation takes longer than the overall stress relaxation of a sample.

- A hypothesis is formed that, upon stretching polymer chains are uncoiled that cannot all move back during relaxation. This leaves the sample in a higher dynamic state where more mobility is possible. This increases the local strain relaxation times for the strained samples tested.

Other Information Obtained
Regarding the choice of materials for a comparison study between DMA and LSI the following can be concluded:

- Besides a turbid material (that creates the speckle pattern of reflected laser light), should samples be stiff enough to remain in shape during the temperature ramp executed in DMA, but not so stiff that the imposed 0,1% strain cannot be maintained at temperatures below T_g.

- The T_g range of the material should lay between the minimum and maximum temperatures the LSI set-up can reach.

- Ideally only one $tan(\delta)$ peak is present in order to interpret the results.

- All monomers used to synthesize the material should be well known, so the material behavior can be explained based on their polymer architecture.

While testing the LSI set-up several conclusions were drawn. Airflow is of influence on the LSI result, higher temperatures in an open set-up increase airflow and thus disturb the signal. This could be reduced by covering the set-up with a cardboard box, but for tests at higher temperatures interference of the signal should be taken into account.

The current analysis method that compiles g_2 and d_2 produces a number for a moment in time compared to the future, so if displacement has occurred at $t_0 + 100s$ this will be visible for $\tau = 100s$ at t_0. Computing the values in this way gives confusing results for the higher correlation ranges, since a look into the future is given. This could be changed by reversing the order in which the frames are compared, resulting in a high d_2 number at t_0 only if a displacement has occurred compared to the past. In this manner there will only occur high d_2 numbers for a certain moment in time if there actually has been a displacement.

Recommendations
In view of the bigger research aim regarding gap closure dynamics of self-healing polymer coatings some recommendations for future research have been formulated. If a measuring protocol has to be developed to measure gap closure dynamics of polymer coatings, LSI is a good candidate. But several things have to be examined in the way towards implementation of such a protocol.

Concerning the materials to test, it would be interesting to test a wider range of polymers. It is recommended that all polymers have one feature standing out from the rest. For example, a polymer not showing any entropy induced retraction to complement the polymers tested for this research which showed a lot and a little entropic induced length changes. Polymers with different temperature ranges and values for $tan(\delta)_{max}$ should also be investigated with LSI, to see if the probed dynamics can be quantified and a universal link between $tan(\delta)$ and dynamics can be established.

The relation between relaxation dynamics and entropy release should be investigated further. Longer relaxation tests should be executed on a range of polymers with different entropic values to investigate if a parameter can be found to relate ΔS_R to relaxation dynamics.

The LSI set-up should be developed further, especially for testing at different temperatures. In order to probe polymer dynamics and link them to temperature dependent polymer properties an environment should be created where temperature can be regulated and airflow is reduced to a minimum. Different test set-ups, like a tensile tester, should still fit in the set-up to keep the versatile possibilities regarding modes of measurement available. Regulating and measuring the temperature accurately is important in order to draw conclusions on measured dynamics in relation to temperature dependent material properties.

The next step regarding this research should be to further confirm and investigate the findings of this research in a statistically relevant context. By doing this, a DMA experiment to establish the T_g range, and thus gap closure and healing temperatures, of a coating would be unnecessary in the future and could be established by LSI only.

Once it is established that bulk material properties can be measured on coatings as well, the following step is to link energy storage measured by DMA in terms of entropy changes to a quantifiable parameter in LSI. Once this parameter is reviewed in terms of gap closure behavior, gap closure behavior can be investigated further. Different scratch modes, material types and temperatures could be tested in order to better understand gap closure behavior of materials in terms of dynamics.

The ability of LSI to probe dynamics in a spatial manner could be added to these results in order to define material characteristics in a spatial manner as well. It can be concluded that enough interesting research can be done regarding gap closure of polymer coatings and LSI.

Bibliography

[1] C. Niemann, "Camera." [Online]. Available: https://www.christophniemann.com/

[2] S. García, H. Fischer, and S. Van Der Zwaag, "A Critical Appraisal of the Potential of Self Healing Polymeric Coatings," *Progress in Organic Coatings*, vol. 72, no. 3, pp. 211–221, 2011.

[3] S. García, "Effect of Polymer Architecture on the Intrinsic Self-Healing Character of Polymers," *European Polymer Journal*, vol. 53, no. 1, pp. 118–125, 2014.

[4] R. P. Wool and K. M. O'Connor, "A Theory of Crack Healing in Polymers," *Journal of Applied Physics*, vol. 52, no. 10, pp. 5953–5963, 1981. [Online]. Available: http://aip.scitation.org/doi/10.1063/1.328526

[5] A. Susa, "Self Healing Polyimides," doctoral thesis, Delft University of Technology, 2019. [Online]. Available: https://doi.org/10.4233/uuid:49ce6618-c9d5-4a46-bbc9-7439484d1ff8

[6] Y. Yang and M. W. Urban, "Self-Healing Polymeric Materials," *Chemical Society Reviews*, vol. 42, no. 17, p. 7446, 2013. [Online]. Available: http://xlink.rsc.org/?DOI=c3cs60109a

[7] V. Montano, W. Vogel, A. Smits, S. Van Der Zwaag, and S. J. Garcia, "From Scratch Closure to Electrolyte Barrier Restoration in Self-Healing Polyurethane Coatings," 2021.

[8] C. C. Hornat, Y. Yang, and M. W. Urban, "Quantitative Predictions of Shape-Memory Effects in Polymers," *Advanced Materials*, vol. 29, no. 7, pp. 1–8, 2017.

[9] V. Montano, "Scratch closure in thermoplastic polyurethanes: an energetic analysis," in *Thesis*, 2021, ch. 5, pp. 125–150.

[10] S. Yoneyama and G. Murasawa, "Digital Image Correlation," p. 10, 2021. [Online]. Available: https://www.eolss.net/Sample-Chapters/C05/E6-194-04.pdf

[11] J. W. Goodman, "Statistical Properties of Laser Speckle Patterns," in *Laser Speckle and Related Phenomena*, J. Dainty, Ed. Springer-Verlag Berlin Heidelberg, 1975, ch. 2, pp. 9 –74.

[12] C. Cane, "Lasers and PEMF [illustration]." [Online]. Available: https://pemfschool.com/lasers-pemf-use-them-together-with-the-new-lllt-pemf-combo-probe/

[13] H. M. Van Der Kooij, R. Fokkink, J. Van Der Gucht, and J. Sprakel, "Quantitative Imaging of Heterogeneous Dynamics in Drying and Aging Paints," *Scientific Reports*, vol. 6, no. September, pp. 1–10, 2016.

[14] H. M. van der Kooij, S. A. Semerdzhiev, J. Buijs, D. J. Broer, D. Liu, and J. Sprakel, "Morphing of Liquid Crystal Surfaces by Emergent Collectivity," *Nature Communications*, vol. 10, no. 1, pp. 1–9, 2019. [Online]. Available: http://dx.doi.org/10.1038/s41467-019-11501-5

[15] H. M. van der Kooij, A. Susa, S. García, S. van der Zwaag, and J. Sprakel, "Imaging the Molecular Motions of Autonomous Repair in a Self-Healing Polymer," *Advanced Materials*, vol. 29, no. 26, pp. 1–6, 2017. [Online]. Available: https://doi-org.tudelft.idm.oclc.org/10.1002/adma.201701017

[16] A. Lendlein and S. Kelch, "Shape-Memory Effect From permanent shape," *Angewandte Chemie (International ed. in English)*, vol. 41, pp. 2034–2057, 2002.

[17] M. Abdolahzadeh, A. C. C. Esteves, S. Van Der Zwaag, and S. J. García, "Healable dual organic-inorganic crosslinked sol-gel based polymers: Crosslinking density and tetrasulfide content effect," *Journal of Polymer Science, Part A: Polymer Chemistry*, vol. 52, no. 14, pp. 1953–1961, 2014.

[18] C. C. Hornat, M. Nijemeisland, M. Senardi, Y. Yang, C. Pattyn, S. van der Zwaag, and M. W. Urban, "Quantitative Predictions of Maximum Strain Storage in Shape Memory Polymers (SMP)," *Polymer*, vol. 186, no. September 2019, 2020.

[19] M. T. Rodríguez, S. J. García, J. J. Gracenea, C. Vitores, and J. J. Suay, "Thermal, mechanical, and anticorrosive characterization of an epoxy primer," *Corrosion*, vol. 63, no. 12, pp. 1075–1084, 2007.

[20] S. Ammu, "Towards improved dual network, disulfide based, self-healing thermosets for fibre reinforced composites," Ph.D. dissertation, TU Delft, 2018. [Online]. Available: https://repository.tudelft.nl/islandora/object/uuid% 3Afc9df535-d6e7-442d-bb7a-3ea87fbfe695?collection=education

[21] C. C. Hornat, M. Nijemeisland, M. Senardi, Y. Yang, C. Pattyn, S. van der Zwaag, and M. W. Urban, "Quantitative Predictions of Maximum Strain Storage in Shape Memory Polymers (SMP) – Supplementary Material," 2020.

[22] P. Hiemenz and T. Lodge, *Polymer Chemistry*.   CRC Press, 2007.

[23] Y. Yang and M. W. Urban, "Thermodynamics of Self-Healing in Polymeric Materials," in *Healable Polymer Systems*, W. Hayes and B. W. Greenland, Eds. Cambridge: Royal Society of Chemistry, 2013, ch. 5, pp. 126–148. [Online]. Available: http://ebook.rsc.org/?DOI=10.1039/ 9781849737470-00126

[24] C. C. Hornat and M. W. Urban, "Entropy and Interfacial Energy Driven Self-healable Polymers," *Nature Communications*, vol. 11, no. 1, pp. 1–9, 2020. [Online]. Available: http://dx.doi.org/10.1038/s41467-020-14911-y

[25] V. Montano, "Structure and Dynamics of Self-Healing Polyurethanes," Ph.D. dissertation, Delft University of Technology, 2021. [Online]. Available: https://doi.org/10.4233/uuid: 6ad1f5f3-c8b0-4d01-b875-5586a25744bd

[26] F. T. Wall and P. J. Flory, "Statistical Thermodynamics of Rubber Elasticity," *The Journal of Chemical Physics*, vol. 19, no. 12, pp. 1435–1439, dec 1951. [Online]. Available: http://aip.scitation.org/doi/10.1063/1.1748098

[27] P. Flory, *Principles of Polymer Chemistry*.   Cornell University Press, 1953.

[28] V. Montano, M. W. Urban, S. van der Zwaag, and S. García, "Storage and Release of Entropic Energy During Damage-Repair Cycle of Self-Healing Polyurethanes," *Unpublished*, 2021.

[29] C. C. Hornat, Y. Yang, and M. W. Urban, "Quantitative Predictions of Shape-Memory Effects in Polymers [Supporting Information]," *Advanced Materials*, 2017.

[30] H. M. James and E. Guth, "Theory of the Elastic Properties of Rubber," *The Journal of Chemical Physics*, vol. 11, no. 10, pp. 455–481, oct 1943. [Online]. Available: http: //aip.scitation.org/doi/10.1063/1.1723785

[31] L. R. G. Treloar, *The Physics of Rubber Elasticity*.   USA: Oxford University Press, 1975.

[32] H. M. van der Kooij, "Let There Be Light : Quantitative Imaging of Nanoscale Dynamics in Polymer Materials," Ph.D. dissertation, Wageningen University, aug 2020. [Online]. Available: https://research.wur.nl/en/publications/3a48ede7-9fcd-4492-9d1a-9196c14fac0b

[33] A. Amon, A. Mikhailovskaya, and J. Crassous, "Spatially Resolved Measurements of Micro-Deformations in Granular Materials Using Diffusing Wave Spectroscopy," *Review of Scientific Instruments*, vol. 88, no. 5, 2017. [Online]. Available: http://dx.doi.org/10.1063/1.4983048

[34] V. Viasnoff, F. Lequeux, and D. J. Pine, "Multispeckle Diffusing-Wave Spectroscopy: A Tool to Study Slow Relaxation and Time-Dependent Dynamics," *Review of Scientific Instruments*, vol. 73, no. 6, p. 2336, 2002.

[35] S. E. Skipetrov, J. Peuser, R. Cerbino, P. Zakharov, B. Weber, and F. Scheffold, "Noise in laser speckle correlation and imaging techniques," *Optics Express*, vol. 18, no. 14, p. 14519, 2010.

[36] P. Zakharov and F. Scheffold, "Single Light Scatterig and Radiative Transfer," in *Light Scattering Reviews 4*, A. A. Kokhanovsky, Ed.   Berlin: Springer, 2009, ch. 8, pp. 433–467.

[37] S. Gomarasca, "On the Use of Laser Speckle Imaging to Study Local Polymer Dynamics," MSc. Thesis, TU Delft University, 2018. [Online]. Available: http://resolver.tudelft.nl/uuid: fc526722-4b8f-4a08-9c37-998a20f62d92

[38] X. Xiong, L. Zhou, R. Ren, S. Liu, and P. Chen, "The thermal decomposition behavior and kinetics of epoxy resins cured with a novel phthalide-containing aromatic diamine," *Polymer Testing*, vol. 68, no. December 2017, pp. 46–52, jul 2018. [Online]. Available: https://doi.org/10.1016/j. polymertesting.2018.02.012https://linkinghub.elsevier.com/retrieve/pii/S014294181731927X

[39] S. Matsumura, A. R. Hlil, C. Lepiller, J. Gaudet, D. Guay, Z. Shi, S. Holdcroft, and A. S. Hay, "Stability and Utility of Pyridyl Disulfide Functionality in RAFT and Conventional Radical Polymerizations," *Journal of Polymer Science: Part A: Polymer Chemistry*, vol. 46, no. April, pp. 7207–7224, 2008.

[40] A. V. Tobolsky, D. W. Carlson, and N. Indictor, "Rubber elasticity and chain configuration," *Journal of Polymer Science*, vol. 54, no. 159, pp. 175–192, 1961.

[41] C. W. Macosko and D. R. Miller, "A New Derivation of Average Molecular Weights of Nonlinear Polymers," *Macromolecules*, vol. 9, no. 2, pp. 199–206, mar 1976. [Online]. Available: https://pubs.acs.org/doi/abs/10.1021/ma60050a003

[42] L. W. Hill, "Calculation of crosslink density in short chain networks," *Progress in Organic Coatings*, vol. 31, no. 3, pp. 235–243, 1997.

[43] J. S. Nakka, K. M. B. Jansen, and L. J. Ernst, "Effect of chain flexibility in the network structure on the viscoelasticity of epoxy thermosets," *Journal of Polymer Research*, vol. 18, no. 6, pp. 1879–1888, nov 2011. [Online]. Available: http://link.springer.com/10.1007/s10965-011-9595-5

A

DMA Entropy Calculations

Instructions:

Output value   (1) **Input** the **required values** into the **red/orange cells.**

Outputs to make equal   (2) Then **change** the **purple cell value** to make the **blue cells** approximately **equal to each other**, to ~ 3-4 decimals at least (try using the goal seek fxn to start)

Variable/Output   (3) Once that is done, the **values** in the **blue, green,** and **purple output cells** are **calculated.**

Required Inputs

In bold the samples that have been used to perform the calculations th[...] These DMA experiments were all run at 10 mm gauge length, 10 Hz, 10 μm amplitude, 2°C/min, 125% force track ratio

Molar ratio	Sample Name↓	εmax (%)	σR (MPa)	σSF @ Lmax (MPa)	ΔSs (kJ/m3)	average ΔSS (kJ/m3)	ΔSR (kJ/m3)	average ΔSR (mol/m^3)	νj Junction-p (mol/m^3)	Mj (g/mol)	ρ Density (g/cm^3)	Lo RT initial L (mm)	w width (mm)	t thickness (mm)	T (Li) Temp @ Li (°C)	Li Length @ "i" (mm)	T (Lmax) Temp Lmax (°C)	Fs @ Lmax SF @ Lmax (N)	L @ "Lmax" (mm)	Lmax (mm)	T (Lmin) Temp Lmin (°C)	Lmin L @ "Lmin" (mm)
1.00	EpiAnc_21 - Bonus	9,5323525	0,258507	0,258507538	12,587366		-10,4561		346,614	3173,56	1,1	9,90511	3,98	0,9	29,49	9,98748	69,49	0,925974		10,8493	93,55	10,2805
1.00	EpiAnc_25 - 2525	3,1786539	0,18999	0,18991579	3,04		-0,66		705,10	1560,06	1,1	9,99228	4,89	0,85	27,4	10,0085	77,4	0,7897		10,3099	89,16	10,2685
1.00	EpiAnc_25 - 2530	3,6906309	0,171117	0,171120846	3,20	4,10	-0,43	-0,47	550,15	1999,45	1,1	9,99531	5,51	0,87	27,06	9,99507	77,06	0,820302		10,3642	89,93	10,332
1.00	EpiAnc_25 - 2566	7,4178268	0,159609	0,159609572	6,05		-0,33		263,687	4171,61	1,1	9,99201	5,31	0,82	27,68	10,0125	77,68	0,694972		10,7332	91,8	10,6977
1.00	EpiAnc_26 - 2531	3,9213014	0,173268	0,173273272	3,43		-1,08		524,40	2097,64	1,1	9,97832	5,15	0,68	27,75	9,99504	77,75	0,608803		10,3696	95,2	10,2942
1.00	EpiAnc_26 - 2532	7,5887488	0,159064	0,159064603	6,18	4,01	-0,90	-0,81	256,27	4292,35	1,1	9,95197	5,12	0,65	29,03	9,96065	79,03	0,529367		10,7072	93,14	10,6249
1.00	EpiAnc_26 - 2572	3,3429083	0,143152	0,143151098	2,41		-0,44		504,98	2178,3	1,1	9,9913	5,17	0,68	28,08	10,0127	78,08	0,503262		10,3253	91,44	10,2873
1.00	EpiEff_31 - 2551	20,74542	0,226346	0,226635713	24,80		-22,98		164,23	6697,92	1,1	10,0051	4,86	1,15	34,69	10,0466	44,69	1,26511		12,0807	64,18	10,5288
1.00	EpiEff_31 - 2555	19,840287	0,189841	0,189848155	19,86	21,97	-18,56	-20,68	142,85	7700,39	1,1	10,018	5,19	1,09	35,2	10,0314	45,20	1,0740		12,0056	67,02	10,4898
1.00	EpiEff_31 - 2556	20,252153	0,199023	0,19902777	21,25		-20,49		147,49	7458,13	1,1	10,1367	5,19	1,09	34,48	10,1192	44,48	1,1259		12,1896	66,65	10,4989
1.00	EpiEff_09 - 17	19,349075	0,167943	0,167944995	17,11		-16,91		131,66	8354,85	1,1	10,1302	5,14	1,1	29,04	10,1792	39,04	0,9496		12,0903	61,88	10,3261
1.00	EpiEff_09 - 19	10,619196	0,188065	0,188066791	10,29	15,34	-4,90	-13,40	251,191	4379,14	1,1	10,0469	4,78	1,08	28,48	10,0886	38,48	0,9709		11,1138	60,08	9,3417
1.00	EpiEff_09 - 20	19,456555	0,181935	0,181940566	18,64		-18,39		142,86	7699,85	1,1	10,3672	4,63	1,12	27,06	10,4082	37,06	0,9435		12,3843	60,22	10,1502

Lo = Either the Length of the sample at room Temp right after loading & "FLOATING", or the Length at the Starting Temp of the EXP after hitting "MEASURE". Either is fine, but it should be true that Lo < Li. I took the first measured length

Li = The sample length during the experiment approximately right before the elongation phase of the VLT begins. Usually the length of the sample about 25-40C below the T(Lmax). I took the length 50C below T(Lmax)

Lmin = The sample length at the minimum point at the end of the VLT, so after the contraction phase has finished.

Figure A.1: Screenshot of the excel file used for entropy calculations with the DMA results.

B

DMA Results

Obtained results from DMA measurements.

Anc Samples

Two batches of the Anc formulation have been prepared. Figures B.1 - B.6 present the DMA results of the two batches.
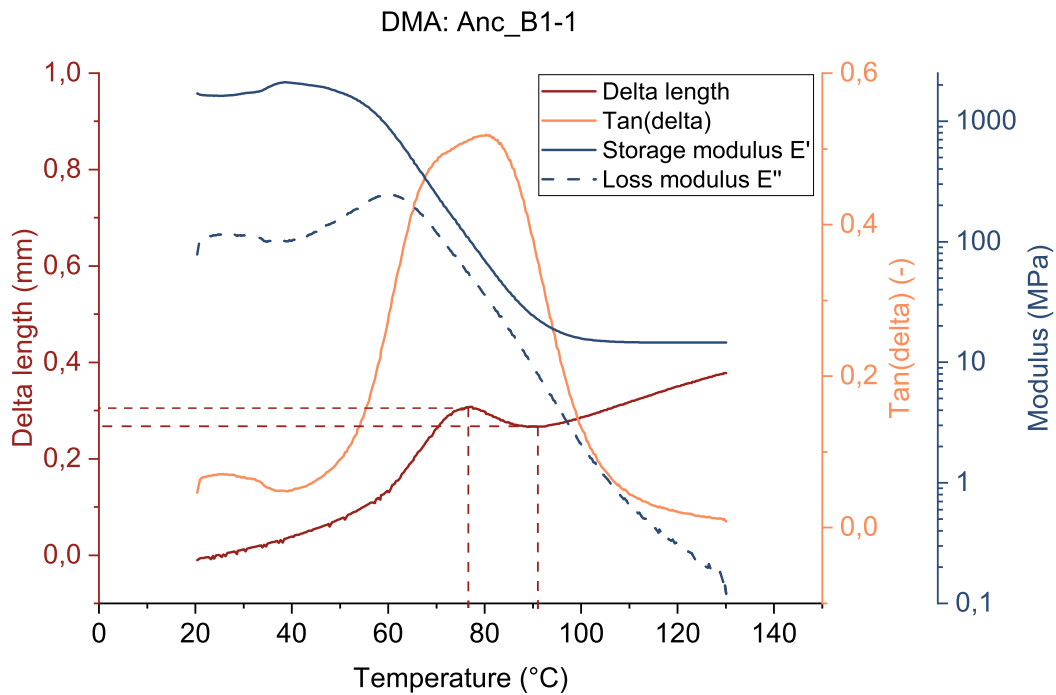
Figure B.1: DMA result AncB_1-1
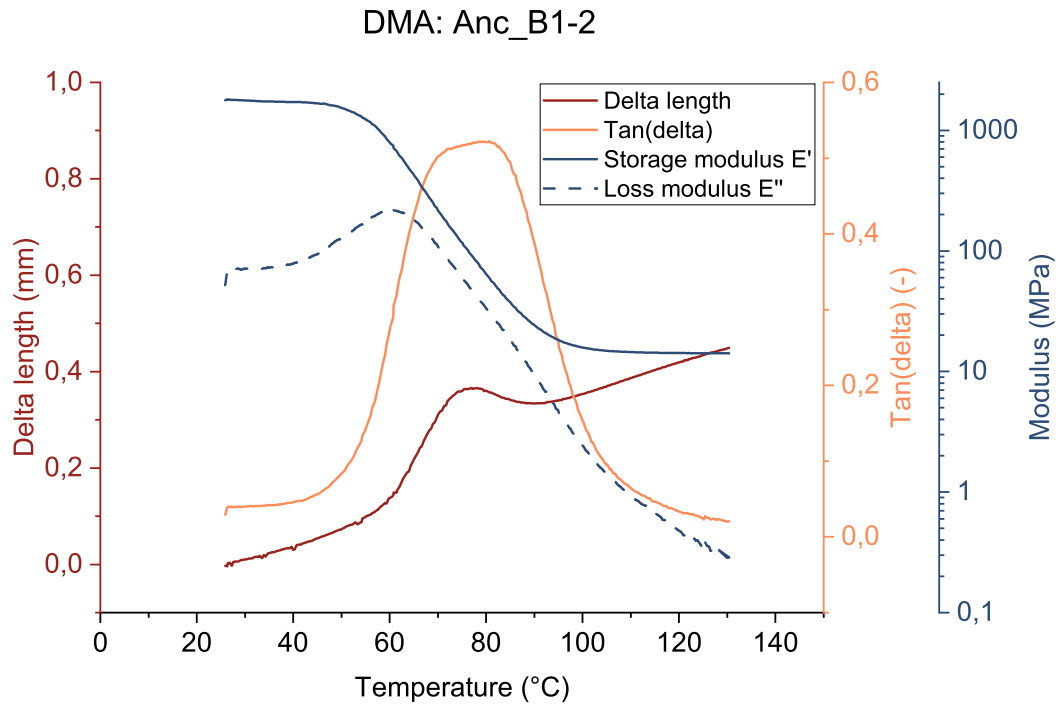
Figure B.2: DMA result AncB_1-2
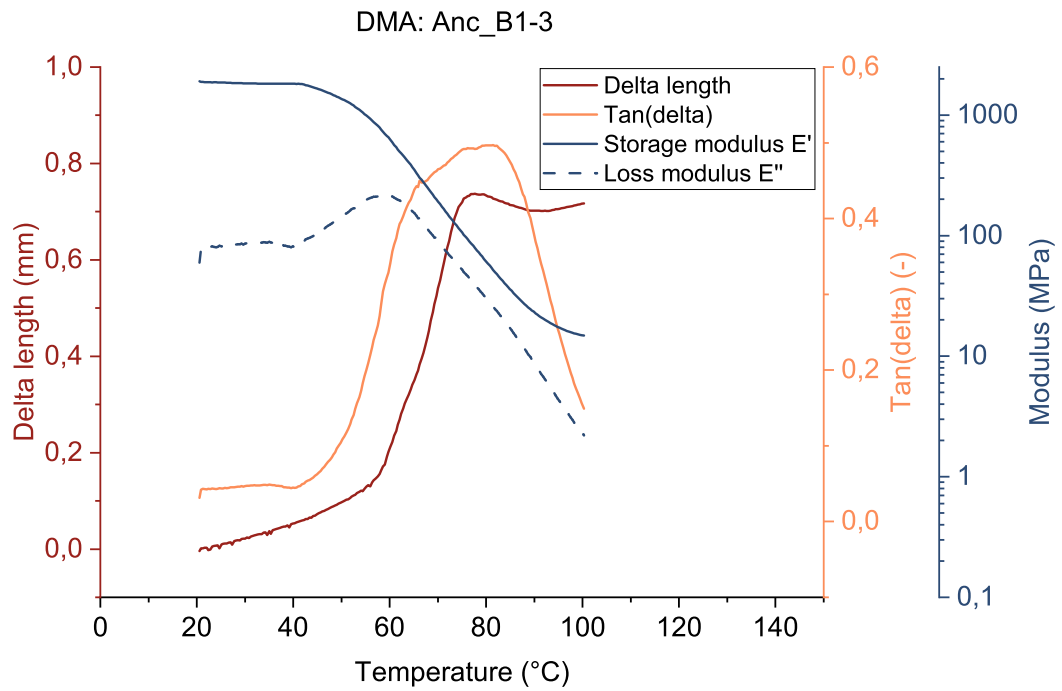
Figure B.3: DMA result AncB_1-3
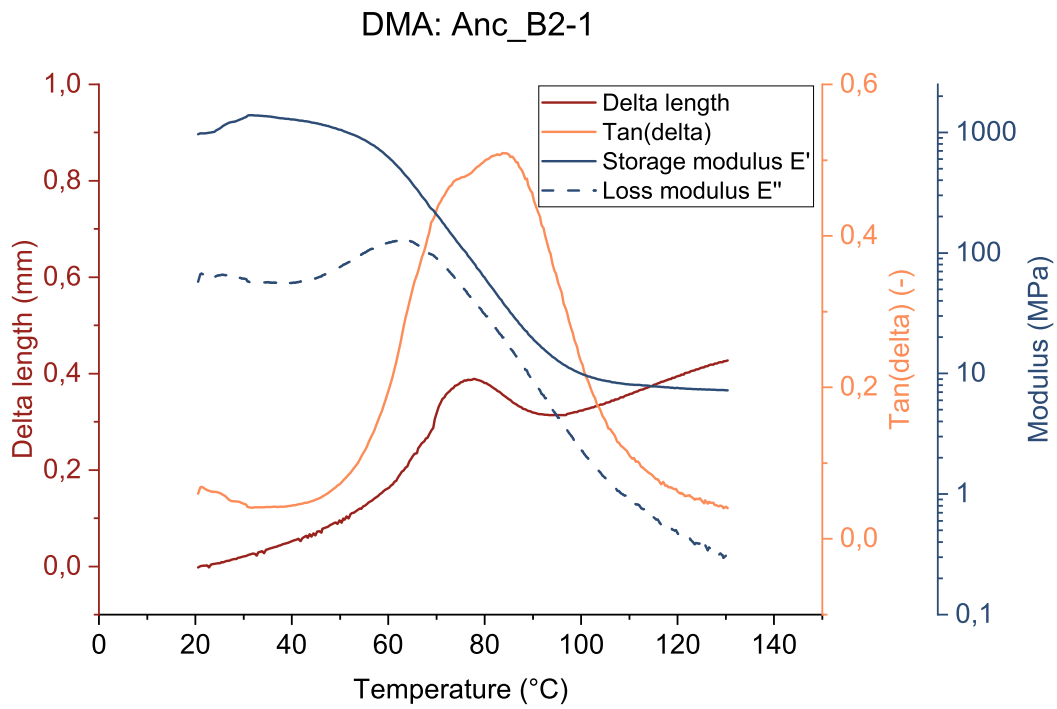
Figure B.4: DMA result AncB_2-1
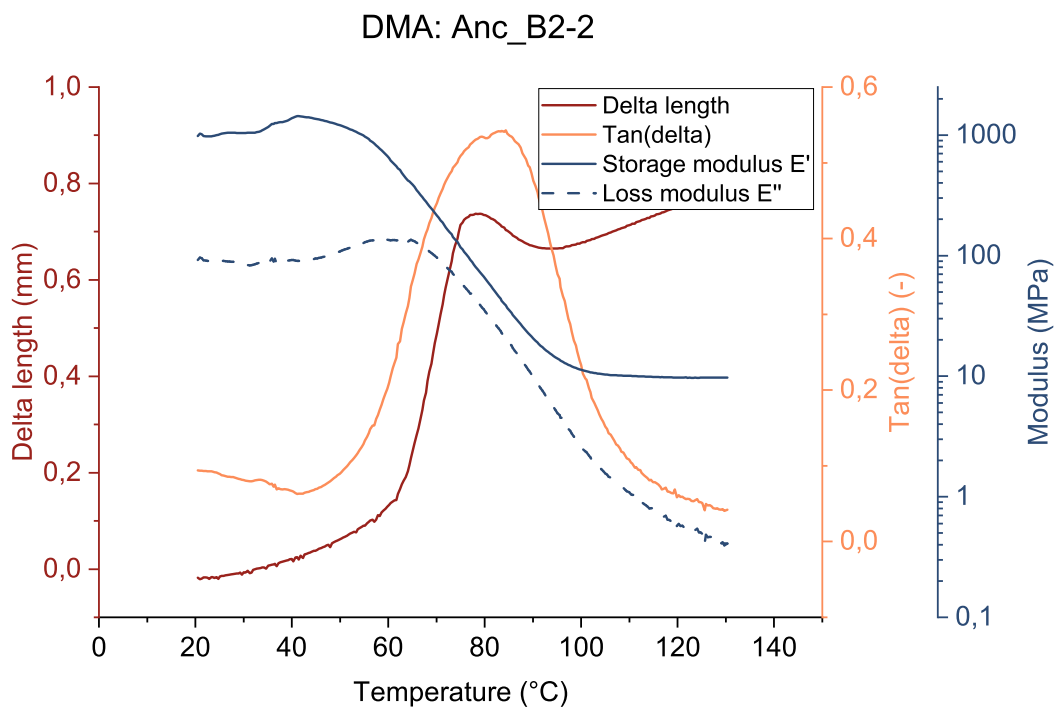
Figure B.5: DMA result AncB_2-2
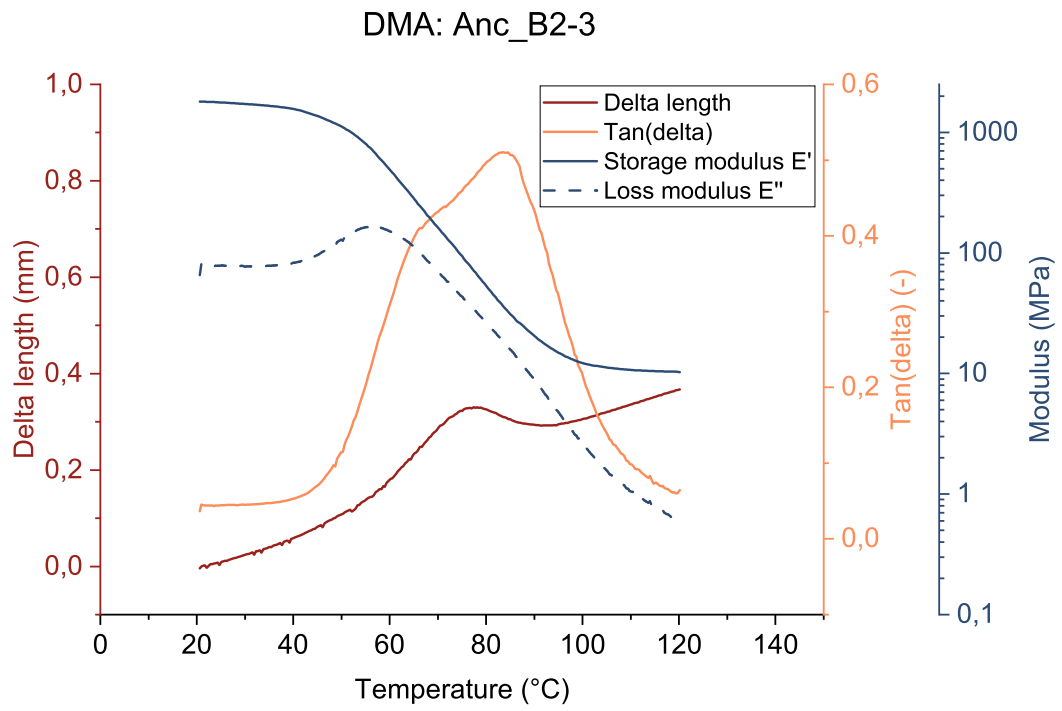
Figure B.6: DMA result AncB_2-3

Jeff Samples

Two batches of the Jeff formulation have been prepared. Figures B.7 - B.12 present the DMA results of the two batches.
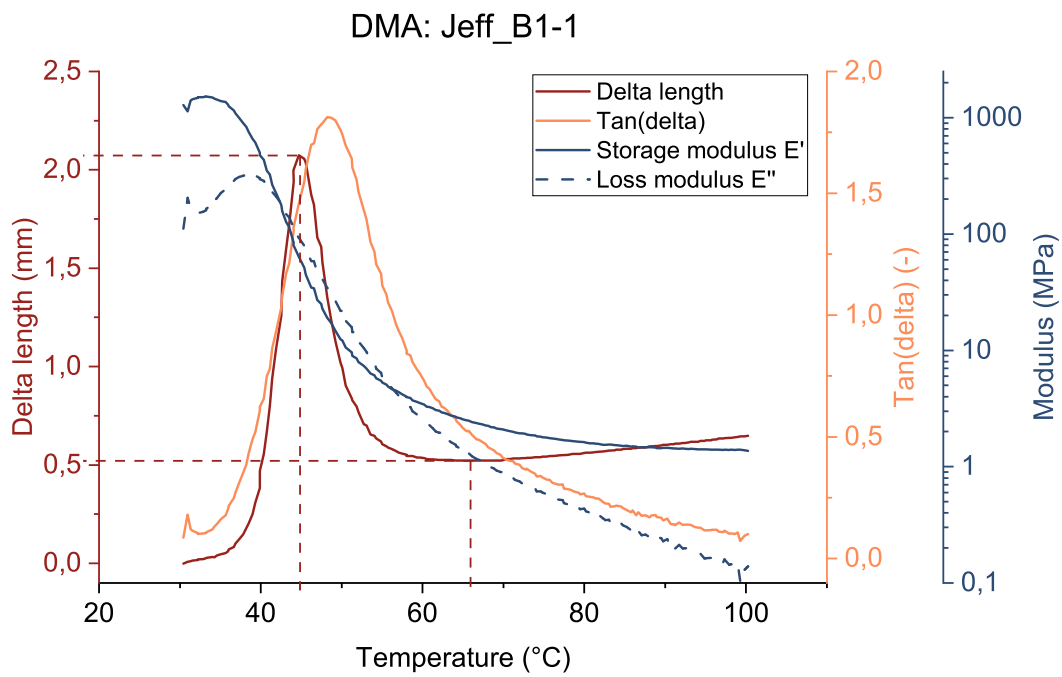
Figure B.7: DMA result Jeff_B1-1
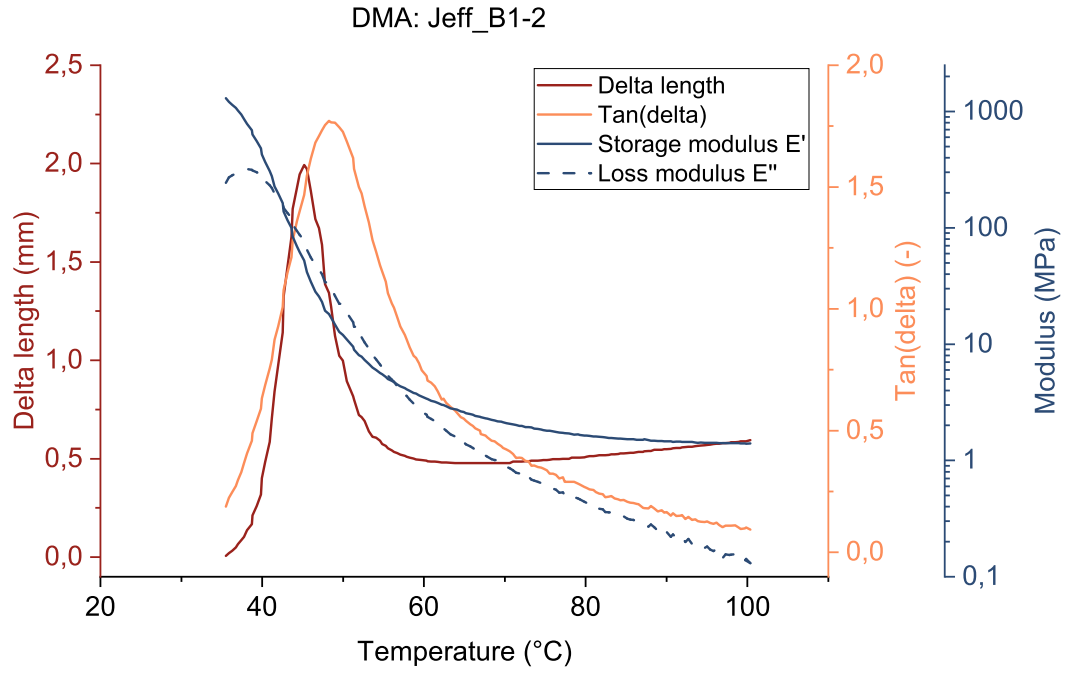
Figure B.8: DMA result Jeff_B1-2
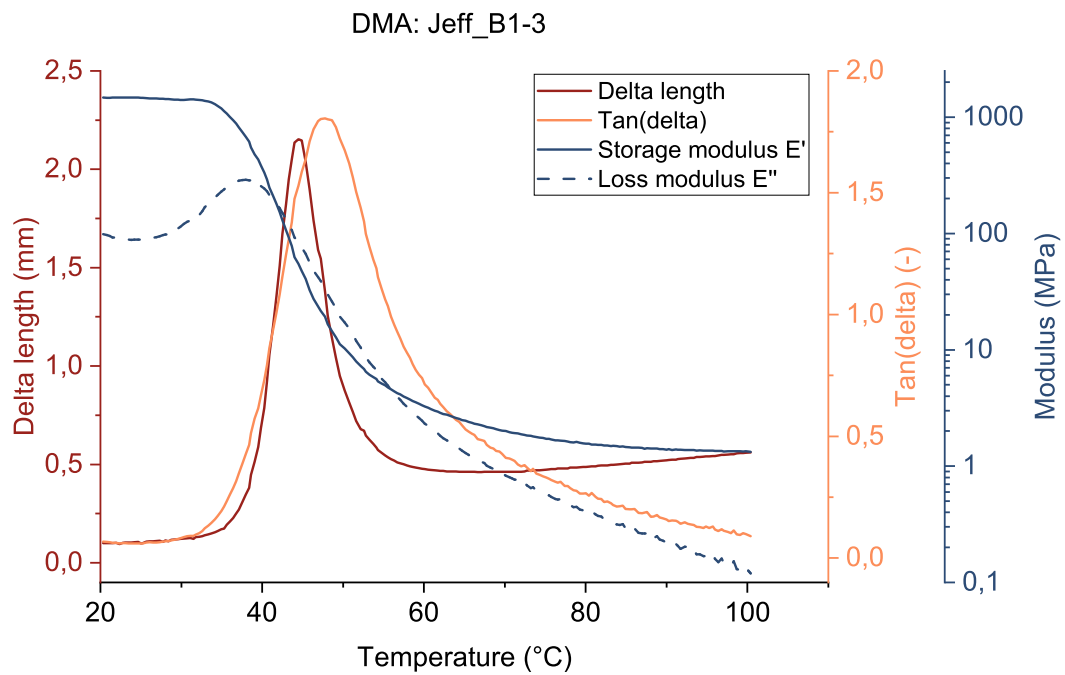
Figure B.9: DMA result Jeff_B1-3
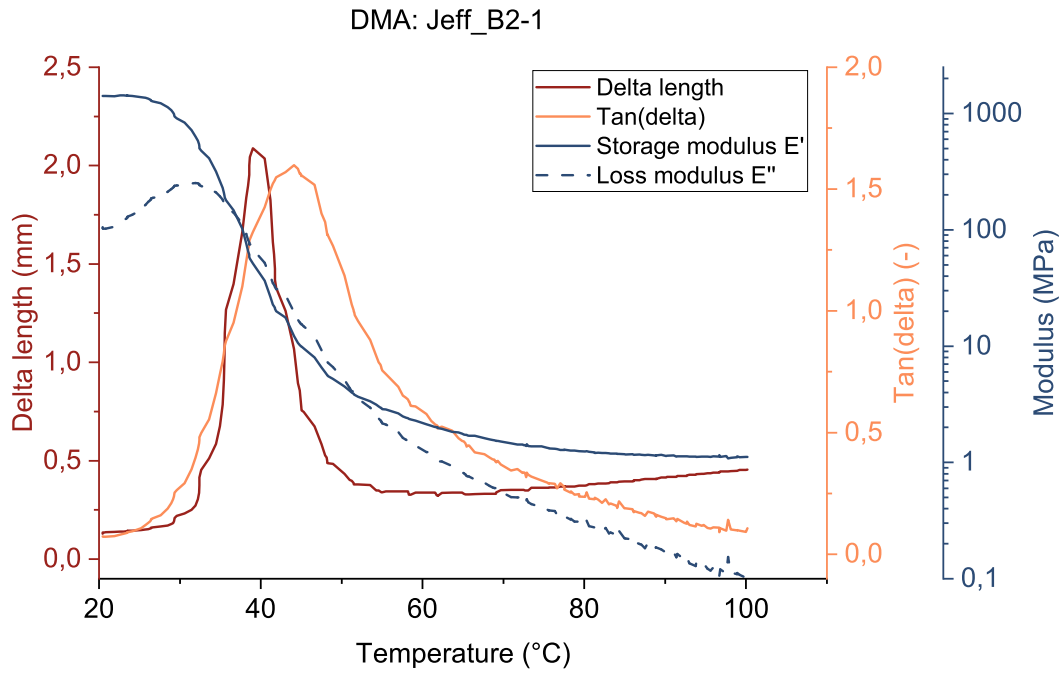
Figure B.10: DMA result Jeff_B2-1
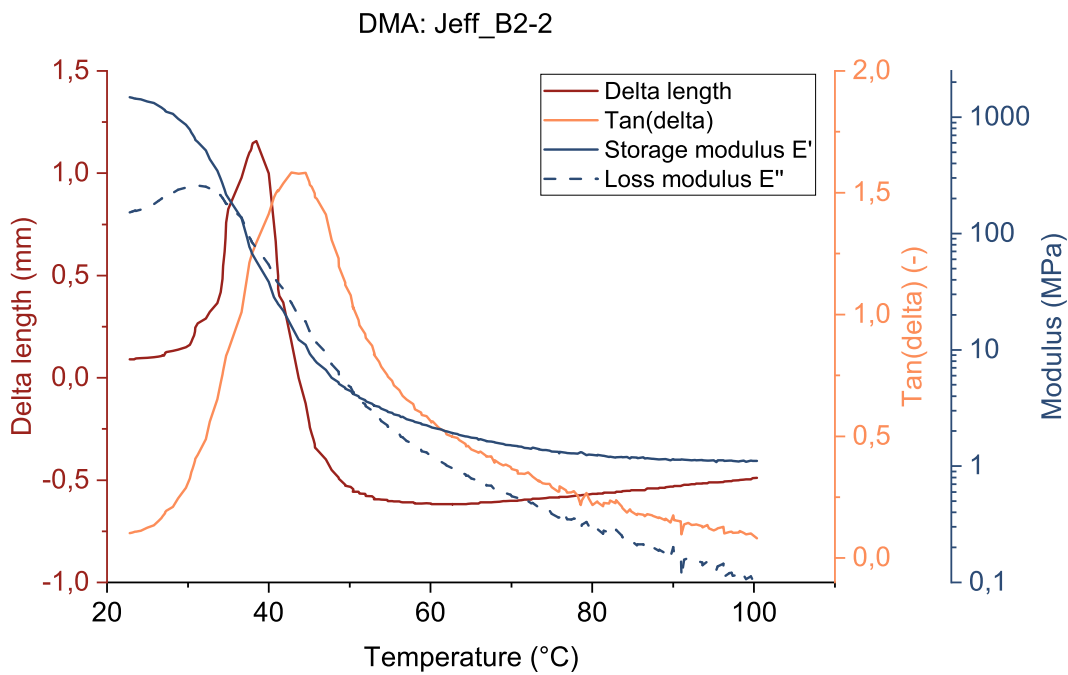
Figure B.11: DMA result Jeff_B2-2
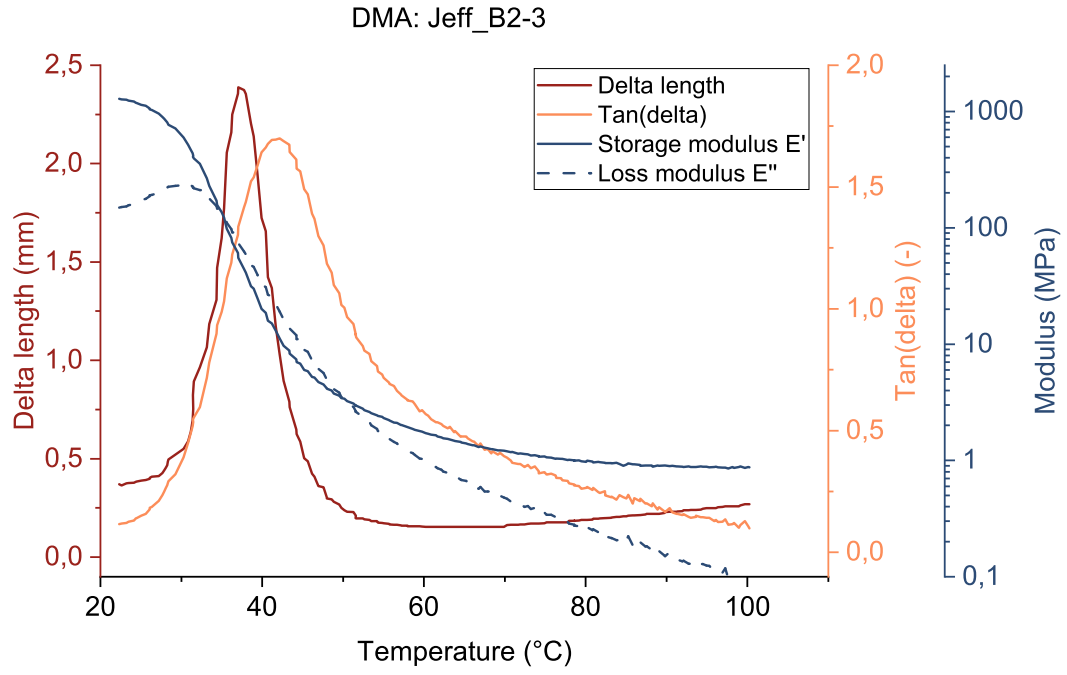
Figure B.12: DMA result Jeff_B2-3

C

LSI Results

Obtained results from LSI measurements.

Non-strained Sample

Anc samples:

Temperature ramp 2,3°C/min (Anc_B1)
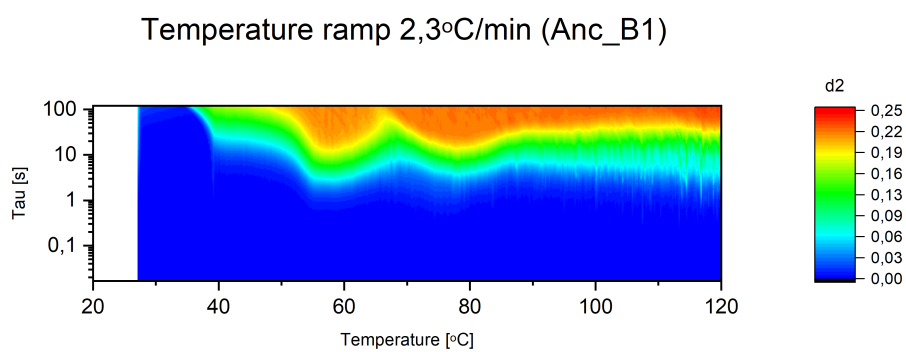
Figure C.1: Non-strained sample temperature ramp Anc_B1

Temperature ramp Anc_B2
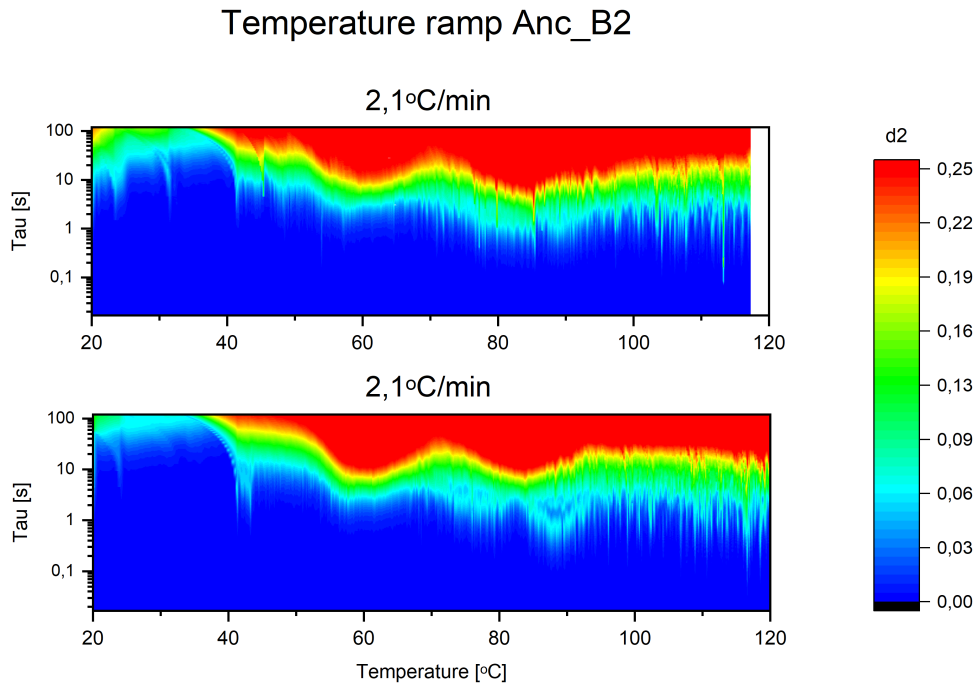
Figure C.2: Two non-strained sample temperature ramps Anc_B2

Jeff samples:

Temperature ramp Jeff_B1
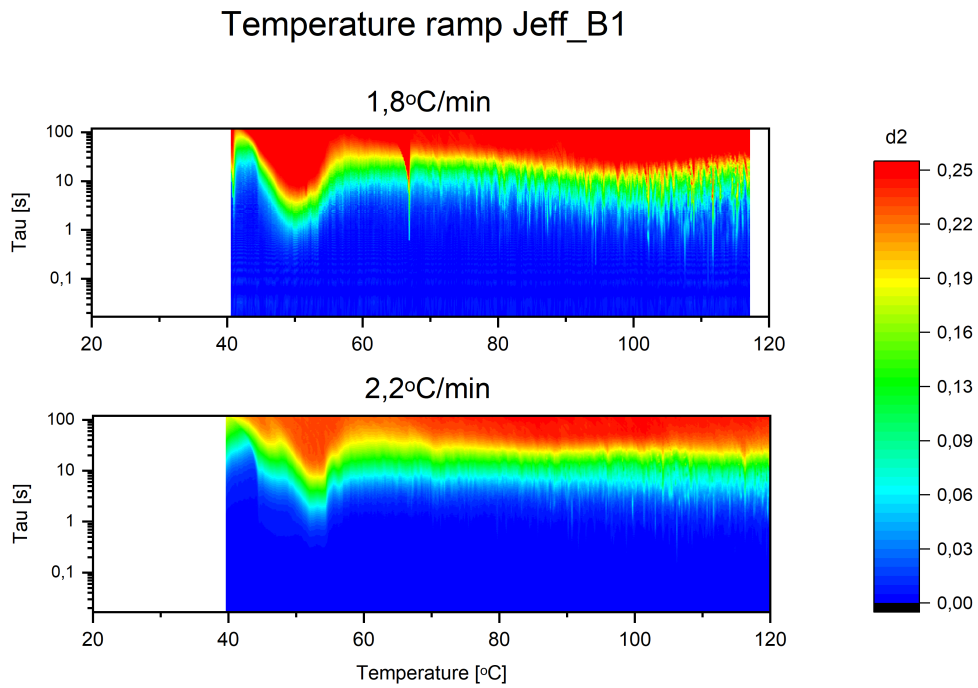
Figure C.3: Two non-strained sample temperature ramps Jeff_B1
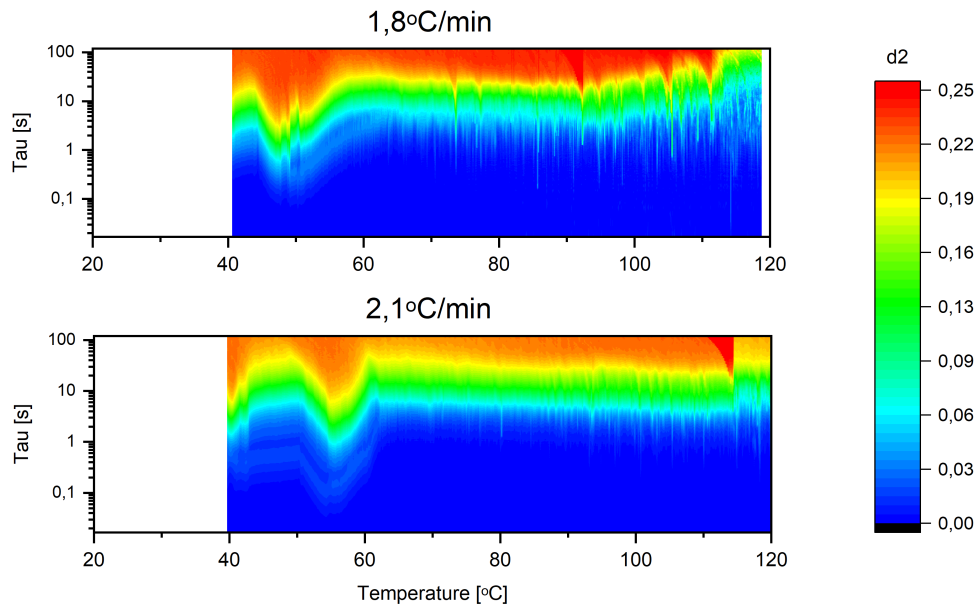
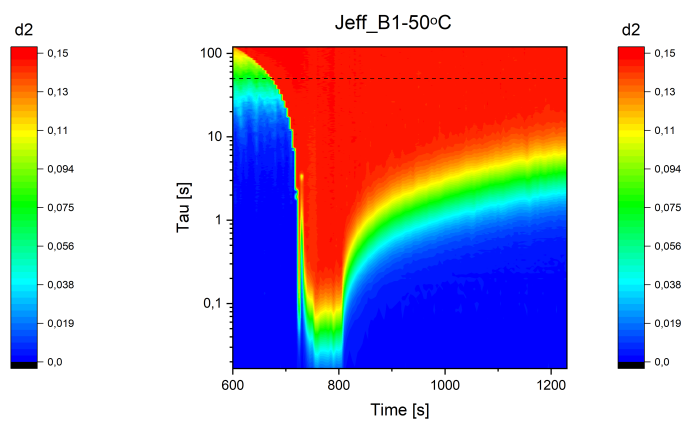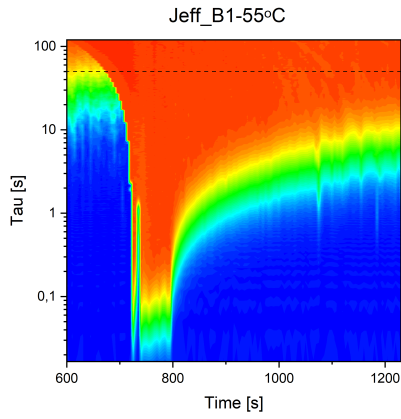Figure C.4: Two non-strained sample temperature ramps Jeff_B2

Strained Sample Room Temperature Tests

Room temperature tensile test to check the method on repeatability. In Figures C.5-C.13 all the color plots are shown.

Before the runs at the indicated temperatures, which followed from DMA measurements, nine tensile tests were executed at "room temperature" (only the heat from the laser was of influence), to test the repeatability of the method.

For the room temperature tests the first two minutes (120s) nothing happened whereafter the elongation started, followed by the relaxation that was measured for five minutes. As can be seen in Figures C.5-C.9 there are marginal differences visible between the plots. Figures C.5 and C.6 show an almost identical development with a difference at about 190 seconds. In Figure C.8 increased dynamics over a wider range of frequencies are visible as opposed to the other plots.
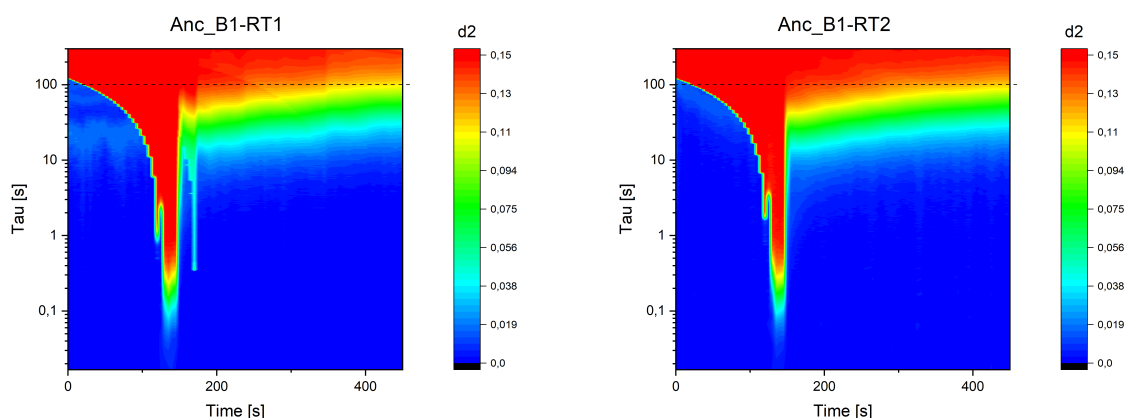
Figure C.5: Strained Sample Temperature Ramp Anc_B1-RT1   Figure C.6: Strained Sample Temperature Ramp Anc_B1-RT2
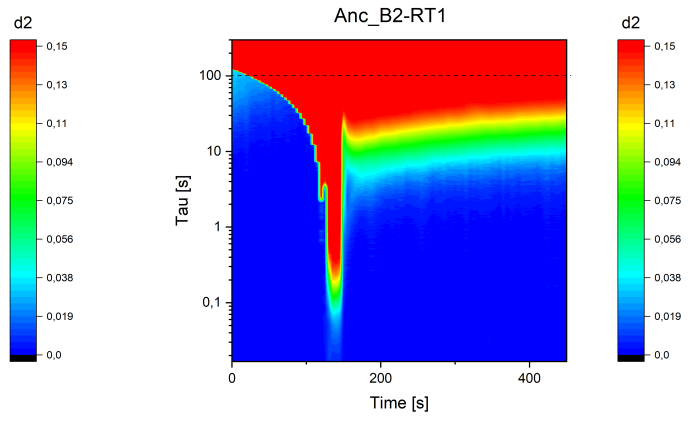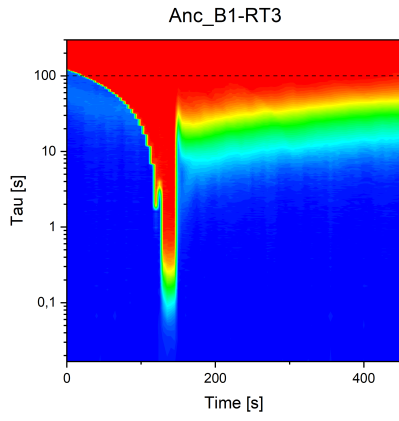
Figure C.7: Strained Sample Temperature Ramp Anc_B1-RT3

Figure C.8: Strained Sample Temperature Ramp Anc_B2-RT1
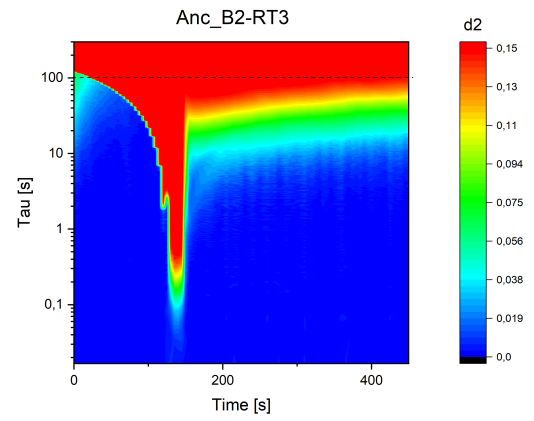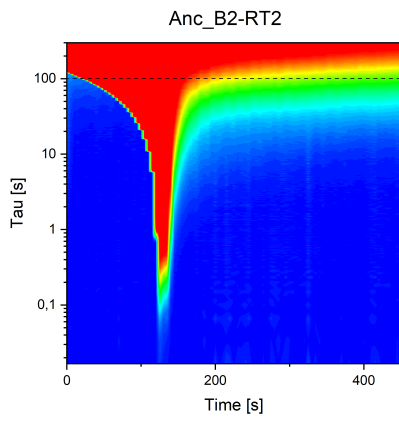
Figure C.9: Strained Sample Temperature Ramp Anc_B2-RT2

Figure C.10: Strained Sample Temperature Ramp Anc_B2-RT3
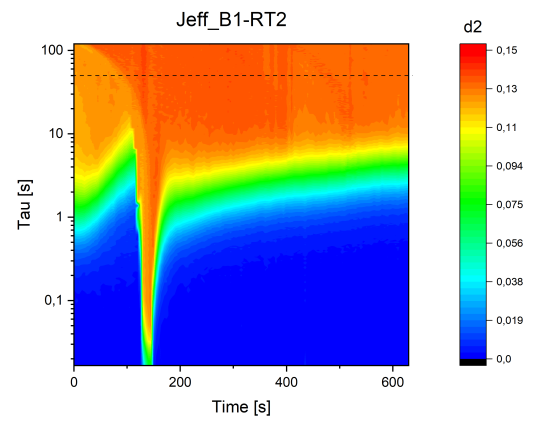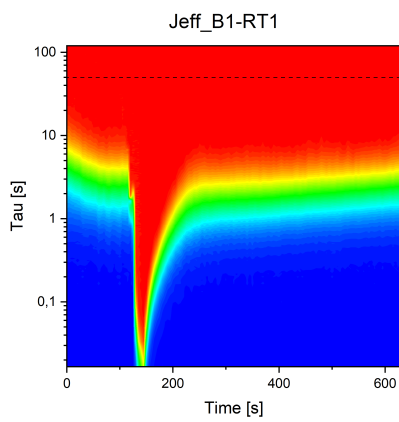
Figure C.11: Strained Sample Temperature Ramp Jeff_B1-RT1

Figure C.12: Strained Sample Temperature Ramp Jeff_B1-RT2
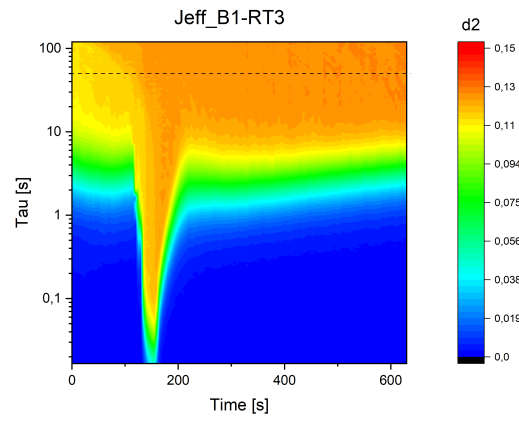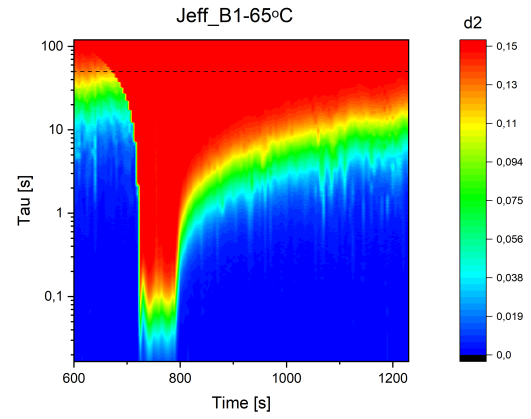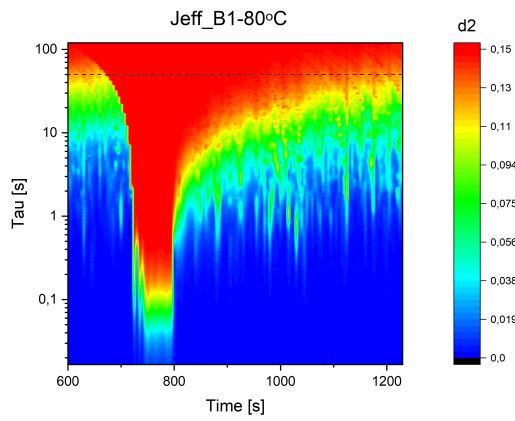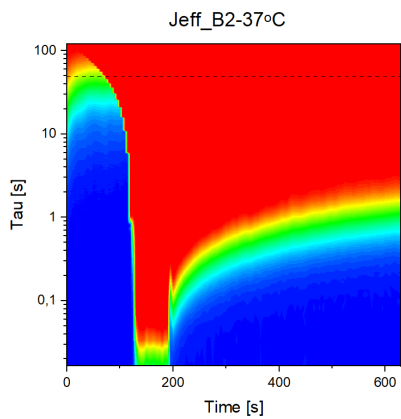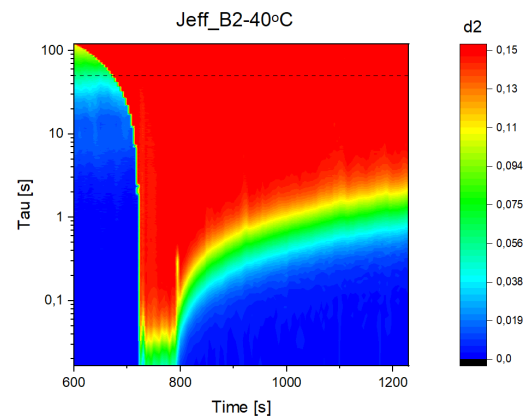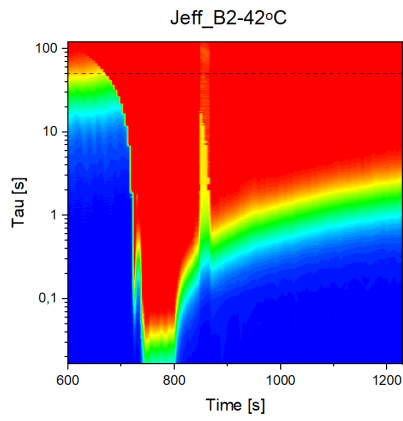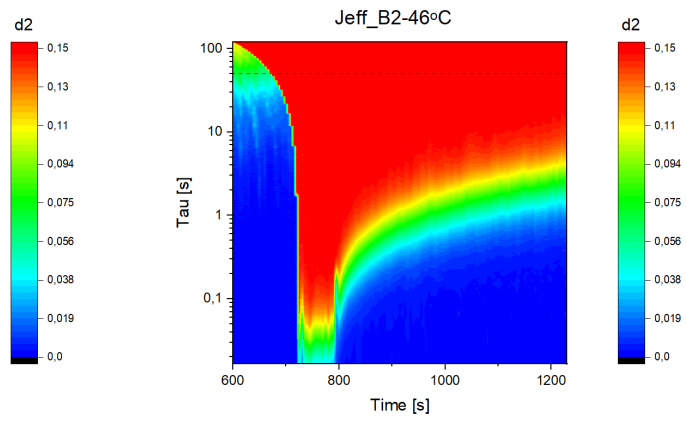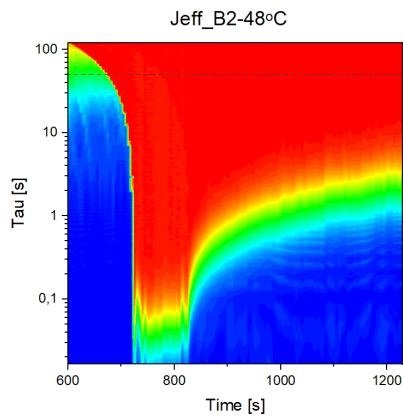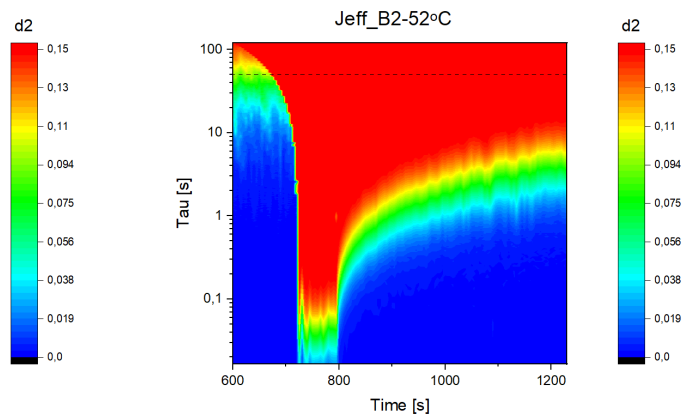
Figure C.13: Strained Sample Temperature Ramp Jeff_B1-RT3

Strained Sample

With samples from both batches one temperature ramp has been carried out, so two ramps per epoxy type.

Anc_B1 Samples
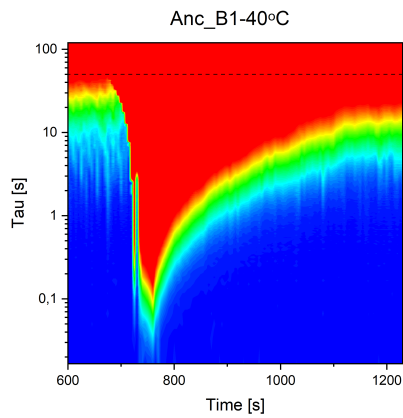
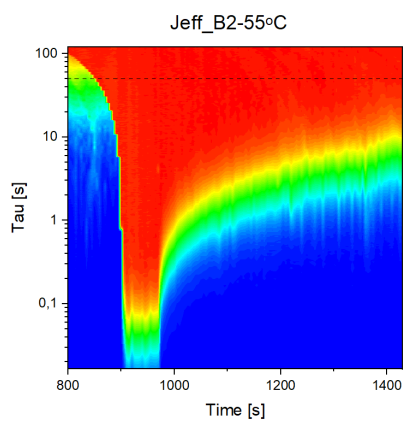

Figure C.14: Strained Sample Temperature Ramp Anc_B1-40°C
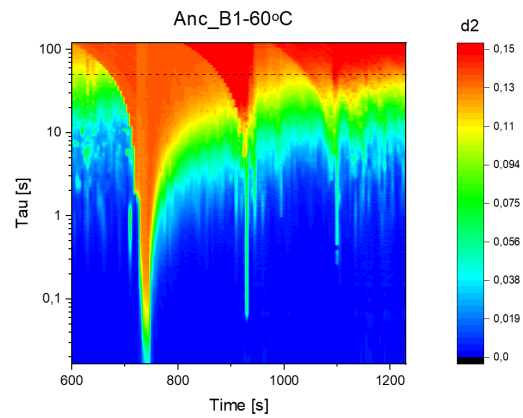
Figure C.15: Strained Sample Temperature Ramp Anc_B1-60°C
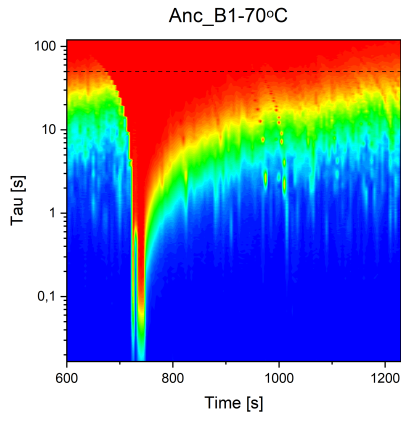
Figure C.16: Strained Sample Temperature Ramp Anc_B1-70°C
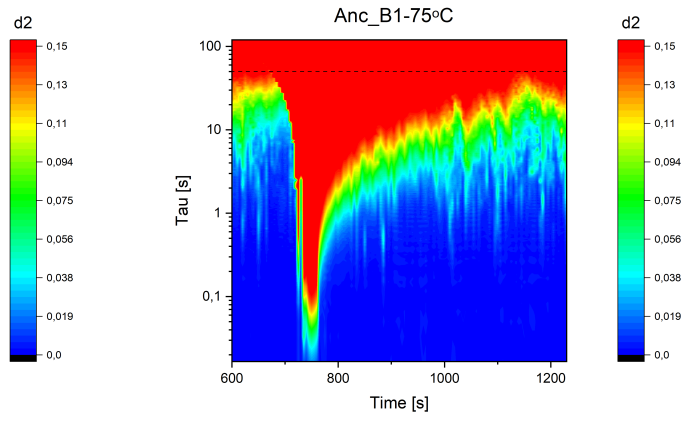
Figure C.17: Strained Sample Temperature Ramp Anc_B1-75°C
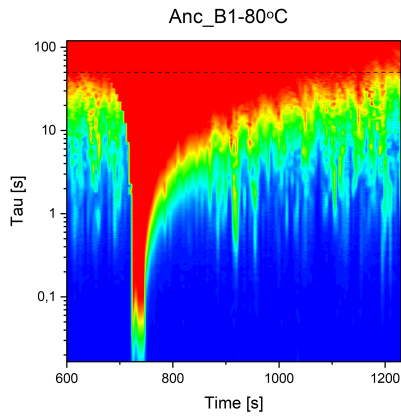
Figure C.18: Strained Sample Temperature Ramp Anc_B1-80°C
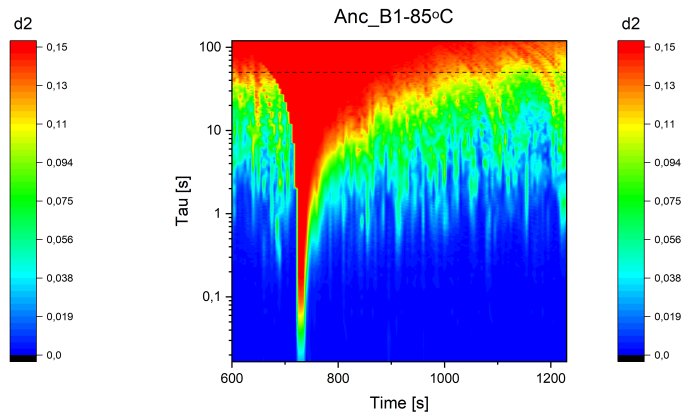
Figure C.19: Strained Sample Temperature Ramp Anc_B1-85°C
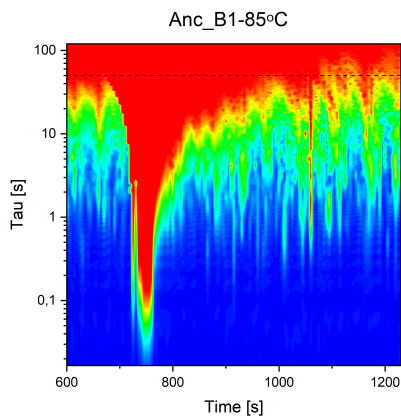
Figure C.20: Strained Sample Temperature Ramp Anc_B1-85°C
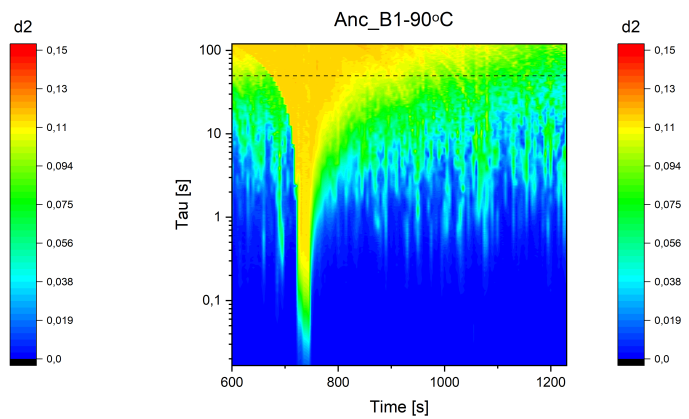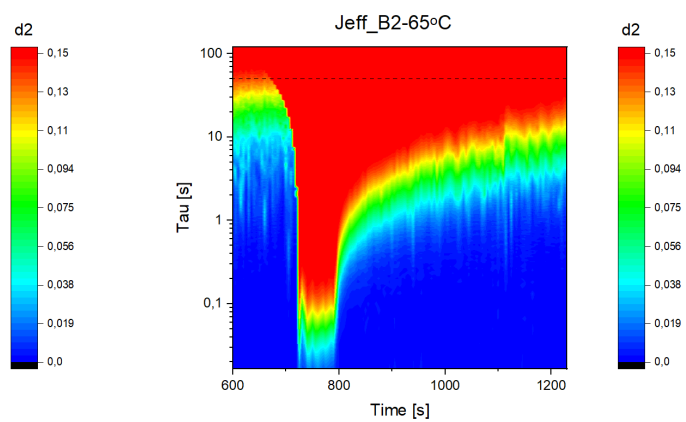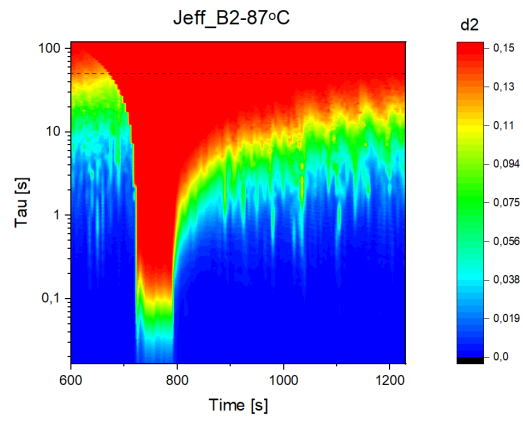

Figure C.21: Strained Sample Temperature Ramp Anc_B1-90°C
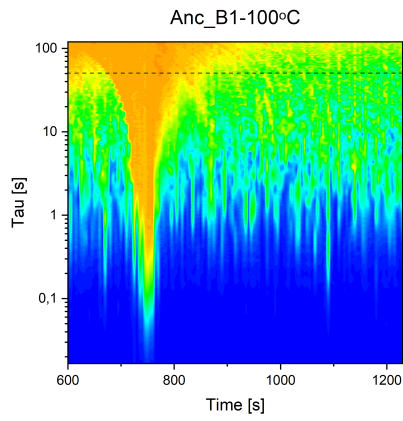
Figure C.22: Strained Sample Temperature Ramp Anc_B1-100°C
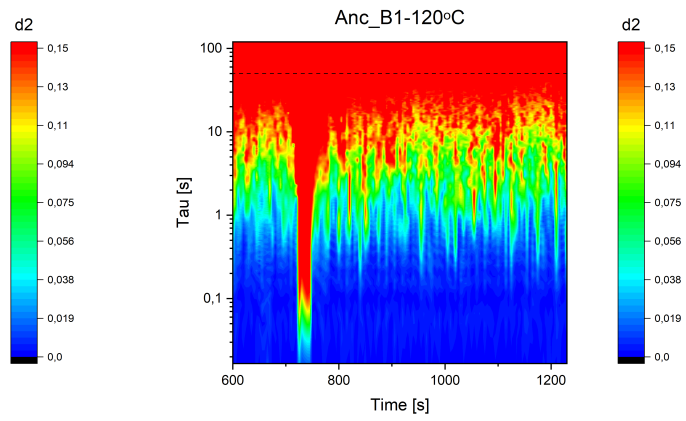
Figure C.23: Strained Sample Temperature Ramp Anc_B1-120°C

Anc_B2 Samples
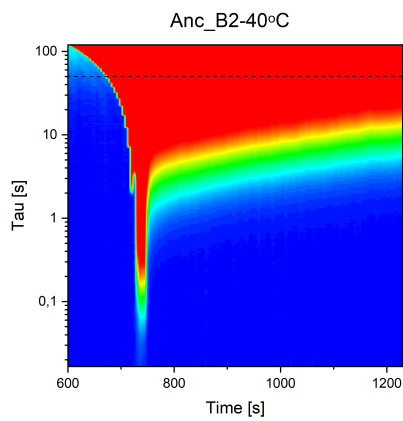
Figure C.24: Strained Sample Temperature Ramp Anc_B2-40°C
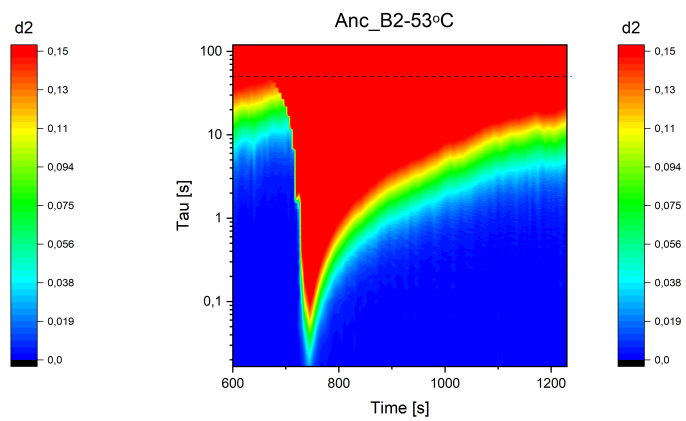
Figure C.25: Strained Sample Temperature Ramp Anc_B2-53°C
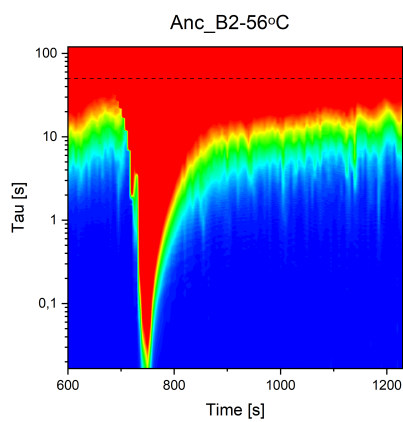
Figure C.26: Strained Sample Temperature Ramp Anc_B2-56°C
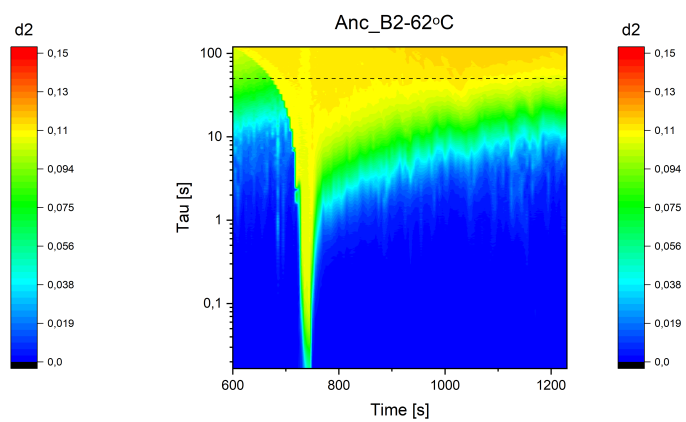
Figure C.27: Strained Sample Temperature Ramp Anc_B2-62°C
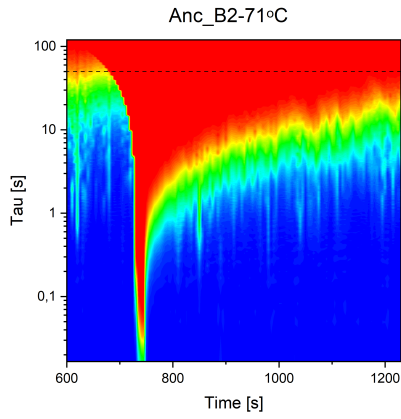
Figure C.28: Strained Sample Temperature Ramp Anc_B2-71°C
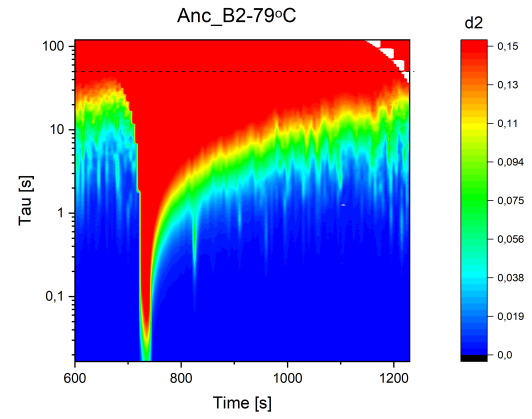
Figure C.29: Strained Sample Temperature Ramp Anc_B2-79°C
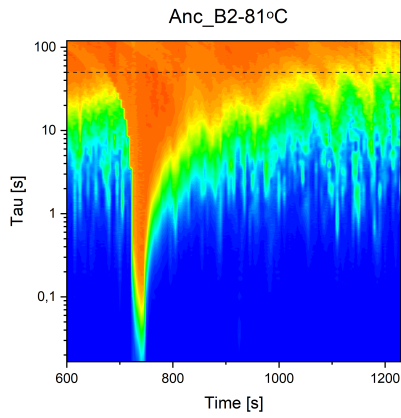
Figure C.30: Strained Sample Temperature Ramp Anc_B2-81°C
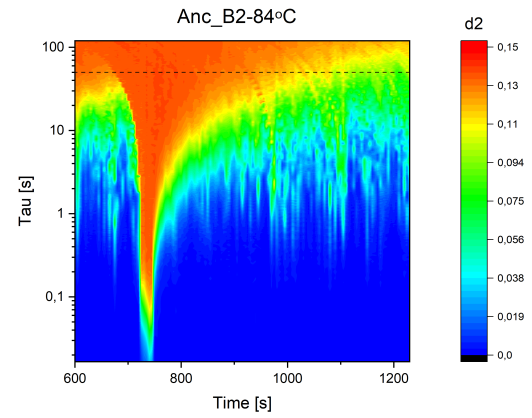
Figure C.31: Strained Sample Temperature Ramp Anc_B2-84°C
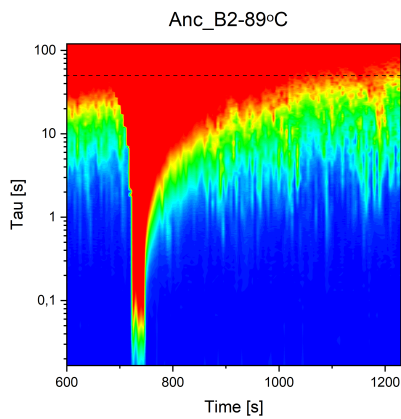
Figure C.32: Strained Sample Temperature Ramp Anc_B2-89°C
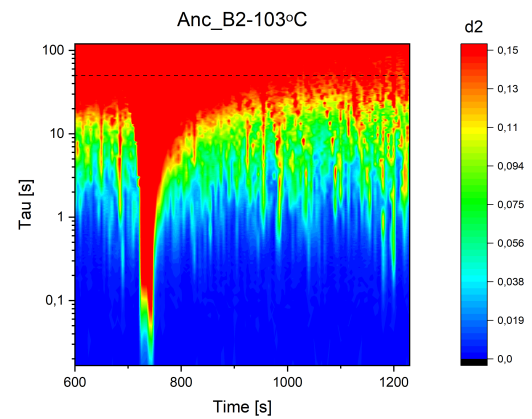
Figure C.33: Strained Sample Temperature Ramp Anc_B2-103°C
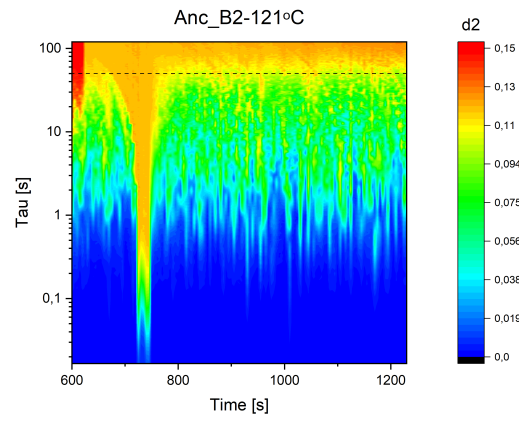
Figure C.34: Strained Sample Temperature Ramp Anc_B2-121°C

Jeff_B1 Samples
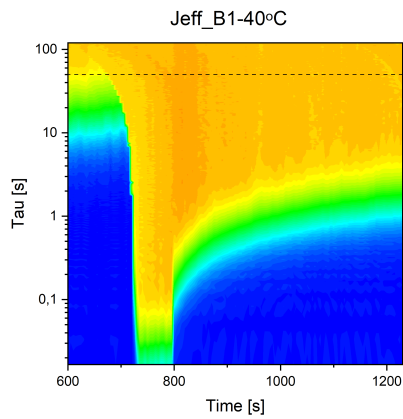
Figure C.35: Strained Sample Temperature Ramp Jeff_B1-40°C
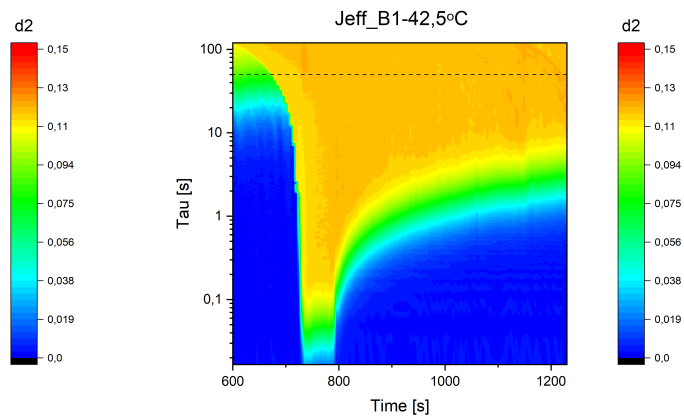
Figure C.36: Strained Sample Temperature Ramp Jeff_B1-42,5°C
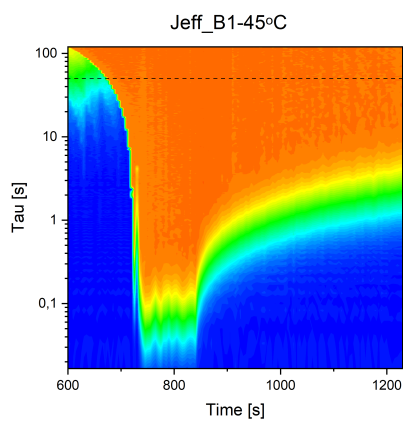
Figure C.37: Strained Sample Temperature Ramp Jeff_B1-45°C

Figure C.38: Strained Sample Temperature Ramp Jeff_B1-50°C

Figure C.39: Strained Sample Temperature Ramp Jeff_B1-55°C

Figure C.40: Strained Sample Temperature Ramp Jeff_B1-65°C

Figure C.41: Strained Sample Temperature Ramp Jeff_B1-80°C

Jeff_B2 Samples

Figure C.42: Strained Sample Temperature Ramp Jeff_B2-37°C

Figure C.43: Strained Sample Temperature Ramp Jeff_B2-40°C

Figure C.44: Strained Sample Temperature Ramp Jeff_B2-42°C

Figure C.45: Strained Sample Temperature Ramp Jeff_B2-46°C

Figure C.46: Strained Sample Temperature Ramp Jeff_B2-48°C

Figure C.47: Strained Sample Temperature Ramp Jeff_B2-52°C

Figure C.48: Strained Sample Temperature Ramp Jeff_B2-55°C

Figure C.49: Strained Sample Temperature Ramp Jeff_B2-65°C

Figure C.50: Strained Sample Temperature Ramp Jeff_B2-87°C

Additional Analysis Method of LSI Strained Sample Temperature Ramp

Another method to look at relaxation of strained samples is explained using an example as depicted for several values in Figure C.51. τ_0 can be obtained for certain moments in time, zero seconds is set as the moment elongation ends and relaxation thus starts. By combining this data for a time interval over all the measured temperatures, relaxation times versus temperature graphs are obtained as shown in Figures C.52-C.55.

In these graphs an increasing relaxation time on a logarithmic scale is depicted on the y-axis, whereas the x-axis depicts a linear temperature gradient. The differences in time are visible by the coloured scale that runs from zero until 150 seconds, where blue is short after elongation and red longer afterwards. For the two Anc plots a similarity can be seen in the neatly arranged data points for lower temperatures until about 80°C whereafter the values of τ_0 intermingle completely and no order can be observed. Another remarkable feature are the drops in τ_0 at about 55°C and between 70°C and 80°C. At the lowest temperature of 40°C both plots show high relaxation times.

The plots showing results from measurements with the Jeff samples are distinctly different from Figure C.52 and C.53 because the relaxation times at the lower temperatures are much shorter to start with. The datapoints stay better separated/organized over the complete measured temperature range as well. From about 50°C on, the relaxation times increase slightly across the entire pack while they show more fluctuations and shorter times before that temperature.
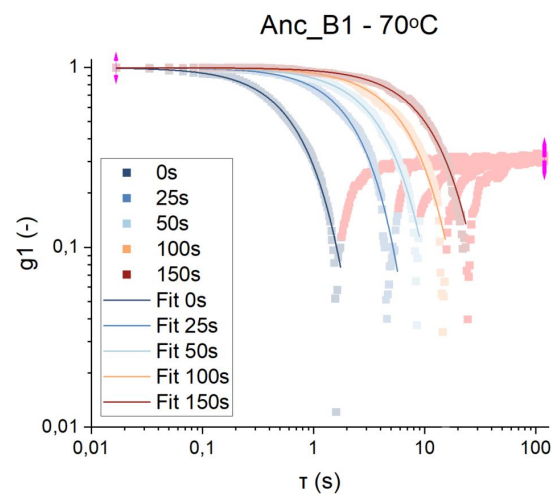
Figure C.51: The g_1 values for several sample times are plotted to show the fitting procedure. The shape of the g_1 data points follows first a decay after which they increase again reaching a plateau value. In order to obtain good fitting results only the first decay is fitted the subsequent data points are masked (red).
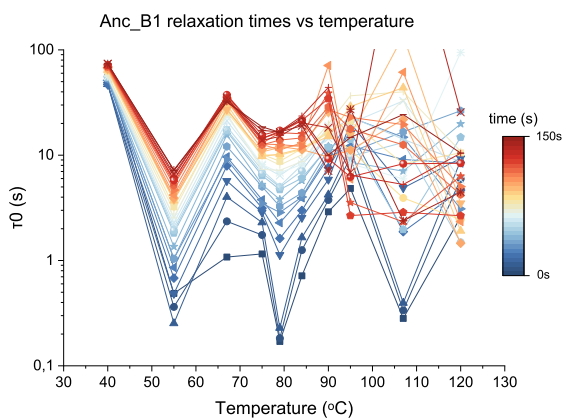

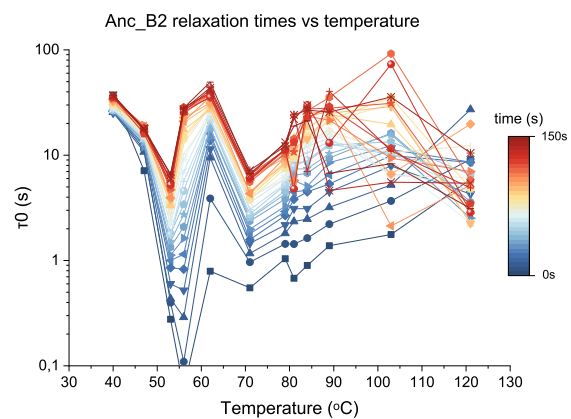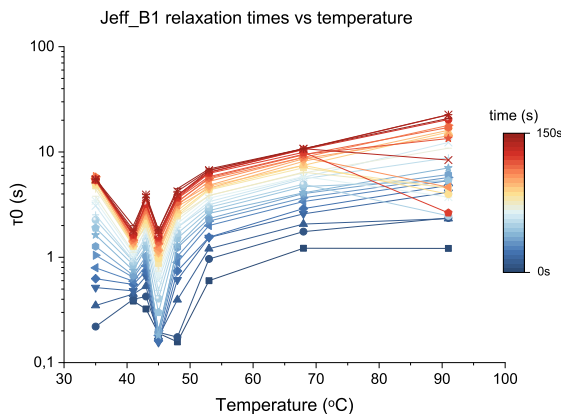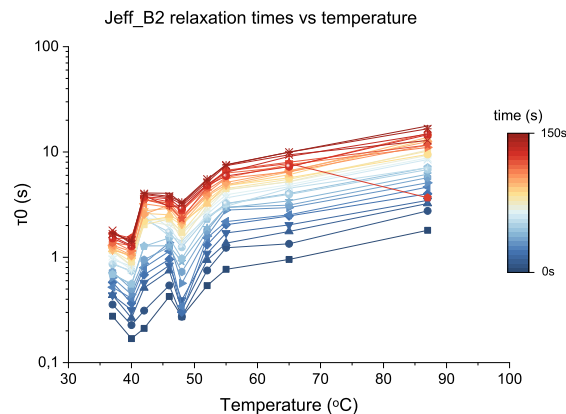Figure C.52: τ_0 vs temperature for Anc_B1 samples.

Figure C.53: τ_0 vs temperature for Anc_B2 samples.

Figure C.54: τ_0 vs temperature for Jeff_B1 samples.

Figure C.55: τ_0 vs temperature for Jeff_B2 samples.

The obtained relaxation times are more difficult to interpret, since τ_0 does not seem to decrease for higher temperatures as was expected. This could be attributed to the type of test executed, where the materials reaction to an imposed displacement is measured at different temperatures. So not only the material response to temperature changes was measured to compute τ_0, as has been the case in previous studies were τ_0 has been used for analysis. More datapoints would aid in a better understanding of the results, nevertheless the obtained results will be discussed here.

In Figures C.56 and C.57 the temperature ramp covers the entire T_g transition ($tan(\delta)$ peak) and length change coincides with the measured range. For the Jeff samples depicted in Figures C.58 and C.59 this is not the case, the peaks lay right at the begin of the temperature ramp.

Combining the results of Figures C.56 and C.57 and their DMA graphs, several characteristics stand out. The first decay in relaxation times coincides with the glassy phase of the material, before the onset points of length change and $tan(\delta)$. The first peak in relaxation time corresponds to the onset point of the length change curve. The peak of length change on the contrary coincides with shorter relaxation time, whereafter $\tau_0(s)$ increases again until the local minimum in delta length. After this moment the entropic length elongation and retraction are finished and $\tau_0(s)$ shows a scattered distribution over a wide range of frequencies.

From Figures C.58 and C.59 the same can be concluded as from the static temperature ramp tests, that the region of interest lies too much at the beginning of the LSI measuring range to see the effect all through the transition. It is difficult to say if the changes in relaxation time measured in the lower temperatures can be attributed to the material behavior or to discrepancies between measurements.

From these observations it may be suggested that LSI is not suitable to measure entropy changes. The course of $tan(\delta)$ seems detectable in LSI by means of τ_0, in the decrease of τ_0 during $tan(\delta)_{max}$. Further research should be conducted in order to see if this trend also holds for other materials (with their region of interest in the measurable range of both LSI and DMA).
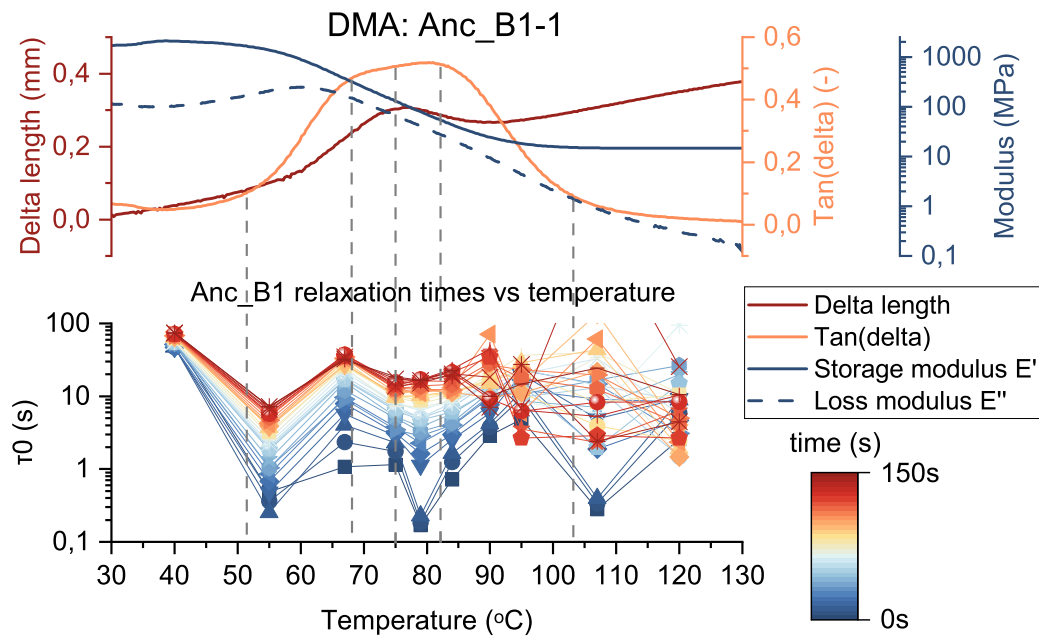
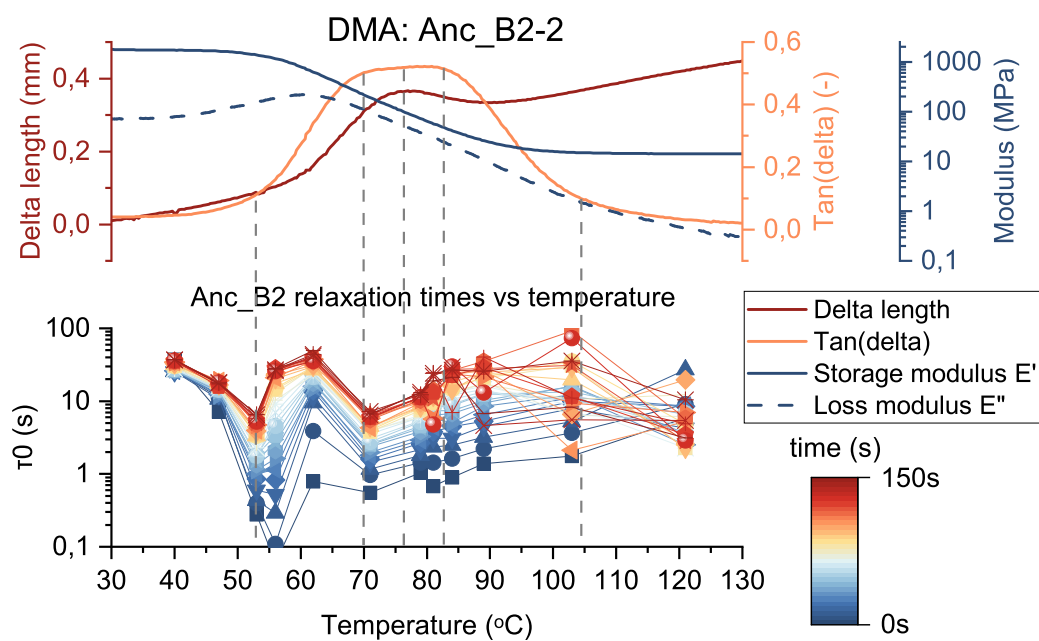Figure C.56: Comparison DMA and Dynamic Temperature Ramp LSI for Anc_B1

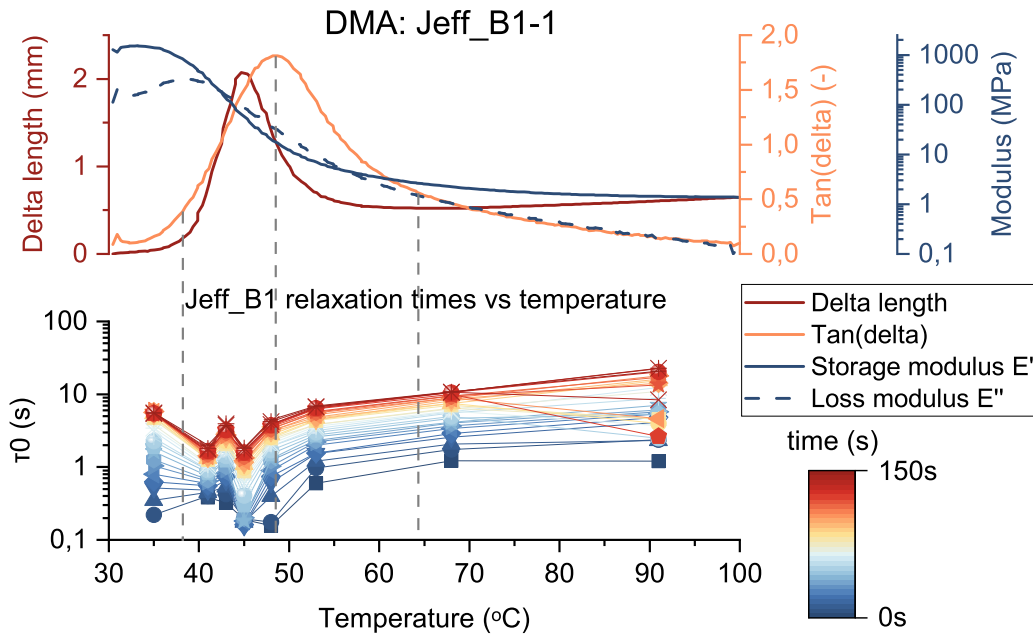Figure C.57: Comparison DMA and Dynamic Temperature Ramp LSI for Anc_B2

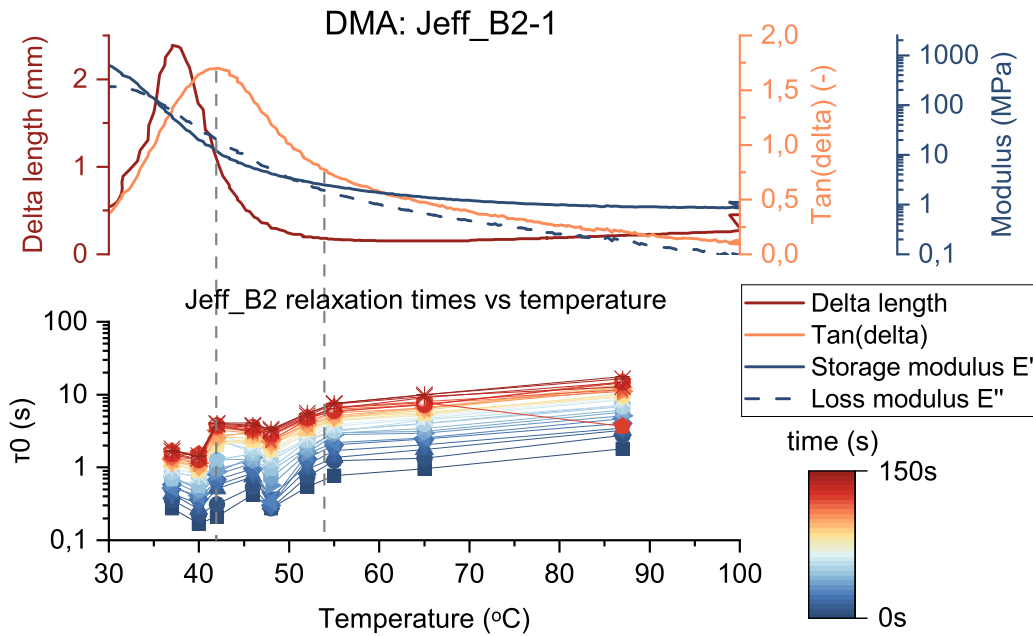Figure C.58: Comparison DMA and Dynamic Temperature Ramp LSI for Jeff_B1

Figure C.59: Comparison DMA and Dynamic Temperature Ramp LSI for Jeff_B2

D

Material Characteristics
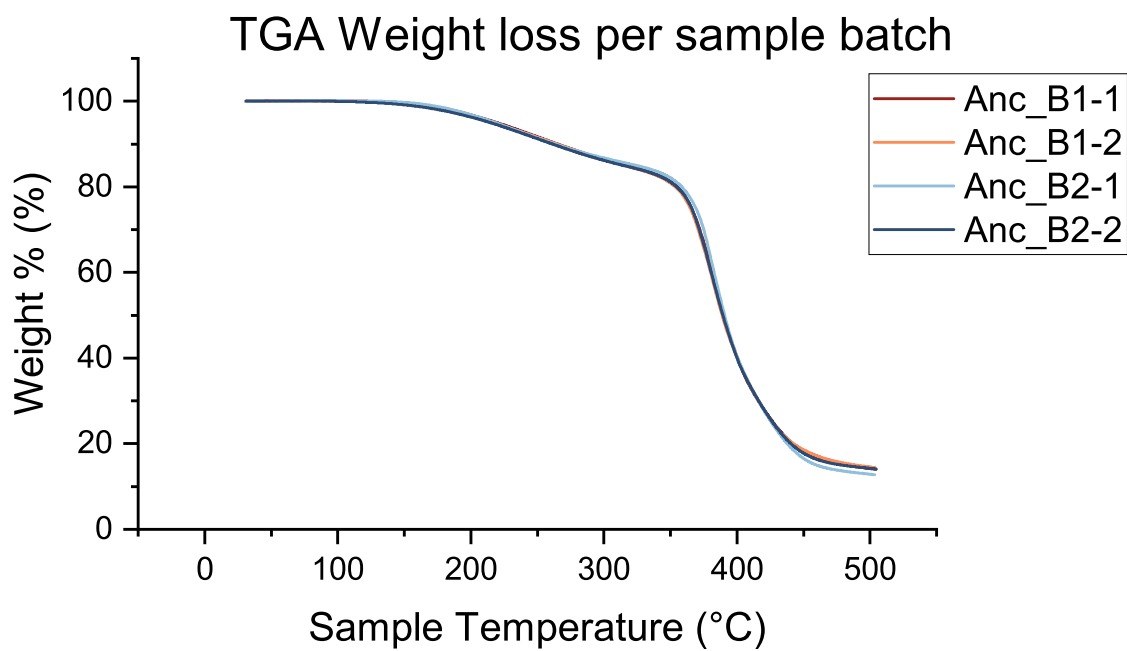
Obtained results from TGA and DSC measurements.

TGA Results
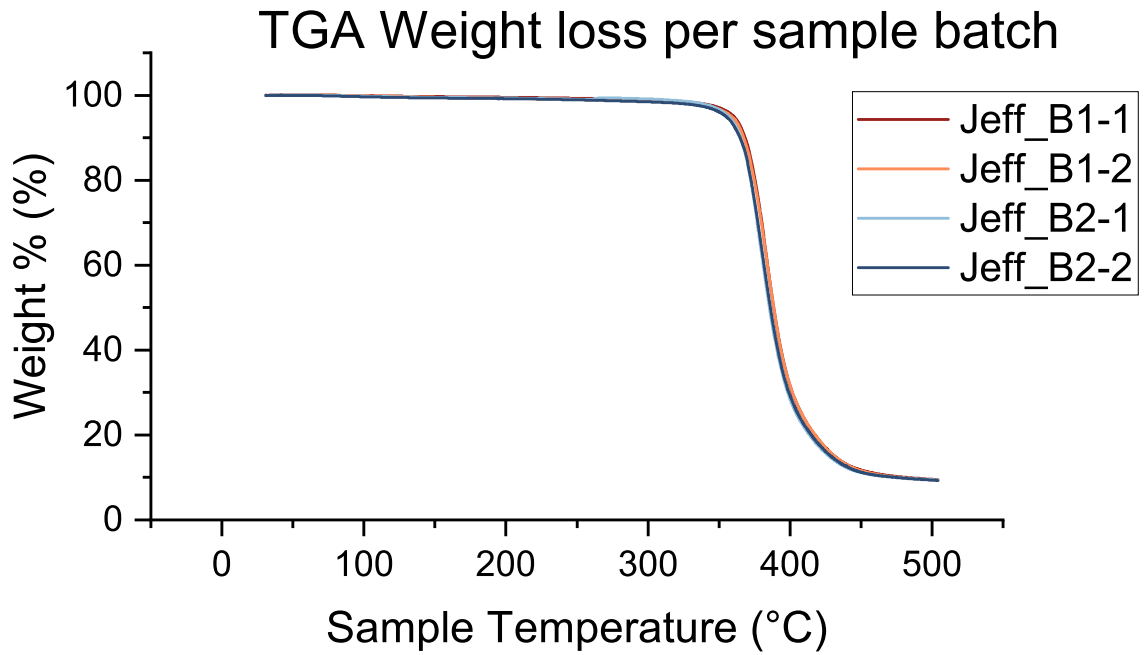

Figure D.1: TGA Results Anc Samples

TGA Weight loss per sample batch

Figure D.2: TGA Results Jeff Samples

DSC Results

The graphs below are obtained with the *TA Instruments TRIOS Software*. All DSC tests are executed in the same order. First the temperature is equilibrated at -30°C and the temperature is kept constant for 1 minute, blue and green curves. A first heating circle is conducted in order to remove the thermal history of the sample, heating to 170°C, kept at 170°C for 1 minute, cooling down to -30°C and kept at -30°C for 1 minute (the red, brown, pink and yellow curves respectively). The last heating ramp is the one used to extract thermal material behavior, the blue curve.

The Jeff samples show a broad endothermic peak around 100°C during the first heating ramp, which is not distinguishable in the Anc tests.
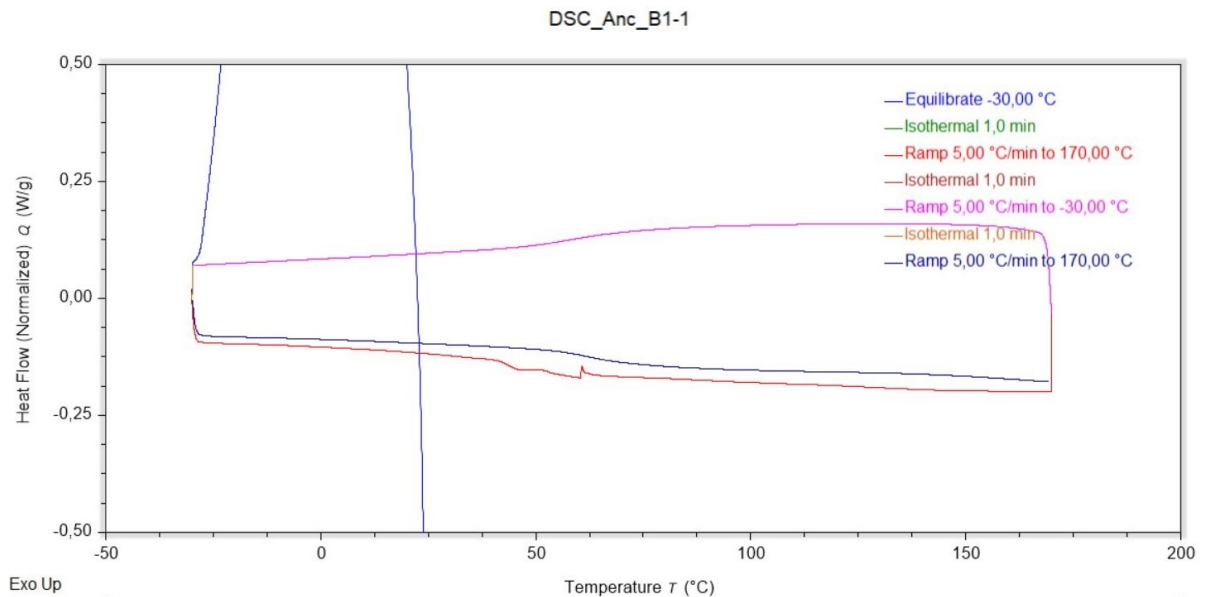
Figure D.3: DSC Result Anc_B1-1
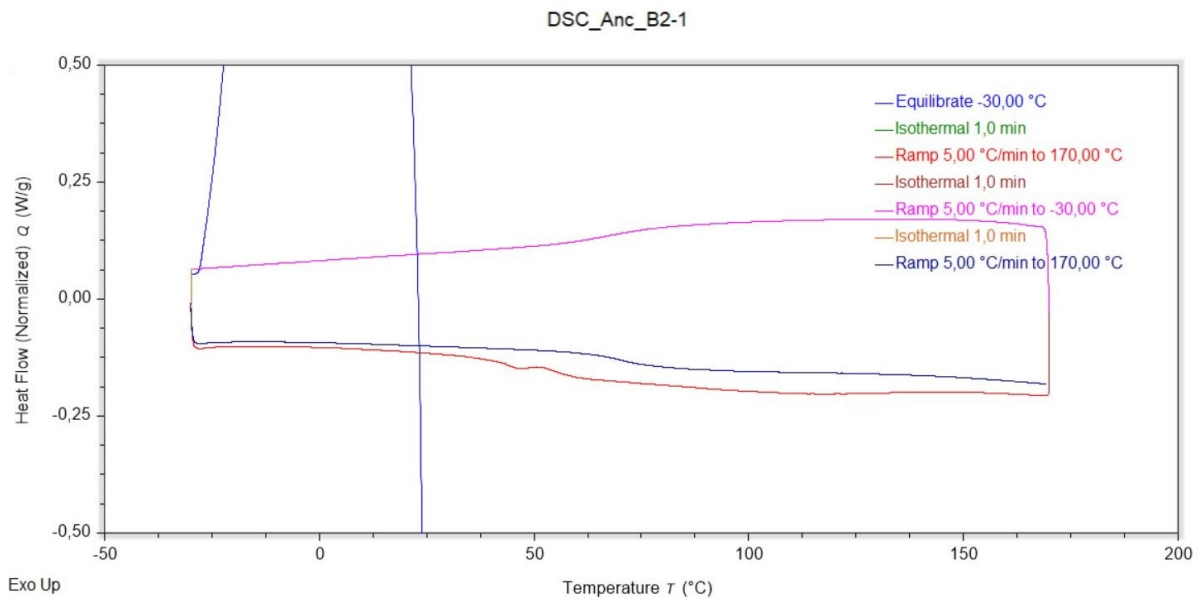
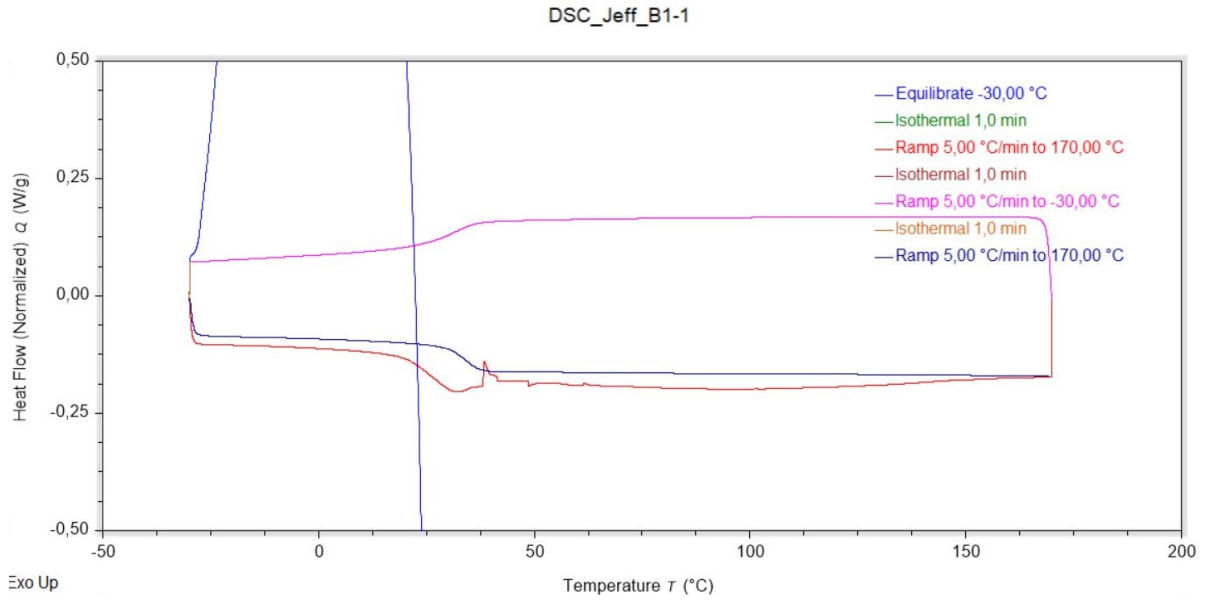Figure D.4: DSC Result Anc_B2-1
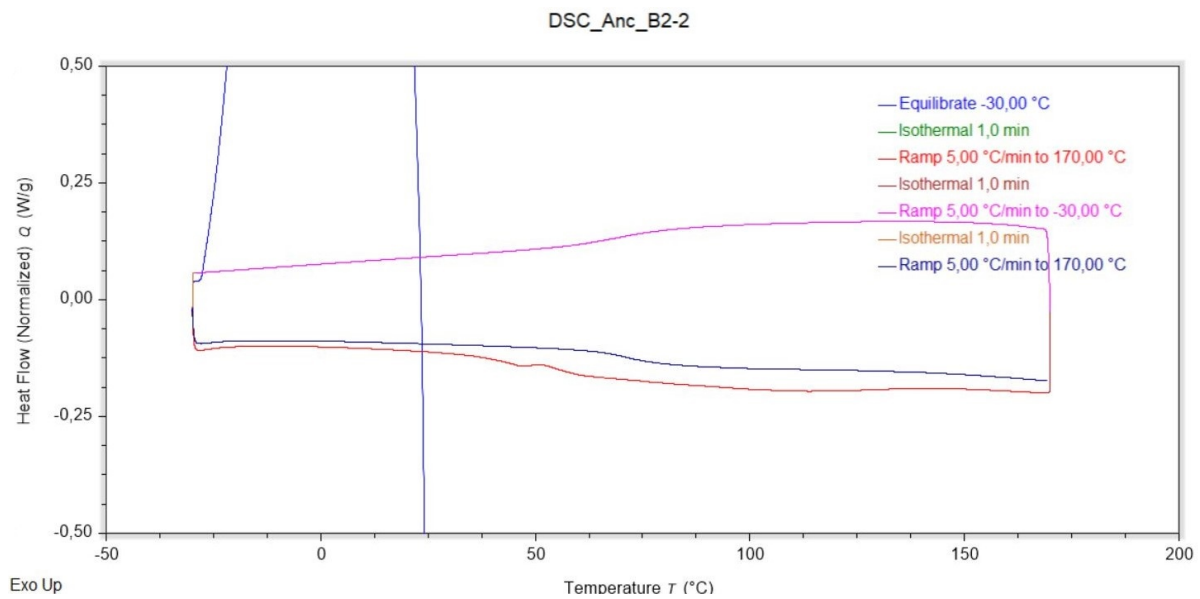
Figure D.5: DSC Result Anc_B2-2

DSC_Jeff_B1-1

Figure D.6: DSC Result Jeff_B1-1
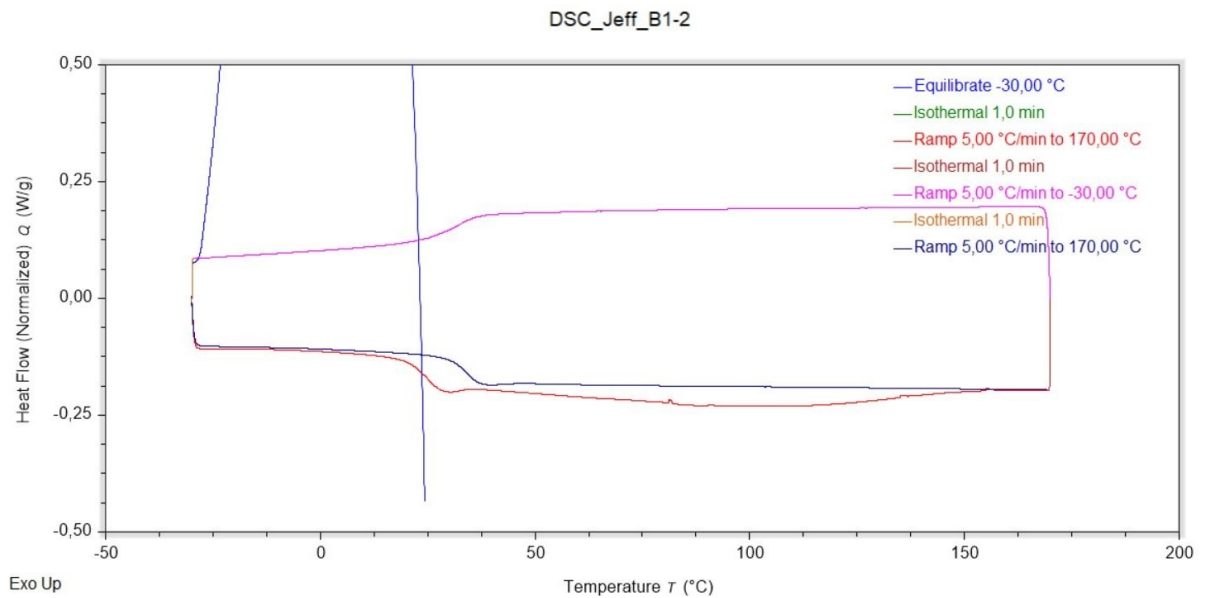
DSC_Jeff_B1-2

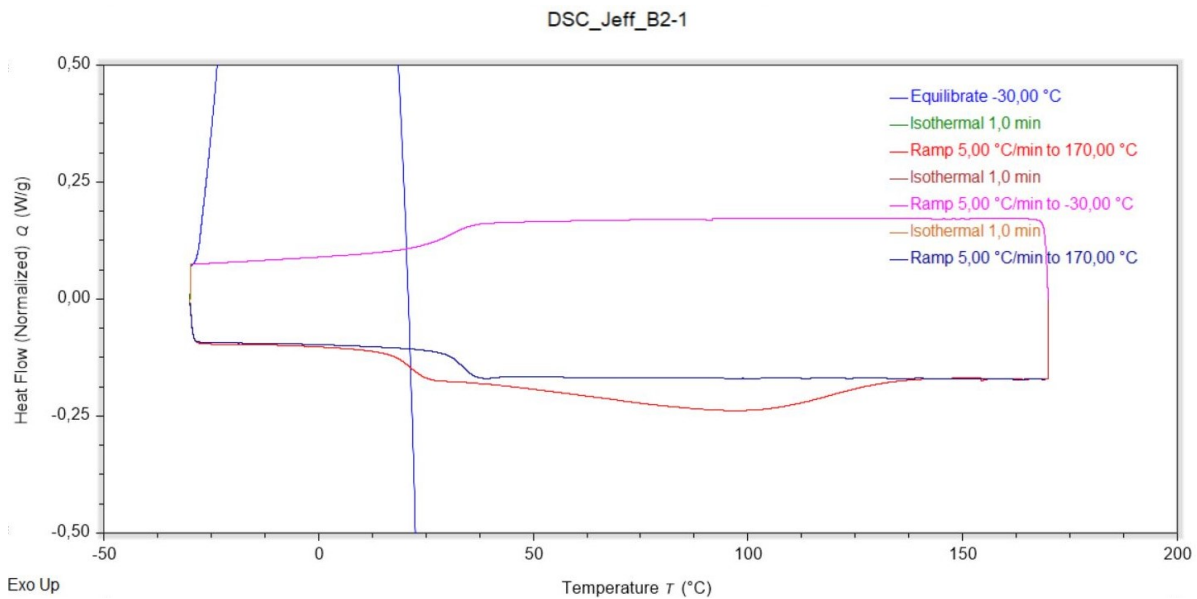Figure D.7: DSC Result Jeff_B1-2
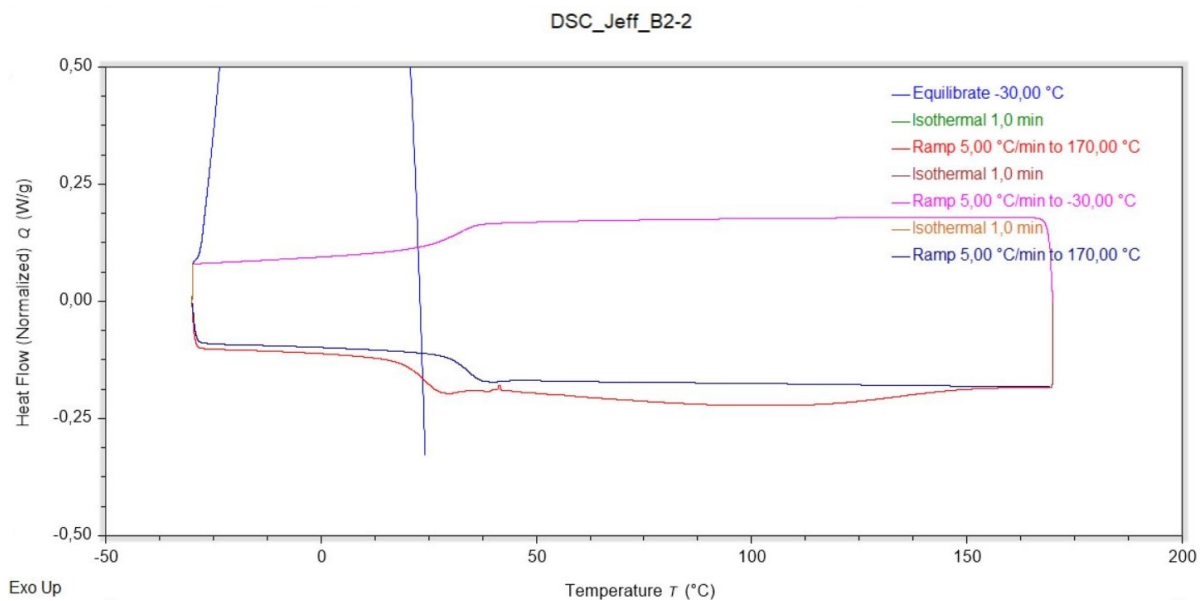
Figure D.8: DSC Result Jeff_B2-1

Figure D.9: DSC Result Jeff_B2-2

Post-curing Check After LSI Measurements

After the LSI temperature ramp for strained samples of Anc_B2 and Jeff_B2, T_g was measured with DSC. Those results with respect to the averaged T_g values as mentioned before can be seen in Figure D.10. The T_g values at 20°C are the same as in Figure 4.2. From Figure D.10 it can be noted that T_g of Anc samples are similar and are all lower than T_g measured before LSI tests, only the values between 80-85°C stand out from the rest. The results for Jeff samples are even more similar. All stay within the error bars established from the previous tests.

The little change in T_g before and after the executed temperature ramps in LSI suggest that no post curing has taken place during the tests. This is interesting to know because post curing could dissipate energy and thus influence the test results. Curing would result in a higher crosslinking density and thus increased T_g.
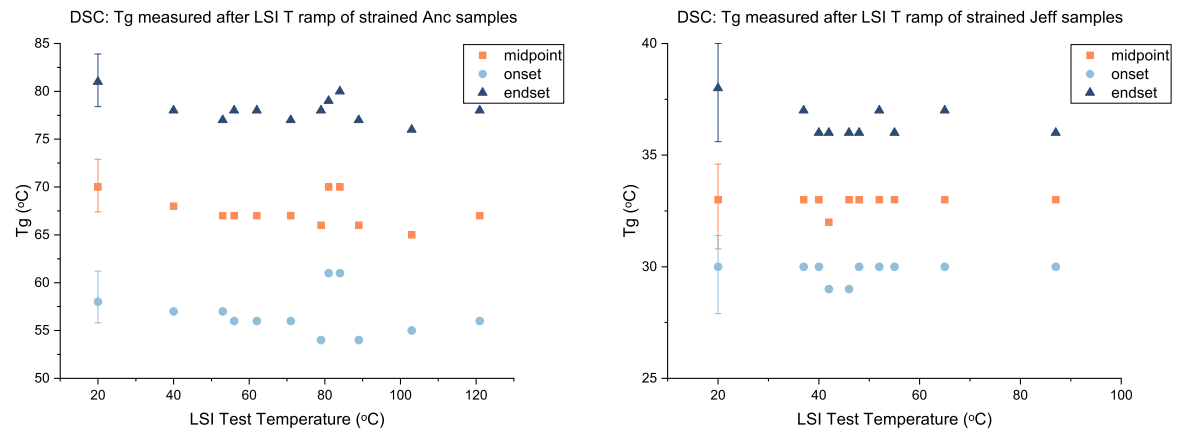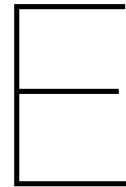
Figure D.10: T_g comparison for the samples before and after a LSI temperature ramp measured by DSC.

Temperature Calibration LSI

Temperature Gradient Sample

Infrared measurements have been carried out that show spatial differences in temperature over the whole area of the sample, for the strained sample temperature ramp set-up. . This method established a gradient in temperature over the whole sample surface with the maximum temperature in the middle. The middle of the sample has been taken as measurement spot to establish the end-of-test temperature with a thermocouple. Since the area of the laser spot is very small, the assumption has been made that in that area temperature is constant. The end-of-test temperatures measured with the thermocouple have been used as true test temperature.

A FLIR A-600 Series thermal imaging camera was used to calibrate the sample temperature for certain voltages of the resistors. The picture was taken after 10 minutes of heating at the following voltages: 0V, 6V, 9V, 12V, 15V, 18V and 24V. In Table E.1 the temperature gradients are summarized per voltage. The pictures taken of the software to illustrate the gradient are depicted in Figures E.1 - E.7.

Table E.1: FLIR Temperature Gradient

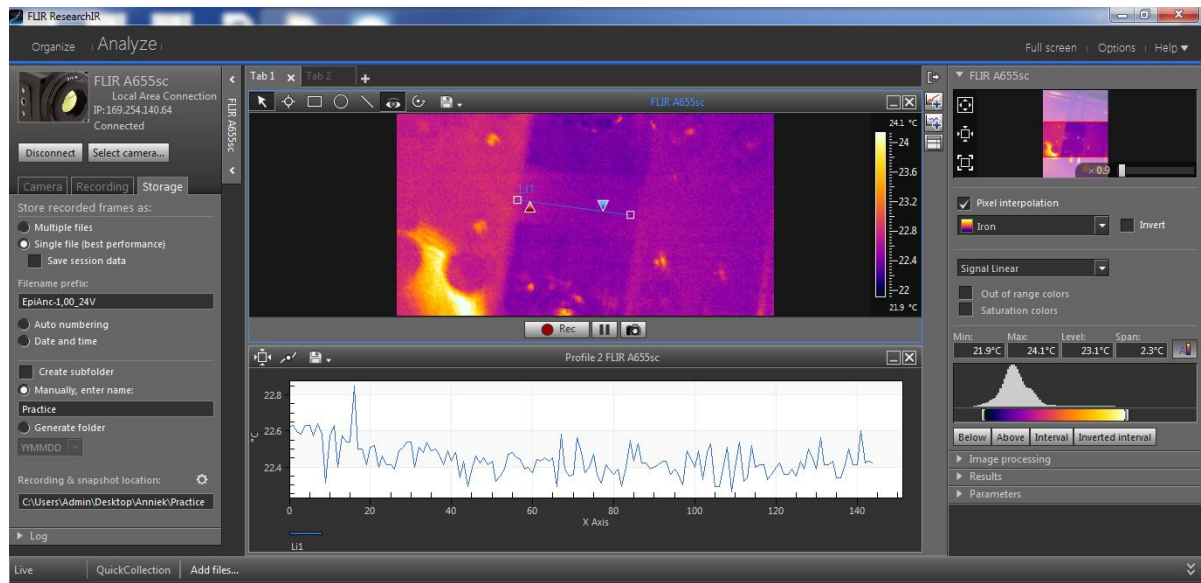| Applied Voltage	Temperature Minimum	Temperature Maximum
0 V	22.2	22.8
6 V	23	29
9 V	24	39
12 V	25	50
15 V	25	65
18 V	30	80
24 V	30	120

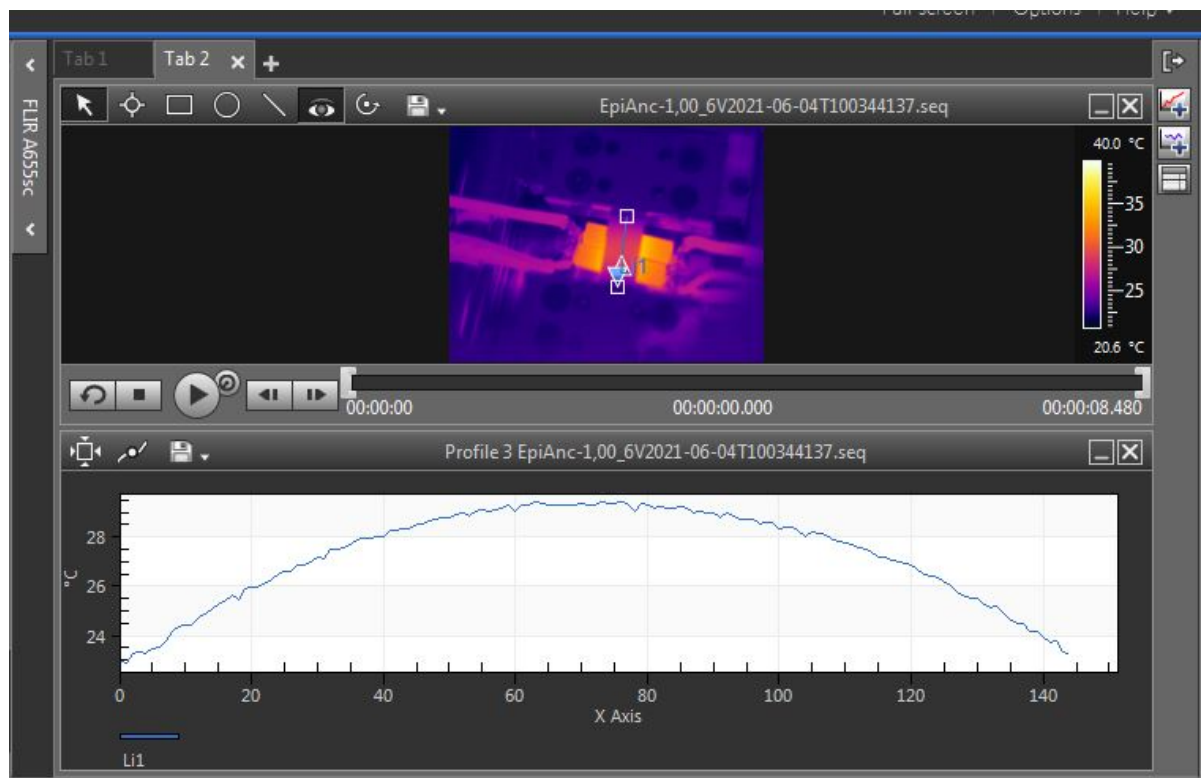Figure E.1: FLIR camera heat map of an epoxy sample at room temperature and 0V

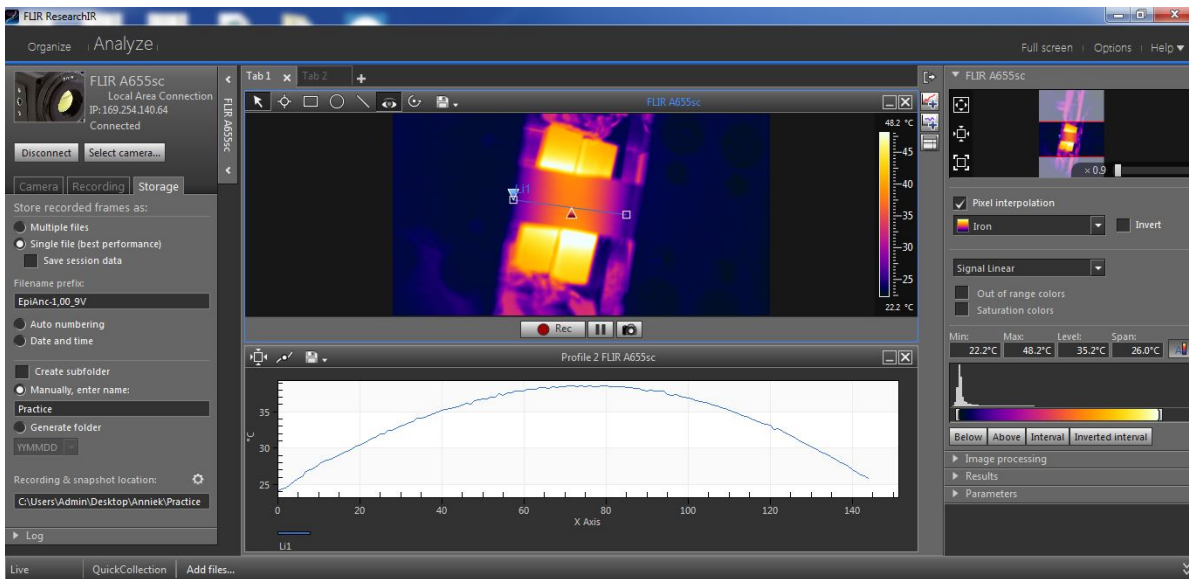Figure E.2: FLIR camera heat map of an epoxy sample at 6V

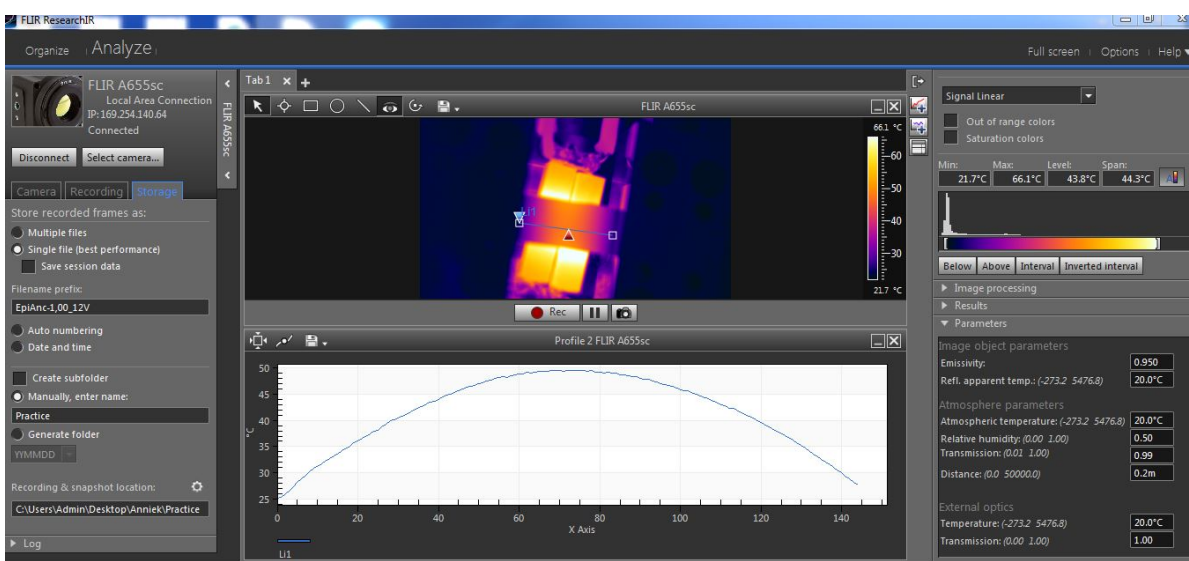Figure E.3: FLIR camera heat map of an epoxy sample at 9V

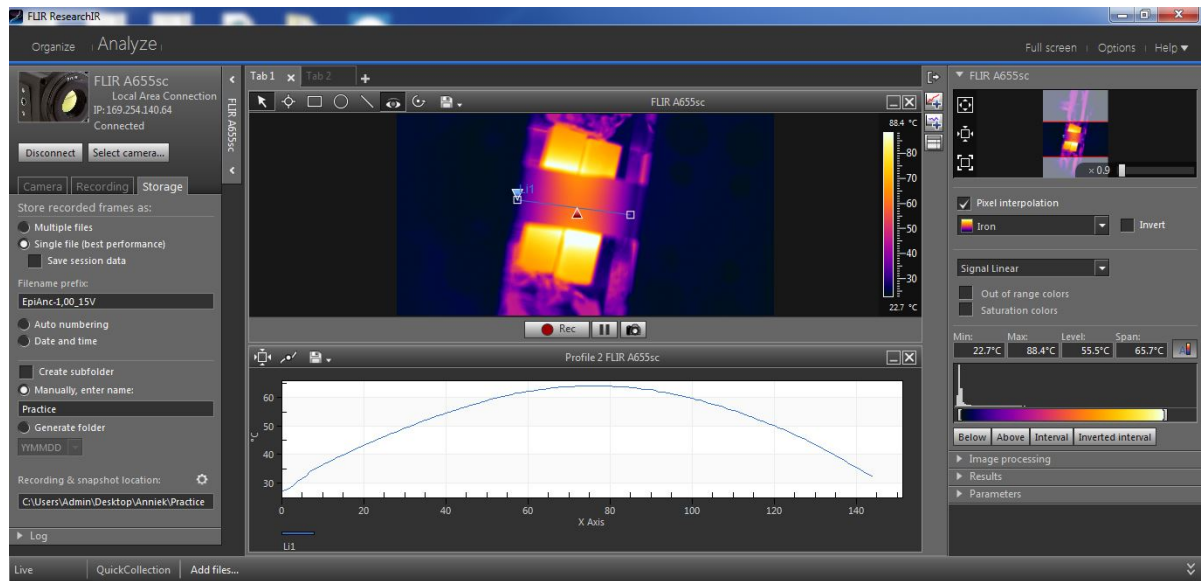Figure E.4: FLIR camera heat map of an epoxy sample at 12V

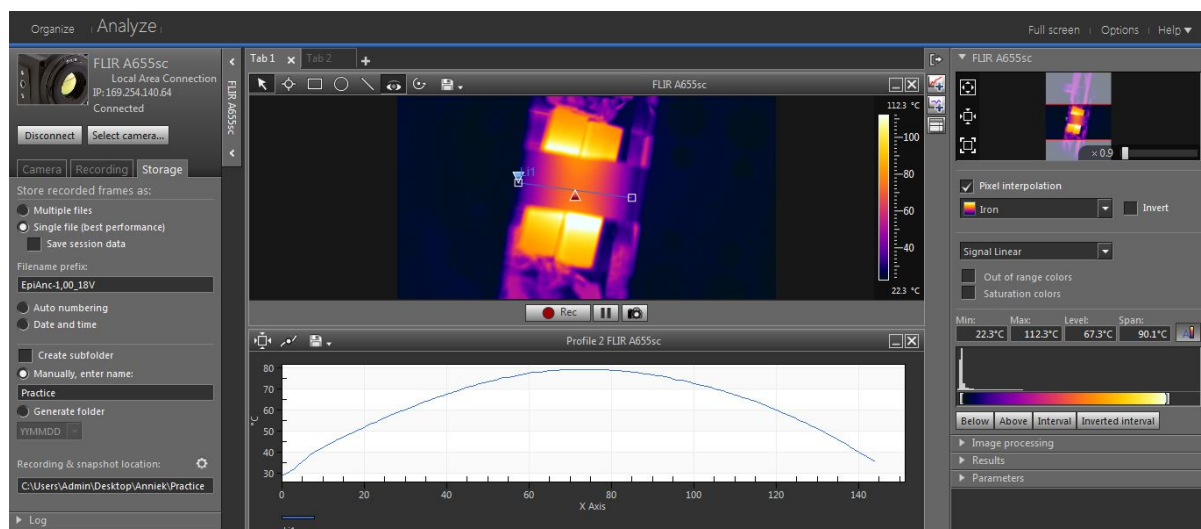Figure E.5: FLIR camera heat map of an epoxy sample at 15V

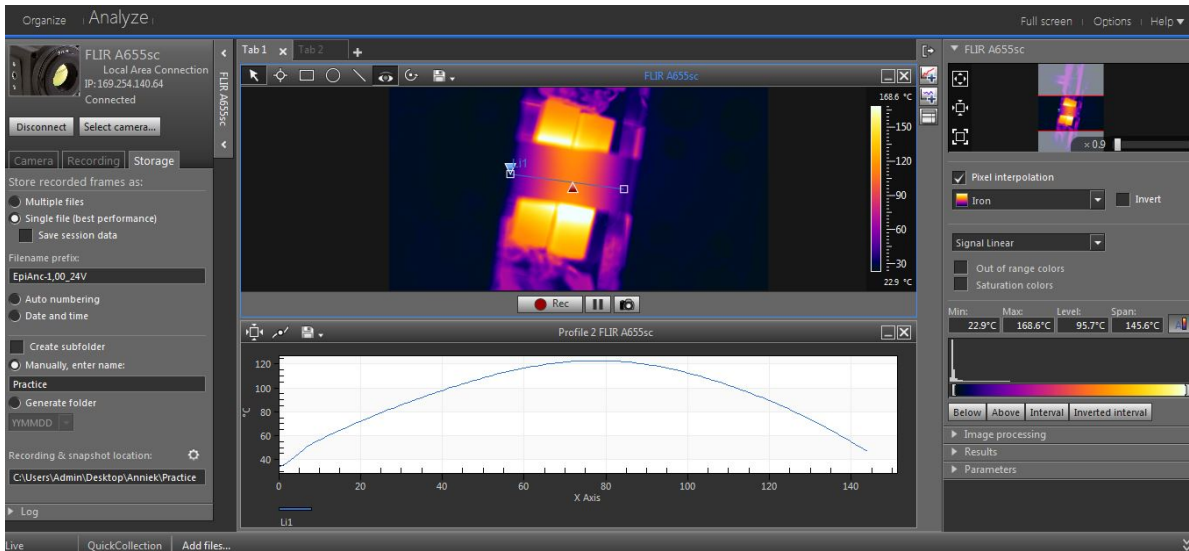Figure E.6: FLIR camera heat map of an epoxy sample at 18V

Figure E.7: FLIR camera heat map of an epoxy sample at 24V

Thermocouple Results LSI Temperature Ramps

Non-strained Sample

A linear line is fitted through the maximum temperature measured and the temperature of the sample surface when the hot stage is turned off but the laser is already a few minutes on. The true sample surface temperature during the test has been established in this manner and thus the heating rate (it should be approximately 2°C/min in order to mimic the rate of the DMA temperature ramp).

Anc_B1	Time [s]	T sample [°C]	
	120	31,8	hot stage off, laser on
	2700	132,3	
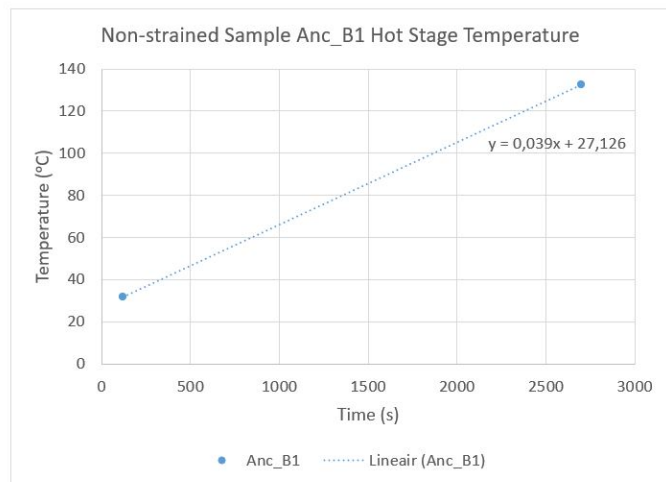
Figure E.8: Temperature Hot Stage Anc_B1

Anc_B2-1	Time [s]	T sample [°C]	
	0	20	hot stage off, laser off
	300	41	hot stage off, laser on
	2700	125	hot stage on, laser on
Anc_B2-2	0	20	hot stage off, laser off
	300	41	hot stage off, laser on
	2700	125	hot stage on, laser on
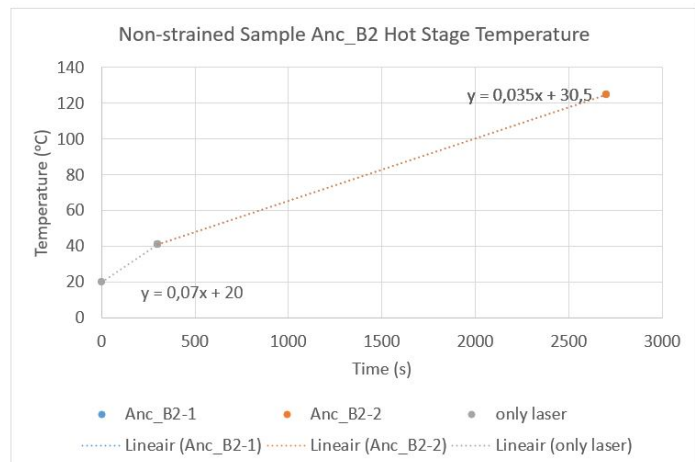
Figure E.9: Temperature Hot Stage Anc_B2

Jeff_B1-1	Time [s]	T sample [°C]	
	120	44,1	hot stage off, laser on
	2660	119,4	end of test
Jeff_B1-2	120	44,1	hot stage off, laser on
	2560	135	end of test

Non-strained Sample Jeff_B1 Hot Stage Temperature

y = 0,0373x + 39,63

y = 0,0296x + 40,543
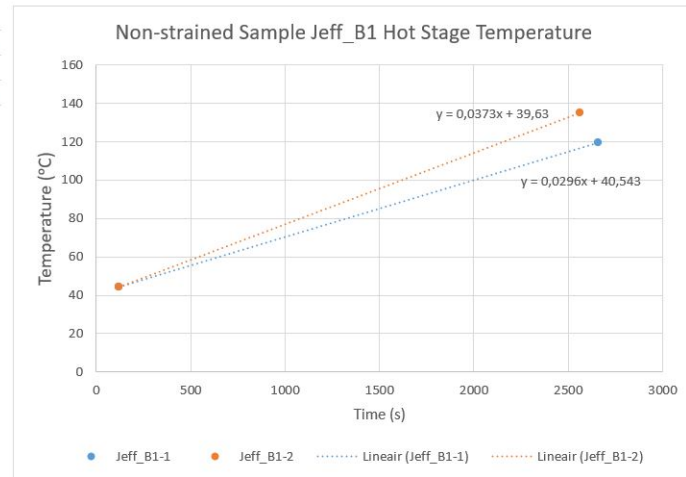
Figure E.10: Temperature Hot Stage Jeff_B1

Jeff_B2-1	Time [s]	T sample [°C]	
	120	44,1	hot stage off, laser on
	2700	120	end of test
Jeff_B2-2	120	44,1	hot stage off, laser on
	2700	133	end of test

Non-strained Sample Jeff_B2 Hot Stage Temperature
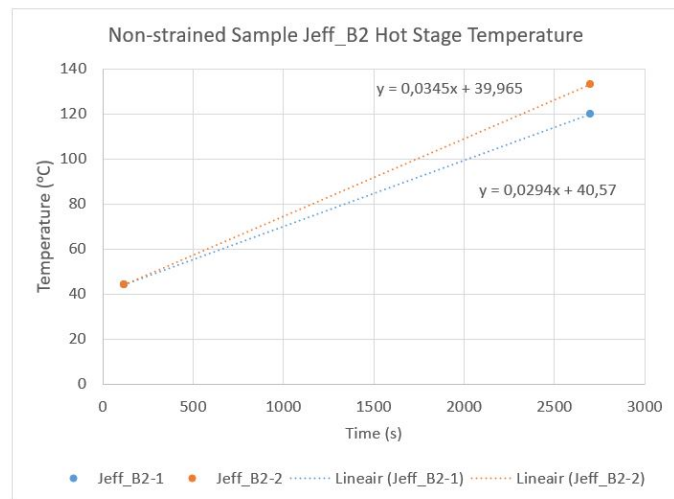
y = 0,0345x + 39,965

y = 0,0294x + 40,57

Figure E.11: Temperature Hot Stage Jeff_B2

Strained Sample

A thermocouple was used to measure the sample temperature before and after the tests. The before measurements have been used to calibrate the resistor heating set-up, since it has not been possible to measure the temperature during LSI experiments. After every LSI measurement the temperature at the middle of the sample, similar to the laser spot place, has been measured and will be reported below. If a temperature has not been measured the corresponding temperature to the voltage used is reported, the fitted lines are used to do so.

Temperature Calibration

Measured temperatures and fitted line of voltage vs temp of the sample temperature heated with the resistors, before strain test have been executed.

Voltage (V)	Temperature (°C)
3,5	40
8,0	53
9,4	55
10,0	56
12,6	62
13,5	67
14,3	71
15,6	75
15,7	79
16,6	79
17,6	81
18,0	84
17,7	84
18,8	89
18,8	90
19,9	95
20,8	103
22	107
24	120
24,0	121

The fitted equation: $y = 0,1248x^2 + 0,3475x + 39,446$, $R^2 = 0,994$
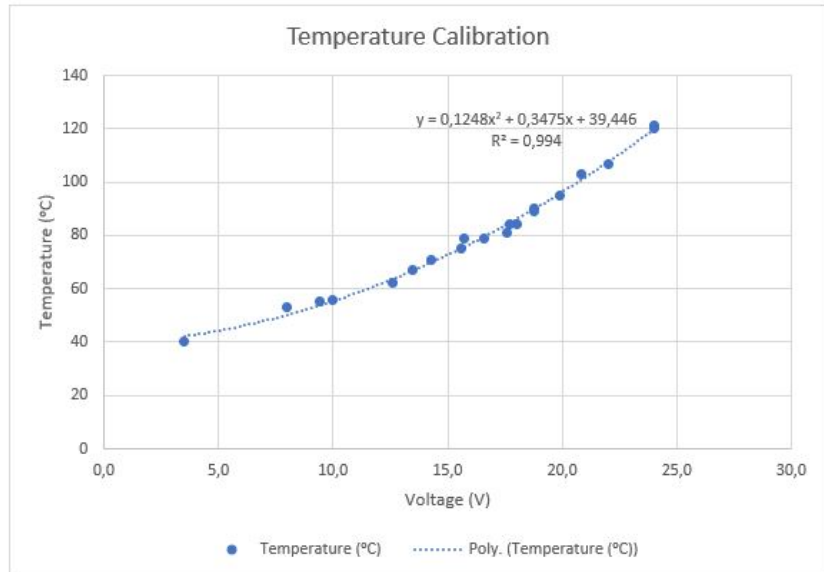

Figure E.12: Temperature calibration of the resistor heating device

After Test Measurements

True test temperatures, measured temperatures after every test.

Voltage [V]	T after test [°C]
0,0	44,7
3,5	47,1
5,5	50
8,0	52,5
10,0	55,7
12,6	62,3
14,3	70,7
15,7	78,8
17,6	80,8
18,0	83,8
18,8	89,2
20,8	102,6
23,9	120,5

The fitted equation: $y = 0,1484x^2 - 0,4627x + 46,17$, $R^2 = 0,9937$
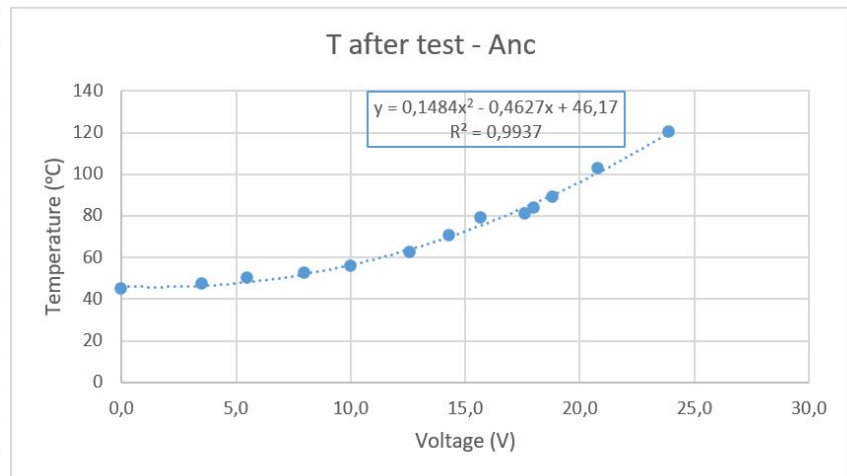
Figure E.13: Sample Temperature Anc Samples

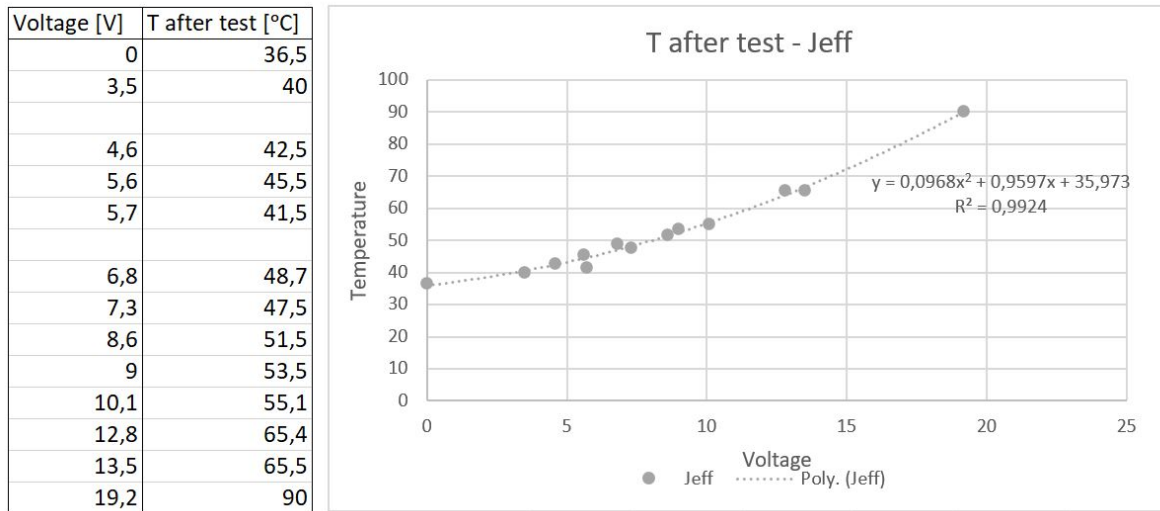| Voltage [V]	T after test [°C]
0	36,5
3,5	40
4,6	42,5
5,6	45,5
5,7	41,5
6,8	48,7
7,3	47,5
8,6	51,5
9	53,5
10,1	55,1
12,8	65,4
13,5	65,5
19,2	90

Figure E.14: Sample Temperature Jeff Samples

Influence of Airflow

To test the expected influence of airflow on LSI tests a few trials were executed. First over a period of four minutes a sample in open air was measured. After one and three minutes the airflow was disturbed with an air blower for one minute. The result shows a clear disturbance in d_2 signal over the whole frequency span during those two minutes.

The other three tests were executed to test the cardboard chamber used in all experiments. The goal was to see if the box could reduce the fluctuations without disturbing or influencing the test results. The difference between Figures E.15B and D shows the decrease in noise at higher temperatures. The result from Figures E.15B and C show how little influence the glass plate has on the signal disturbance. Therefore it was decided to use the box and glass cover as depicted in Figures 3.11B and 3.12B.
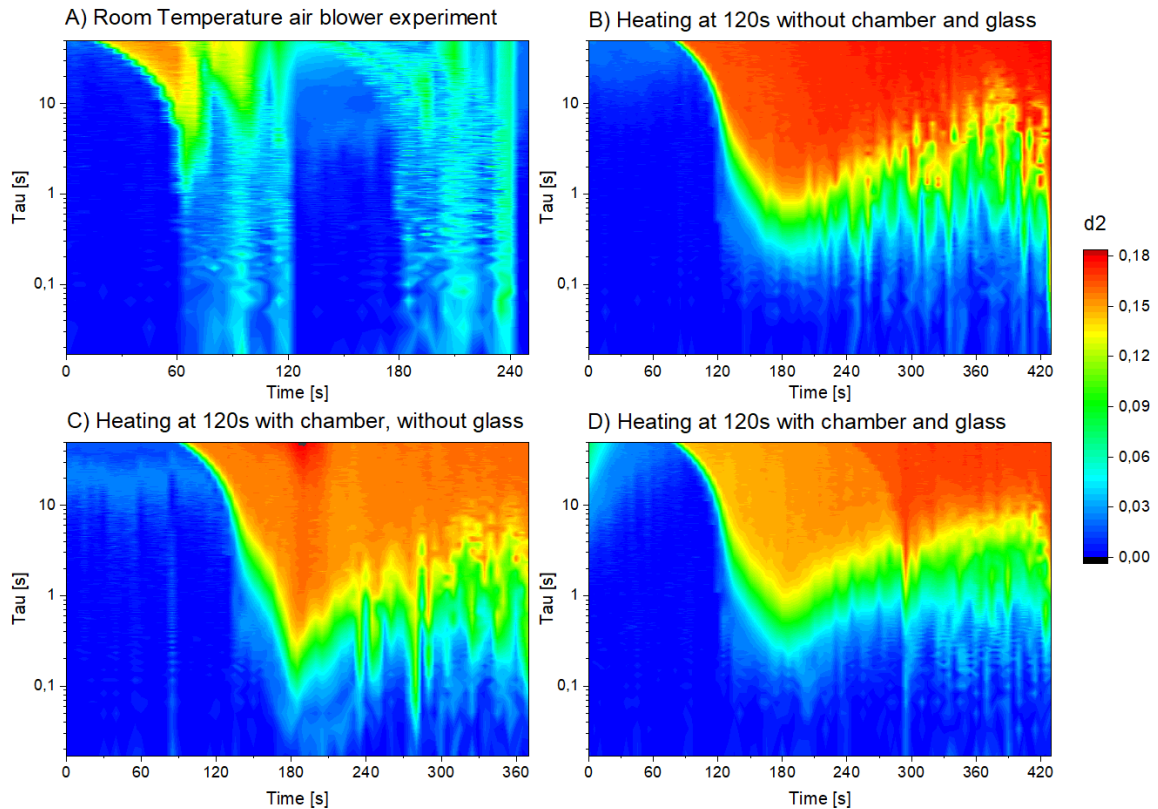

Figure E.15: Tests airflow and influence cardboard chamber. A) Test with air blower and non-heated sample in open air, B) Heating of a sample in open air. C) Heating of a sample in a chamber but without glass top plate . D) Heating of a sample in a chamber with a glass top plate.